CLOSED PATH APPROACH TO CASIMIR EFFECT IN RECTANGULAR CAVITIES AND PISTONS

A Dissertation

by

ZHONGHAI LIU

Submitted to the Office of Graduate Studies of
Texas A&M University
in partial fulfillment of the requirements for the degree of

DOCTOR OF PHILOSOPHY

December 2009

Major Subject: Physics

CLOSED PATH APPROACH TO CASIMIR EFFECT IN RECTANGULAR CAVITIES AND PISTONS

A Dissertation

by

ZHONGHAI LIU

Submitted to the Office of Graduate Studies of
Texas A&M University
in partial fulfillment of the requirements for the degree of

DOCTOR OF PHILOSOPHY

Approved by:

Chair of Committee,	Stephen Fulling
Committee Members,	Christopher Pope
	Wayne Saslow
	Peter Kuchment
Head of Department,	Edward Fry

December 2009

Major Subject: Physics

ABSTRACT

Closed Path Approach to Casimir Effect in Rectangular
Cavities and Pistons. (December 2009)
Zhonghai Liu, B.S., University of Science and Technology of China;
M.S., Texas A&M University
Chair of Advisory Committee: Dr. Stephen Fulling

We studied thoroughly Casimir energy and Casimir force in a rectangular cavity and piston with various boundary conditions, for both scalar field and electromagnetic (EM) field. Using the cylinder kernel approach, we found the Casimir energy exactly and analyzed the Casimir energy and Casimir force from the point of view of closed classical paths (or optical paths). For the scalar field, we studied the rectangular cavity and rectangular piston with all Dirichlet conditions and all Neumann boundary conditions and then generalized to more general cases with any combination of Dirichlet and Neumann boundary conditions. For the EM field, we first represented the EM field by 2 scalar fields (Hertz potentials), then related the EM problem to corresponding scalar problems. We studied the case with all conducting boundary conditions and then replaced some conducting boundary conditions by permeable boundary conditions. By classifying the closed classical paths into 4 kinds: Periodic, Side, Edge and Corner paths, we can see the role played by each kind of path. A general treatment of any combination of boundary conditions is provided. Comparing the differences between different kinds of boundary conditions and exploring the relation between corresponding EM and scalar problems, we can understand the effect of each kind of boundary condition and contribution of each kind of classical path more clearly.

ACKNOWLEDGMENTS

I would like to thank my friend in Dr. Fulling's group, Todd Zapata, who shared lots of valuable things by discussing problems in the research as well as in life. I also want to thank Dr. Kaplan from Tulane University, Dr. Villarreal from Mexico (UNAM), Dr. Kirsten from Baylor University, Dr. Milton from Oklahoma University for their helpful conversations and instructions on many topics.

I deeply appreciate the advice and the supervision by Dr. Fulling. Whenever I had problems with my research, he is the person I would turn to for help. He would always point out what needed to be improved and what direction I should go. He often prevented me from going in the wrong direction. I also appreciate my committee members, Dr. Pope, Dr. Kuchment, Dr. Saslow, Dr. Belyanin and Dr. Berkolaiko. Their classes and their direction were always good for understanding my research problems.

TABLE OF CONTENTS

CHAPTER Page

CHAPTER Page

LIST OF TABLES

LIST OF FIGURES

FIGURE Page

FIGURE Page

CHAPTER I

INTRODUCTION

A. Origin of Casimir Effect

In 1948, H.G.Casimir predicted the well-known Casimir effect [1], that is, two extremely clean, neutral, parallel, micro-flat conducting surfaces, in a vacuum environment, at zero temperature, attract one another by a very weak force that varies inversely as the fourth power of the distance between them [2] :

$$F(a) = -\frac{\pi^2 \hbar c}{240 a^4} A \tag{1.1}$$

where a is the separation between two parallel plates, $A \gg a^2$ is their area and c is the speed of light. In the following we set $\hbar$=c=1. From dimensional analysis with $\hbar$, c and the separation a, the Casimir force per unit area is inversely proportional to the fourth power of the separation a. The Casimir effect was first demonstrated by M.J. Sparnaay in 1958 [3] and was confirmed to good accuracy by S. K. Lamoreaux's experiment in 1997 [4].

The Casimir Effect is a prediction of quantum electrodynamics (QED). However, Casimir and Polder's first attempt to compute the Casimir energy (force) was not based on QED; instead, they investigate the Van der Waals forces in colloidal fluids [5]. There is an interesting story on the history of the Casimir Effect that H.B.G.Casimir stated on his own words [6]:

During a visit I paid to Copenhagen, it must have been in 1946 or 1947, Bohr asked me what I had been doing and I explained our work on Van der Waals forces. "That's nice, that is something new", he said. I then explained I should like to find a simple and elegant derivation of my results. Bohr thought it over, then mumbled something like "must have

---

The journal model is *Journal of Physics A* .

something to do with the zero-point energy". That was all, but in retrospect I have to admit that I owe much to this remark.

It turns out that zero-point energy is the key word to understand Casimir effect.

B. Understanding of Casimir Effect

The Casimir effect is widely regarded as a rising from the zero-point fluctuations intrinsic to any quantum system. The QED vacuum is a sea of virtual photons; in another words, it may be regarded as an enormously large collection of harmonic oscillators representing the fluctuations. A harmonic oscillator with frequency ω has a ground state energy which is nonzero:

$$\varepsilon(\omega) = \frac{1}{2}\omega \tag{1.2}$$

For free Minkowski space, the spectrum of frequency is continuous, so integration over possible frequency gives the energy density:

$$\varepsilon = \int_0^\infty \varepsilon(\omega)\rho(\omega)\, d\omega = \int_0^\infty \frac{1}{2}\omega\rho(\omega)\, d\omega \tag{1.3}$$

When boundaries are introduced into free Minkowski space, the spectrum of frequency will be discrete; the integration in (1.3) has to be replaced by a summation:

$$\varepsilon = \sum_J \frac{1}{2}\omega_J \tag{1.4}$$

With boundaries the field is constrained to a finite spatial volume and is forced to satisfy certain boundary conditions on the boundaries. It is the presence of boundaries that makes the field constrained and changes the spectrum from continuous to discrete [7]. The Casimir effect can be understood as resulting from the modification of zero-point fluctuations of QED vacuum [8]. For the original model, parallel plates, Casimir energy corresponds to

the energy difference between constrained field and unconstrained field (free field) [7]:

$$\triangle\varepsilon = \varepsilon_{plates} - \varepsilon_{free} = \sum_{J} \frac{1}{2}\omega_J - \int_0^\infty \frac{1}{2}\omega\rho(\omega)d\omega \tag{1.5}$$

One is faced with the problem of ultraviolet divergence when summing the zero-point energy over all modes [9]. Careful renormalization is needed to take care of the divergence. There are many approaches to yield finite results for Casimir energy with different mechanisms.

C. Various Approaches to Casimir Effect

Various methods have been developed to evaluate Casimir energy since H.B.G. Casimir's famous paper [1] in 1948. The Casimir energy can be defined directly as the sum of half-frequencies that is interpreted via ζ-function regularization [10]. Multiple reflection expansion [11] and optical approximation [12] are based on the analysis of density of states and they develop general methods to deal with either flat or curved surfaces by bringing in stationary path/optical path analysis. The Green function formalism [13], and heat kernel expansion [14] find systematic applications to quite a lot of problems.

Our approach to scalar field Casimir problems is closed path analysis based on the cylinder kernel [15, 16]. For the electromagnetic (EM) field, we find that the Hertz potential approach is convenient to convert the EM problem to a scalar problem; thus we can analyze it by closed paths as well [17].

Casimir energy depends strongly on geometry and the relation between sign of Casimir force and geometry is nontrivial. The earliest and simplest geometry is parallel plates, which can be dealt with by almost every approach. The piston geometry has attracted much interest since Cavalcanti published his first piston paper [18]. The piston geometry is our focus in this dissertation, for both scalar field and EM field. The measurement of

the force between two parallel plates is not as easy as its derivation because of alignment. An experimentally interesting geometry is a sphere above a plate, since that is a highly symmetrical geometry. We will discuss more about measurement in the following section.

D. Measurement and Application of Casimir Effect

One of the main pioneers in measuring the Casimir force was M.J. Sparnaay in 1958 [3]. He used the standard parallel plate geometry with a spring balance, measuring the capacitance between the two plates to determine distances, obtaining results not in contradiction with the Casimir theory, but with large experimental errors. Since then greater and greater accuracy was achieved through a succession of different techniques. The Casimir effect was measured more accurately by S. K. Lamoreaux in 1997 [4] and by U. Mohideen's group in 1999 with the use of an atomic force microscope (AFM) [19]. In practice, rather than using two parallel plates, which would require phenomenally accurate alignment to ensure they were parallel, the experiments use one plate that is flat and another plate that is a part of a sphere with a large radius. In 2001, a group at the University of Padua finally succeeded in measuring the Casimir force between parallel plates using micro-resonators [20].

Presently there are many applications of the Casimir effect to modern physics. Perhaps most directly applicable to theoretical physics is the Casimir effect's role in the extremely small distance scales at which quarks interact; physicists studying QCD have modeled hadron interactions within nucleons using the chiral bag model [9]. The dynamical Casimir effect is one of the more interesting predictions in modern physics. Physicists have theorized that such an effect might explain the phenomenon of sonoluminescence [21].

Moreover, it has been suggested that the Casimir forces have application in nanotechnology, in particular silicon integrated circuit technology.

E. Structure of This Dissertation

We shall begin in Chapter II with the foundation of the closed path approach based on the cylinder kernel, with a brief review of other approaches; by applying every approach to the parallel plates model we explore the relation between our approach and others. In Chapter III a thorough study of the scalar piston will be presented, starting from a 3-D rectangular cavity and extending to the piston. Comparison with existing results will be conducted. By means of Hertz potentials, we deal with the EM piston in Chapter IV. Once the EM field is converted to scalar fields, the systematic method for scalar fields developed in Chapter III is convenient to apply. The Casimir effect for a curved boundary such as a sphere will be investigated in Chapter V, where the idea of multiple reflection expansion (MRE) is applied to compute the corresponding Green's function. Chapter VI presents conclusions.

CHAPTER II

FOUNDATION OF CLOSED PATH APPROACH

Although the vacuum energy observable in the laboratory arises from quantum electrodynamics (QED), the simpler model of a scalar field is frequently studied and casts light on most of the questions of principle that arise for QED. In Chapter IV we will treat an electromagnetic field by decomposing it into two corresponding scalar fields by means of Hertz potentials.

This chapter presents a systematic study of the relationship between vacuum energy and Green's function for a massless scalar field since the scalar field model provides a simple relationship to classical paths which can improve our understanding intuitionally. Since our concern is vacuum energy or vacuum energy density, it's a good idea to explore the stress tensor, which has energy density as its first component, T_{00}. It turns out that vacuum energy density is closely related to the propagators.

A. Relation Between Vacuum Energy and Propagator of Klein-Gorden Equation

A massless scalar field satisfies the Klein-Gordon equation (K-G equation or wave equation):

$$\frac{\partial^2 \phi}{\partial t^2} - \nabla^2 \phi = 0 \tag{2.1}$$

For the whole space, the normal-mode solution satisfying the K-G equation, with its standard normalization, is:

$$\phi(\mathbf{r}, t) = \phi(\mathbf{r})\, e^{-\imath\omega t} = \frac{1}{\sqrt{2\omega}}\, e^{\imath\omega r} e^{-\imath\omega t} \tag{2.2}$$

The corresponding propagator (Green's function) $G(t-t', \mathbf{r}, \mathbf{r}')$ satisfies the inhomogeneous Klein-Gordon equation:

$$(\frac{\partial^2}{\partial t^2} - \nabla^2)G(t-t', \mathbf{r}, \mathbf{r}') = -\delta^{(D)}(\mathbf{r}-\mathbf{r}')\delta(t-t') \tag{2.3}$$

and it is understood as the vacuum expectation value (VEV) of the time-ordered product of two fields [21]:

$$G(t-t', \mathbf{r}, \mathbf{r}') = \imath\langle T\phi(\mathbf{r}, t)\phi(\mathbf{r}', t')\rangle \tag{2.4}$$

where T is the time ordering operator.

It's necessary to discuss the reduced Green's function $G(t-t', \mathbf{r}, \mathbf{r}')$ by taking the inverse Fourier transform of $G(t-t', \mathbf{r}, \mathbf{r}')$ with respect to time t:

$$G(\mathbf{r}, \mathbf{r}', \omega) = \int_{-\infty}^{\infty} dt\, \mathbf{e}^{-\imath\omega(t-t')}G(t-t', \mathbf{r}, \mathbf{r}') \tag{2.5}$$

it thus satisfies

$$(\omega^2 + \nabla^2)G(\mathbf{r}, \mathbf{r}', \omega) = -\delta^{(D)}(\mathbf{r}-\mathbf{r}') \tag{2.6}$$

Correspondingly, $G(t-t', \mathbf{r}, \mathbf{r}')$ can be achieved by taking Fourier transform of $G(t-t', \mathbf{r}, \mathbf{r}')$ with respect to ω:

$$G(t-t', \mathbf{r}, \mathbf{r}') = \int_{-\infty}^{\infty} \frac{d\omega}{2\pi}\, e^{\imath\omega(t-t')}G(\mathbf{r}, \mathbf{r}', \omega) \tag{2.7}$$

The reduced Green's function $G(\mathbf{r}, \mathbf{r}', \omega)$ is a good starting point. The eigenfunction expansion for the reduced Green's function is

$$G(\mathbf{r}, \mathbf{r}', \omega) = \sum_n \frac{\phi_n(\mathbf{r})\phi_n(\mathbf{r}')}{k_n^2 - \omega^2} \tag{2.8}$$

For the whole space, however, eigenfunctions $\phi_n(\mathbf{r})$ should be replaced by the usual set of plane waves normalized to a δ-function. This gives

$$G^f(\mathbf{r}, \mathbf{r}', \omega) = \int \frac{d^3p}{(2\pi)^3}\frac{e^{\imath\mathbf{p}\cdot(\mathbf{r}-\mathbf{r}')}}{p^2-\omega^2} = \frac{e^{\imath\omega|\mathbf{r}-\mathbf{r}'|}}{4\pi \mid \mathbf{r}-\mathbf{r}' \mid} \tag{2.9}$$

We call the reduced Green's function for the whole space *free propagator*; it will be useful later.

Now we derive the relation between the stress tensor and the Green's function. The stress tensor, for flat space and minimal coupling, is [2]

$$\begin{aligned} T_{00}(t-t',\mathbf{r},\mathbf{r}') &= \frac{1}{2}\left[\partial_0\phi\partial_{0'}\phi' + \partial_1\phi\partial_{1'}\phi' + \partial_2\phi\partial_{2'}\phi' + \partial_3\phi\partial_{3'}\phi'\right] \\ &= \frac{1}{2}[\partial_0\partial_{0'} + \partial_1\partial_{1'} + \partial_2\partial_{2'} + \partial_3\partial_{3'}]\frac{G(\mathbf{r},t;\mathbf{r}',t')}{\iota} \end{aligned} \tag{2.10}$$

Taking the inverse Fourier transform on both side, we find from (2.4),

$$T_{00}(t-t',\mathbf{r},\mathbf{r}') = \frac{1}{2}[\omega^2 + \partial_1\partial_{1'} + \partial_2\partial_{2'} + \partial_3\partial_{3'}]\frac{G(\mathbf{r},\mathbf{r}',\omega)}{\iota} \tag{2.11}$$

We now integrate over ω; the relation between vacuum energy density and the reduced Green's function comes out as

$$\begin{aligned} T_{00}(t-t',\mathbf{r},\mathbf{r}') &= \int_{-\infty}^{\infty}\frac{d\omega}{2\pi}\,T_{00}(\mathbf{r},\mathbf{r}',\omega)\,e^{-\iota\omega(t-t')} \\ &= \frac{1}{2}\int_{-\infty}^{\infty}\frac{d\omega}{2\pi}\,e^{-\iota\omega(t-t')}\,[\omega^2 + \partial_1\partial_{1'} + \partial_2\partial_{2'} + \partial_3\partial_{3'}]\frac{G(\mathbf{r},\mathbf{r}',\omega)}{\iota} \end{aligned} \tag{2.12}$$

From the analysis above, we see that once we know the reduced Green's function, the energy density can be evaluated by integration over ω. Now we apply Green's function's approach to the parallel plates with separation a. For parallel, the Green's function is [21]:

$$G^{\shortparallel}(t-t',\mathbf{r},\mathbf{r}') = \int\frac{d^2\mathbf{k}_\perp}{(2\pi)^2}\,e^{\iota\mathbf{k}_\perp\cdot(\mathbf{x}-\mathbf{x}')}\int\frac{d\omega}{2\pi}\,e^{-\iota\omega(t-t')}g(z,z',\lambda) \tag{2.13}$$

Here $\lambda^2 = \omega^2 - k_\perp^2$ and the reduced Green's function $g(z,z',\lambda)$ satisfies

$$(-\frac{\partial^2}{\partial z^2} - \lambda^2)g(z,z',\lambda) = \delta(z-z') \tag{2.14}$$

Take into account the Dirichlet boundary condition on plates, $g(0,z',\lambda) = g(a,z',\lambda) = 0$,

we got the reduced Green's function as

$$g(z, z', \lambda) = -\frac{1}{\lambda \sin \lambda a} \sin \lambda z \sin \lambda (z - a) \tag{2.15}$$

Substituting into (2.13) and (2.10), the vacuum energy density for parallel plates is:

$$\begin{aligned} T_{00}^{\shortparallel}(\mathbf{r}, \mathbf{r}) &= -\frac{1}{2\imath} \int_{-\infty}^{\infty} \frac{d\omega}{2\pi} \frac{d^2 k_\perp}{(2\pi)^2} \frac{1}{\lambda \sin \lambda a} [(\omega^2 + k_\perp^2) \sin \lambda z \sin \lambda (z - a) + \lambda^2 \cos \lambda z \cos \lambda (z - a)] \\ &= -\frac{1}{16\pi^3 \imath} \int_{-\infty}^{\infty} d\omega d^2 k_\perp \frac{1}{\lambda \sin \lambda a} [\omega^2 \cos \lambda a - k_\perp^2 \cos \lambda (2z - a)] \end{aligned} \tag{2.16}$$

Perform a complex frequency rotation: $\omega \to \imath\zeta, \lambda \to \imath\kappa$

$$T_{00}^{\shortparallel}(\mathbf{r}, \mathbf{r}) = -\frac{1}{16\pi^3} \int d\zeta \int dk_\perp^2 \frac{\zeta^2}{\kappa} \coth \kappa a + \frac{1}{16\pi^3} \int d\zeta \int dk_\perp^2 \frac{k_\perp^2 \cosh \kappa (2z - a)}{\kappa \sin \kappa a} = -\frac{\pi^2}{1440} \frac{1}{a^4} \tag{2.17}$$

This recovers the well known result for the 3-D parallel plates model. However, this is not the only way to construct the Green's function.

An alternate way to construct the Green's function possibly more instructively is to introduce the method of images. By the method of images, we can construct the Green's function for parallel plates starting from the free propagator in (2.9),

$$G^{\shortparallel}(\mathbf{r}, \mathbf{r}', \omega) = \sum_{n=-\infty}^{\infty} \left[\frac{e^{\imath\omega(2na + z - z')}}{4\pi(2na + z - z')} - \frac{e^{\imath\omega(2na + z + z')}}{4\pi(2na + z + z')} \right] \tag{2.18}$$

Knowing this Green's function is enough to evaluate the energy density for parallel plates. Before doing that, let's study the contribution to the stress tensor from the free propagator. Substituting (2.9) into (2.13), and performing a complex frequency rotation $\omega \to \imath\zeta$, we

can get the 00-component of the stress tensor contributed by the free propagator:

$$\begin{aligned} T^f_{00}(\mathbf{r},\mathbf{r}') &= \frac{1}{2}\int_{-\infty}^{\infty}\frac{d\omega}{2\pi}[\omega^2+\partial_1\partial_{1'}+\partial_2\partial_{2'}+\partial_3\partial_{3'}]\frac{G^f(\mathbf{r},\mathbf{r}',\omega)}{\imath} \\ &= \frac{1}{4\pi^2}\int_0^{\infty} d\omega\,\omega^2\frac{e^{\imath\omega|\mathbf{r}-\mathbf{r}'|}}{\imath\mid\mathbf{r}-\mathbf{r}'\mid} = -\frac{1}{4\pi^2}\int_0^{\infty} d\zeta\,\zeta^2\frac{e^{-\zeta|\mathbf{r}-\mathbf{r}'|}}{\mid\mathbf{r}-\mathbf{r}'\mid} \\ &= -\frac{1}{2\pi^2}\frac{1}{\mid\mathbf{r}-\mathbf{r}'\mid^4} \end{aligned} \tag{2.19}$$

To obtain the energy density we would like to set $\mathbf{r}=\mathbf{r}'$. However, (2.19) is determined by the distance between the two points and inversely proportional to the fourth power of that length. In (2.18) we see that the Green's function for plates can be constructed as a summation of free Green's functions with different path lengths. From the point of view of the method of images, the summation is over number of reflections. Different numbers of reflection indicate different lengths of path between the two points, d_n. When putting the two points identical, the contribution from the free propagator is divergent, hence it should be excluded. But all other terms in (2.18) contributes a finite result.

$$T^{\shortparallel}_{00}(\mathbf{r},\mathbf{r}) = \sum_{n=-\infty}^{\infty} -\frac{1}{2\pi^2}\frac{1}{d_n^4} = -\frac{1}{2\pi^2}\sum_{n=-\infty}^{\infty}[\frac{1}{(2na)^4}-\frac{1}{(2na+2z)^4}] \tag{2.20}$$

The total vacuum energy is the integral of energy density over space. The integral of the second sum in (2.20) yields a surface divergent term which is independent of the plate separation a and hence does not affect the Casimir energy. We will discuss this issue in later chapters, see [22, 23] for more extensive discussion. The integral of the first sum in (2.20), which is position-independent, yields the total energy of the parallel plates:

$$\varepsilon = -\frac{a}{2\pi^2}\sum_{n=-\infty}^{\infty}\frac{1}{(2na)^4} = -\frac{\pi^2}{1440}\frac{1}{a^3} \tag{2.21}$$

B. Relation Between Vacuum Energy and Propagator of Laplace Equation

1. Definition of Cylinder Kernel and Its Relation to Vacuum Energy Density

The Laplace equation relates to the K-G equation by converting the time parameter t in K-G to an imaginary time parameter $t \to \imath t$:

$$\frac{\partial^2 \phi}{\partial t^2} + \nabla^2 \phi = 0 \tag{2.22}$$

The Green's function of Laplace equation is named as Poisson kernel or cylinder kernel, we will use the second name "cylinder kernel" throughout this dissertation. We should understand that cylinder kernel is just a name for one special kind of Green's function (for Laplace equation) and has nothing to do with circular symmetry. The cylinder kernel in unconstrained space is defined as:

$$\begin{aligned} \overline{T}(t, \mathbf{r}, \mathbf{r}') = -\int d\omega\, \phi(\mathbf{r})\phi^*(\mathbf{r}')e^{-t\omega} &= -\int d\omega\, \frac{1}{\omega} e^{\imath\omega(r-r')} e^{-\omega t} \\ &= -\frac{1}{2\pi^2} \frac{1}{t^2 + \mid \mathbf{r} - \mathbf{r}' \mid^2} \end{aligned} \tag{2.23}$$

Correspondingly, the cylinder kernel in constrained space has discrete spectrum other than continuous spectrum.

$$\overline{T}(t, \mathbf{r}, \mathbf{r}') = -\sum_n \phi_n(\mathbf{r})\phi_n^*(\mathbf{r}')e^{-t\omega_n} \tag{2.24}$$

On the other hand, the stress tensor of a scalar field in flat surface is,

$$T_{\mu\nu} = (1 - 2\xi)\partial_\mu\phi\partial_\nu\phi + (2\xi - \frac{1}{2})\eta_{\mu\nu}\partial_\lambda\phi\partial^\lambda\phi - 2\xi\phi\partial_\mu\partial_\nu\phi \tag{2.25}$$

where R is the curvature scalar, and ξ labels different possible gravitational couplings. Note that ξ does not affect the total energy. Throughout this dissertation we choose ξ=$\frac{1}{4}$ because doing so simplifies the relation between the stress tensor and the total energy. When ξ is

set to $\frac{1}{4}$, the energy density (00-component of the stress tensor) is simplified as [22]:

$$T_{00} = \frac{1}{2}\sum_n \omega_n |\phi(r)|^2 \tag{2.26}$$

Based on the definition of cylinder kernel in (2.23) and (2.24) and the definition of vacuum energy density in (2.26), we can see the relation between cylinder kernel and vacuum energy density directly. By taking second derivative of cylinder kernel with respect to t we get the vacuum energy density:

$$\varepsilon(t, \mathbf{r}, \mathbf{r}) = T_{00}(t, \mathbf{r}, \mathbf{r}) = -\frac{1}{2}\lim_{t\to 0}\frac{\partial^2}{\partial t^2}\overline{T}(t, \mathbf{r}, \mathbf{r}) = \frac{1}{2}\int \omega e^{t\omega(r-r')}e^{-t\omega}d\omega \tag{2.27}$$

The exponential term $e^{-t\omega}$ can be understood as a cutoff function. The structure of cutoff dependence is simple and clear since we have an asymptotic expansion in t. For instance, the leading divergent term depending on cutoff is proportional to the volume V of the rectangular cavity and t^{-4}, as we will discuss in detail later. The inverse of t here is the counterpart of Λ (upper limit of frequency) in [12]. However, not all divergences are removed even after the cutoff. Be aware that there are also other divergences such as a surface divergence proportional to $1/d^3$ appearing in the expression of energy density; here d is the distance from $\mathbf{r}$ to $\mathbf{r}'$. we will talk about that when studying the rectangular cavity in the next section.

2. An Alternate Derivation of the Relation Between Cylinder Kernel and Vacuum Energy

It is worthwhile to investigate the relation between energy density and free propagator as in (2.11) in more detail.

$$\begin{aligned} T_{00}(\mathbf{r},\mathbf{r}',\omega) &= \frac{1}{2}[\omega^2+\partial_1\partial_{1'}+\partial_2\partial_{2'}+\partial_3\partial_{3'}]\frac{G^f(\mathbf{r},\mathbf{r}',\omega)}{\iota} \\ &= \frac{\omega^2}{\iota}G^f(\mathbf{r},\mathbf{r}',\omega) = \frac{\omega^2}{4\pi\iota}\frac{e^{\iota\omega|\mathbf{r}-\mathbf{r}'|}}{\mid\mathbf{r}-\mathbf{r}'\mid} = \frac{\omega^2}{4\pi}\frac{\sin\omega\mid\mathbf{r}-\mathbf{r}'\mid-\iota\cos\omega\mid\mathbf{r}-\mathbf{r}'\mid}{\mid\mathbf{r}-\mathbf{r}'\mid} \end{aligned} \tag{2.28}$$

If we take Laplace transform on both sides of (2.28) with respect to ω, we get,

$$T_{00}(\mathbf{r},t;\mathbf{r}',t') = \frac{1}{4\pi}L[\omega^2\frac{\sin\omega\mid\mathbf{r}-\mathbf{r}'\mid}{\mid\mathbf{r}-\mathbf{r}'\mid},\omega\to t]-\iota\frac{1}{4\pi}L[\omega^2\frac{\cos\omega\mid\mathbf{r}-\mathbf{r}'\mid}{\mid\mathbf{r}-\mathbf{r}'\mid},\omega\to t] \tag{2.29}$$

where $L[f(\omega),\omega\to t]$ represents Laplace transform operation of $f(\omega)$ with respect to ω. We take the real part since the energy density is a real number. To go forward, refer to the formula [24]

$$L[\omega^2 f(\omega),\omega\to t] = \frac{\partial^2}{\partial t^2}L[f(\omega),\omega\to t] \tag{2.30}$$

so ω^2 inside the L operation is equivalent to two t derivative outside L, so

$$\begin{aligned} T_{00}(\mathbf{r},t;\mathbf{r}',t') = \frac{1}{4\pi}\frac{\partial^2}{\partial t^2}L[\frac{\sin\omega\mid\mathbf{r}-\mathbf{r}'\mid}{\mid\mathbf{r}-\mathbf{r}'\mid}] &= \frac{1}{4\pi^2}\frac{\partial^2}{\partial t^2}\frac{1}{(t-t')^2+\mid\mathbf{r}-\mathbf{r}'\mid^2} \\ &= -\frac{1}{2}\frac{\partial^2}{\partial t^2}[-\frac{1}{2\pi^2}\frac{1}{(t-t')^2+\mid\mathbf{r}-\mathbf{r}'\mid^2}] \end{aligned} \tag{2.31}$$

The cylinder kernel $\overline{T}$ is defined as :

$$\overline{T}(\mathbf{r},t;\mathbf{r}',t') = -\frac{1}{2\pi^2}\frac{1}{(t-t')^2+\mid\mathbf{r}-\mathbf{r}'\mid^2} \tag{2.32}$$

Since we get this expression from the free propagator, it is the cylinder kernel for the whole space; we call it *free cylinder kernel*. The relation between energy density and cylinder

kernel is [22]:

$$T_{00}(\mathbf{r},t;\mathbf{r}',t') = -\frac{1}{2}\frac{\partial^2}{\partial t^2}\overline{T}(\mathbf{r},t;\mathbf{r}',t') = -\frac{1}{2\pi^2}\frac{1}{|\ \mathbf{r}-\mathbf{r}'\ |^4} \tag{2.33}$$

Thus we have reproduced the result from Green's function analysis in (2.19) by cylinder kernel analysis.

Let's recall the differential equation which the reduced Green's function satisfies:

$$(\omega^2+\nabla^2)G(\mathbf{r},\mathbf{r}',\omega) = -\delta^{(D)}(\mathbf{r}-\mathbf{r}') \tag{2.34}$$

As mentioned in (2.7), reduced Green's function and Green's function are related by Fourier transform (with respect to ω). Starting from the reduced Green's function, we can get more information besides the corresponding Green's function. As we see above, taking the Laplace transform (with respect to ω) of the reduced Green's function leads to the cylinder kernel (Poisson kernel),

$$\overline{T}(\mathbf{r},t;\mathbf{r}',t') = \int_0^\infty d\omega\, \mathbf{e}^{-\omega(t-t')}G(\mathbf{r},\mathbf{r}',\omega) \tag{2.35}$$

which is the 4-D Green's function of the inhomogeneous Laplace equation

$$(\frac{\partial^2}{\partial t^2}+\nabla^2)\overline{T}(\mathbf{r},t;\mathbf{r}',t') = -\delta^{(D)}(\mathbf{r}-\mathbf{r}')\delta(t-t') \tag{2.36}$$

The term $e^{-\omega(t-t')}$ is understood as a cut off function, and the parameter t is a manifestation of cut off frequency; that is, $\frac{1}{t}\sim\Lambda$ with Λ the cut-off frequency [12, 25].

3. Application to 3-D Parallel Plates

For the parallel plates, we can build the cylinder kernel from the free cylinder kernel by the method of images. It is helpful if we define an operator D_a as

$$D_a\overline{T}(t,x,\mathbf{r}_\perp,x',\mathbf{r}'_\perp) = -\overline{T}(t,2a-x,\mathbf{r}_\perp,x',\mathbf{r}'_\perp) \tag{2.37}$$

the cylinder kernel satisfying both Dirichlet boundary conditions at $x = 0$ and $x = a$ is

$$\overline{T}_{DD}(t, x, \mathbf{r}_\perp, x', \mathbf{r}'_\perp) = \overline{T}^f + D_0\overline{T} + D_a\overline{T} + D_0D_a\overline{T} + D_aD_0\overline{T} + ... \tag{2.38}$$

the cylinder kernel is organized by number of reflections:

$$\overline{T}_{DD}(t, x, \mathbf{r}_\perp, x', \mathbf{r}'_\perp) = -\frac{1}{2\pi^2}\sum_{-\infty}^{\infty}\frac{1}{t^2 + (2la)^2} + \frac{1}{2\pi^2}\sum_{-\infty}^{\infty}\frac{1}{t^2 + (2la + 2x)^2} \tag{2.39}$$

The corresponding energy density is:

$$\varepsilon_{DD}(\mathbf{r}, t; \mathbf{r}, t') = -\frac{1}{2}\frac{\partial^2}{\partial t^2}\overline{T}_{DD}(\mathbf{r}, t; \mathbf{r}, t') = -\frac{1}{2\pi^2}\sum_{-\infty}^{\infty}[\frac{1}{(2la)^4} - \frac{1}{(2la + 2x)^4}] \tag{2.40}$$

The vacuum energy density derived from cylinder kernel using methods of images in (2.40) recovers the expression in (2.20) which is derived from the Green's function of K-G equation. Integrate the vacuum energy density in (2.40) over space to get the total energy, it will definitely recover the result in (2.21):

$$E_{DD} = \int \varepsilon_{DD}(\mathbf{r}, t; \mathbf{r}, t')\, d^3\mathbf{r} = -\frac{a}{2\pi^2}\sum_{n=-\infty}^{\infty}\frac{1}{(2na)^4} = -\frac{\pi^2}{1440}\frac{1}{a^3} \tag{2.41}$$

4. Heat Kernel Analysis

If instead we take Laplace transform of the reduced Green's function with respect to $E = \omega^2$, we will get the heat kernel [9],

$$K(\mathbf{r}, t; \mathbf{r}', t') = \int_0^\infty dE\, e^{-E(t-t')}G(\mathbf{r}, \mathbf{r}', \omega) = t^{-\frac{3}{2}}e^{-\frac{|\mathbf{r}-\mathbf{r}'|^2}{4t}} \tag{2.42}$$

which is the Green's function of the inhomogeneous heat equation

$$(\frac{\partial}{\partial t} - \nabla^2)K(\mathbf{r}, t; \mathbf{r}', t') = -\delta^{(D)}(\mathbf{r} - \mathbf{r}')\delta(t - t') \tag{2.43}$$

C. Optical Approximation Analysis

Let's land our discussion on the free propagator one more time.

$$T^f_{00}(\mathbf{r},\mathbf{r}',\omega) = \frac{1}{2}[\omega^2 + \partial_1\partial_{1'} + \partial_2\partial_{2'} + \partial_3\partial_{3'}]\frac{G^f(\mathbf{r},\mathbf{r}',\omega)}{\imath} = \frac{\omega^2}{\imath}G^f(\mathbf{r},\mathbf{r}',\omega) \tag{2.44}$$

The energy density is thus

$$\begin{aligned} T^f_{00}(\mathbf{r},\mathbf{r}') &= \int_{-\infty}^{\infty}\frac{d\omega}{2\pi}T^f_{00}(\mathbf{r},\mathbf{r}',\omega) = \int_0^{\infty} d\omega\frac{\omega^2}{\pi\imath}G^f(\mathbf{r},\mathbf{r}',\omega) \\ &= \int_0^{\infty}\frac{1}{2}\omega d\omega[\frac{2\omega G(\mathbf{r},\mathbf{r}',\omega)}{\pi\imath}] = \int_0^{\infty}\frac{1}{2}\omega d\omega[\frac{2\omega}{\pi}\mathtt{Im}G(\mathbf{r},\mathbf{r}',\omega)] \end{aligned} \tag{2.45}$$

where

$$\frac{2\omega}{\pi}\mathtt{Im}G(\mathbf{r},\mathbf{r}',\omega) = \rho(\mathbf{r},\mathbf{r}',\omega) \tag{2.46}$$

is the density of states.

For the parallel plates, we can build the corresponding Green's function by method of images as we did in (2.18). As we already argued, the Green's function is a summation over number of reflections, n. The nth Green's function is related to a length of path, d_n:

$$G^{flat}(\mathbf{r},\mathbf{r}',\omega) = \sum_n(-1)^n G^n(\mathbf{r},\mathbf{r}',\omega) = \sum_n(-1)^n\frac{e^{\imath\omega d_n}}{4\pi d_n} \tag{2.47}$$

$(-1)^n$ marks the difference between odd and even numbers of reflections. The energy density is therefore:

$$\begin{aligned} T^{flat}_{00}(\mathbf{r},\mathbf{r}') &= \int_0^{\infty}\frac{d\omega}{\pi\imath}\,\omega^2 G^{flat}(\mathbf{r},\mathbf{r}',\omega) = \sum_n(-1)^n\int_0^{\infty}\frac{d\omega}{\pi\imath}\,\frac{e^{\imath\omega d_n}}{4\pi d_n} \\ &= -\frac{1}{2\pi^2}\sum_n(-1)^n\frac{1}{d_n^4} \end{aligned} \tag{2.48}$$

The optical approximation developed by Scardicchio and Jaffe [12] provides a formula

for Casimir energy density for general surfaces [12],

$$T_{00}(\mathbf{r},\mathbf{r}') = -\frac{1}{2\pi^2}\sum_r (-1)^r \frac{\sqrt{\triangle_r(x)}}{d_r^3(x)} \tag{2.49}$$

where the parameter $\triangle_r$ is called 'enlargement factor' in [12], which is the modification of the inverse-square law of radiation intensity caused by the curvature of a boundary. Determining the enlargement factor is the key part of the optical approximation and that is not easy. We will investigate the enlargement factor for a spherical surface in Chapter V. However, for a flat surface, the enlargement factor is simple, $\triangle_r = 1/d_r^2$. Therefore, for flat surface case, the optical approximation reduces to (2.48) which is derived from method of images. From the point of view of the cylinder kernel, for a flat surface, if we construct the cylinder kernel by method of images and express the cylinder kernel as a summation over number of reflections, we can reproduce the optical approximation's result for flat surface and it turns out that the energy density varies inversely as the fourth power of the lengths of the closed paths as the optical approximation.

CHAPTER III

3-D PISTON WITH MIXED BOUNDARY CONDITIONS FOR SCALAR FIELD

Since R. M. Cavalcanti introduced a 2-dimensional piston model obeying Dirichlet boundary condition (B.C.) for massless scalar field [18], the piston geometry has attracted more and more interest and been generalized to higher dimension, different B.C. (Neumann B.C. or mixed B.C.) and even different kind of field (Electromagnetic field) [26, 27, 28, 29, 30, 31, 32, 33, 34, 22]. A 3-dimensional piston has a movable partition inside a rectangular cylinder as shown in Fig.1. A great advantage of piston geometry is the cancelation of surface divergent terms of region A and region B [18] in the force calculation. When it comes to the B.C., the movable partition and the 6 faces of the rectangular cylinder may obey different B.C.. Edery studied the scalar piston with purely Dirichlet B.C. and purely Neumann B.C. on all faces and the partition [29, 30]. Zhai&Li studied the scalar piston with hybrid B.C. (Neumann B.C. on partition and Dirichlet B.C. elsewhere) [31]. Lim&Teo studied both scalar piston with purely Dirichlet/Neumann B.C. and electromagnetic piston with perfect electric conductor/perfect magnetic conductor [32, 33, 34]. Jaffe's group studied the electromagnetic piston with perfect conductor conditions using their optical approxi-

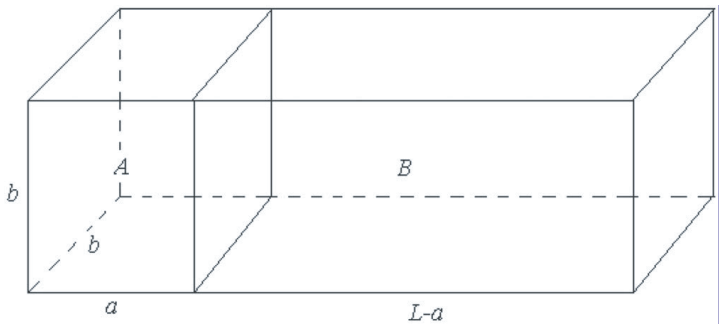

Fig. 1. 3-dimensional piston model. The freely moving partition divides the rectangular cylinder into 2 regions: A and B.

mation method [26, 28]. Electromagnetic pistons with cross sections other than rectangular are considered by Marachevsky [35, 36].

In this chapter, we will investigate the 3-Dimensional piston obeying general B.C. for scalar field. For a rectangular cavity, the B.C. on each pair of opposite faces could be both Dirichlet B.C., both Neumann B.C. or mixed B.C., where mixed B.C. means Dirichlet B.C. on one face and Neumann B.C. on another for a pair of opposite faces. Therefore there are $3 \times 3 \times 3 = 27$ possible B.C. for a rectangular cavity. For the purpose of studying piston geometry, we fix the movable piston plate (partition) at $x = a$, and after considering the symmetry of interchanging y with z, only 18 B.C. are essentially different. They can be classified into 4 kinds, listed in Table I:

Table I. Table of 4 kinds of B.C.

B.C. kind	Description/Examples
B.C. of 1st kind:	no mixed B.C. included
Examples:	NN-NN-NN, NN-NN-DD, NN-DD-DD,
	DD-NN-NN, DD-DD-NN, DD-DD-DD
B.C. of 2nd kind:	one mixed B.C. included
Examples:	DN-NN-NN, DN-NN-DD, DN-DD-DD,
	NN-DN-NN, NN-DN-DD, DD-DN-NN, DD-DN-DD
B.C. of 3rd kind:	two mixed B.C. included
Examples:	DN-DN-NN, DN-DN-DD, NN-DN-DN, DD-DN-DN
B.C. of 4th kind:	three mixed B.C. included
Examples:	DN-DN-DN

We will provide a general method for the scalar piston with B.C. of each kind. Starting from the cylinder kernels, we can find out the Casimir energy for an individual rectangular cavity. To obtain Casimir energy of a piston, we need to sum up Casimir energy of two rectangular cavities. It is straightforward to go from piston energy to piston force. Next we will analyze the piston force in detail for the 4 kinds of B.C. one by one.

A. Scalar Piston with B.C. of 1st Kind

1. Cylinder Kernel for a Rectangular Cavity

a. Cylinder Kernel for Dirichlet Rectangular Cavity Constructed By the Method of Images

To construct the cylinder kernel is always our starting point. Knowing the cylinder kernel we can derive vacuum energy and then Casimir force. To find the corresponding cylinder kernel for 3-D rectangular cavity which satisfies Dirichlet B.C. on each face of the cavity, say $\overline{T}^{DD-DD-DD}$, we start with the free cylinder kernel $\overline{T}^{f}$ and then construct $\overline{T}^{DD-DD-DD}$ by the method of images.

Let's start from a simpler problem: how to construct the cylinder kernel which satisfies Dirichlet B.C. on just one face of the cavity, say $x = a$. By the method of images, it is

$$\begin{aligned}\overline{T}^{D}_{x=a}(t,\mathbf{r},\mathbf{r}') &= \overline{T}^{f}(t,x,\mathbf{r}_\perp,x',\mathbf{r}'_\perp) - \overline{T}^{f}(t,2a-x,\mathbf{r}_\perp,x',\mathbf{r}'_\perp)\\ &= -\frac{1}{2\pi^2}\frac{1}{t^2+(x-x')^2+(y-y')^2+(z-z')^2} + \frac{1}{2\pi^2}\frac{1}{t^2+(2a-x-x')^2+(y-y')^2+(z-z')^2}\end{aligned} \tag{3.1}$$

It will be helpful if we define a Dirichlet reflection operator D^a_x as [37, 23]

$$D^a_x f(x) = -f(2a-x) \tag{3.2}$$

The cylinder kernel can then be simplified as

$$\overline{T}^{D}_{x=a}(t,\mathbf{r},\mathbf{r}') = \overline{T}^{f}(t,x,\mathbf{r}_\perp,x',\mathbf{r}'_\perp) + D^a_x\overline{T}^{f}(t,2a-x,\mathbf{r}_\perp,x',\mathbf{r}'_\perp) \tag{3.3}$$

The next problem would naturally be: how to construct the cylinder kernel which satisfies Dirichlet B.C. on both the face $x = 0$ and the face $x = a$, say the slab $(0, a) \times R^2$. It turns out to be [23]

$$\begin{aligned}&\overline{T}^{DD}_{x}(t,x,\mathbf{r}_\perp,x',\mathbf{r}'_\perp) = \\ &\quad\sum_{n=0}^{\infty}(D^a_xD^0_x)^n\overline{T}^{f} + \sum_{n=1}^{\infty}(D^0_xD^a_x)^n\overline{T}^{f} + \sum_{n=0}^{\infty}(D^a_xD^0_x)^nD^a_x\overline{T}^{f} + \sum_{n=0}^{\infty}(D^0_xD^a_x)^nD^0_x\overline{T}^{f}\end{aligned} \tag{3.4}$$

The first two terms represent even numbers of reflections and the last two terms represent odd numbers of reflections. So (3.4) can be reorganized by number of reflections:

$$\overline{T}^{DD}_{x}(t,x,\mathbf{r}_\perp,x',\mathbf{r}'_\perp) = \overline{T}^{f} + D^0_x\overline{T}^{f} + D^a_x\overline{T}^{f} + D^0_xD^a_x\overline{T}^{f} + D^a_xD^0_x\overline{T}^{f} + ... \tag{3.5}$$

all odd number reflections on either $x = 0$ or $x = a$ are summed up as $D^{odd}_x\overline{T}^{f}$, all even number reflections are summed up as $D^{even}_x\overline{T}^{f}$.

$$\begin{aligned}\overline{T}^{DD}_{x}(t,\mathbf{r},\mathbf{r}') =& D^{even}_x\overline{T}^{f} + D^{odd}_x\overline{T}^{f} \\ =& -\frac{1}{2\pi^2}\sum_{n=-\infty}^{\infty}\frac{1}{t^2+(2na+x-x')^2+(y-y')^2+(z-z')^2} \\ &+\frac{1}{2\pi^2}\sum_{n=-\infty}^{\infty}\frac{1}{t^2+(2na-x-x')^2+(y-y')^2+(z-z')^2}\end{aligned} \tag{3.6}$$

Now we get the cylinder kernel $\overline{T}^{DD}_{x}$ which satisfies Dirichlet B.C. on both the face $x = 0$ and the face $x = a$.

Go further to the next problem: how to construct the cylinder kernel which satisfies Dirichlet B.C. on both the face $y = 0$ and the face $y = b$ and at the same time it satisfies Dirichlet B.C. on both the face $x = 0$ and the face $x = a$ as well. If we build the cylinder kernel from $\overline{T}^{DD}_{x}$, the B.C. along x direction is naturally satisfied. For the tube $(0, a) \times$

$(0, b) \times R^1$, we got a similar expression to 3.4

$$\overline{T}_{xy}^{DD-DD}(t, x, \mathbf{r}_\perp, x', \mathbf{r}'_\perp) = \sum_{n=0}^{\infty}(D_y^b D_y^0)^n \overline{T}_x^{DD} + \sum_{n=1}^{\infty}(D_y^0 D_y^b)^n \overline{T}_x^{DD} + \sum_{n=0}^{\infty}(D_y^b D_y^0)^n D_y^0 \overline{T}_x^{DD} + \sum_{n=0}^{\infty}(D_y^0 D_y^b)^n D_y^0 \overline{T}_x^{DD} \tag{3.7}$$

Rewrite by number of reflections:

$$\begin{aligned}\overline{T}_{xy}^{DD-DD}(t, \mathbf{r}, \mathbf{r}') =& D_{xy}^{[even][even]}\overline{T}^f + D_{xy}^{[even][odd]}\overline{T}^f + D_{xy}^{[odd][even]}\overline{T}^f + D_{xy}^{[odd][odd]}\overline{T}^f \\ =& -\frac{1}{2\pi^2}\sum_{l,m=-\infty}^{\infty}\frac{1}{t^2 + (2na + x - x')^2 + (2mb + y - y')^2)^2} \\ &+ \frac{1}{2\pi^2}\sum_{n=-\infty}^{\infty}\frac{1}{t^2 + (2na - x - x')^2 + (2mb + y + y')^2} \\ &+ \frac{1}{2\pi^2}\sum_{l,m,n=-\infty}^{\infty}\frac{1}{t^2 + (2na + x + x')^2 + (2mb - y - y')^2} \\ &- \frac{1}{2\pi^2}\sum_{l,m,n=-\infty}^{\infty}\frac{1}{t^2 + (2na + x + x')^2 + (2mb + y + y')^2}\end{aligned} \tag{3.8}$$

Finally we are on the problem for 3-D rectangular cavity: how to construct the cylinder kernel $\overline{T}_{xyz}^{DD-DD-DD}$ which satisfies Dirichlet B.C. on each face of the cavity. Based on $\overline{T}_{xy}^{DD-DD}$,

$$\begin{aligned}\overline{T}_{xyz}^{DD-DD-DD}(t, x, \mathbf{r}_\perp, x', \mathbf{r}'_\perp) =& \sum_{n=0}^{\infty}(D_z^c D_z^0)^n \overline{T}_{xy}^{DD-DD} + \sum_{n=1}^{\infty}(D_z^0 D_z^c)^n \overline{T}_{xy}^{DD-DD} \\ &+ \sum_{n=0}^{\infty}(D_z^c D_z^0)^n D_{z:c}\overline{T}_{xy}^{DD-DD} + \sum_{n=0}^{\infty}(D_z^0 D_z^c)^n D_z^0 \overline{T}_{xy}^{DD-DD}\end{aligned} \tag{3.9}$$

We can rewrite (3.9) as a summation over number of reflections:

$$
\begin{aligned}
\overline{T}_{xyz}^{DD-DD-DD} =& D_{xyz}^{[even][even][even]}\overline{T}^f + D_{xyz}^{[even][even][odd]}\overline{T}^f + D_{xyz}^{[even][odd][even]}\overline{T}^f + D_{xyz}^{[odd][even][even]}\overline{T}^f \\
&+ D_{xyz}^{[even][odd][odd]}\overline{T}^f + D_{xyz}^{[odd][even][odd]}\overline{T}^f + D_{xyz}^{[odd][odd][even]}\overline{T}^f + D_{xyz}^{[odd][odd][odd]}\overline{T}^f \\
=& -\frac{1}{2\pi^2}\sum_{l,m,n=-\infty}^{\infty}\frac{1}{t^2+(2na+x-x')^2+(2mb+y-y')^2+(2lc+z-z')^2}) \\
&+\frac{1}{2\pi^2}\sum_{n=-\infty}^{\infty}\frac{1}{t^2+(2na-x-x')^2+(2mb+y-y')^2+(2lc+z-z')^2}) \\
&+\frac{1}{2\pi^2}\sum_{l,m,n=-\infty}^{\infty}\frac{1}{t^2+(2na+x-x')^2+(2mb-y-y')^2+(2lc+z-z')^2}) \\
&+\frac{1}{2\pi^2}\sum_{l,m,n=-\infty}^{\infty}\frac{1}{t^2+(2na+x-x')^2+(2mb+y-y')^2+(2lc-z-z')^2}) \\
&-\frac{1}{2\pi^2}\sum_{l,m,n=-\infty}^{\infty}\frac{1}{t^2+(2na-x-x')^2+(2mb-y-y')^2+(2lc+z-z')^2}) \\
&-\frac{1}{2\pi^2}\sum_{l,m,n=-\infty}^{\infty}\frac{1}{t^2+(2na-x-x')^2+(2mb+y-y')^2+(2lc-z-z')^2}) \\
&-\frac{1}{2\pi^2}\sum_{l,m,n=-\infty}^{\infty}\frac{1}{t^2+(2na+x-x')^2+(2mb-y-y')^2+(2lc-z-z')^2}) \\
&+\frac{1}{2\pi^2}\sum_{l,m,n=-\infty}^{\infty}\frac{1}{t^2+(2na-x-x')^2+(2mb-y-y')^2+(2lc-z-z')^2})
\end{aligned}
\tag{3.10}
$$

For abbreviation, define

$$
V_1^{\varepsilon_1\varepsilon_2\varepsilon_3} = -\frac{1}{2\pi^2}\sum_{l,m,n=-\infty}^{\infty}\frac{1}{t^2+(2la+x+\varepsilon_1 x')^2+(2mb+y+\varepsilon_2 y')^2+(2nc+z+\varepsilon_3 z')^2} \tag{3.11}
$$

Values for ε_i ($i = 1, 2, 3$) are either '$-$' or '$+$', where '$-$' means even number of reflections and '$+$' means odd number of reflections. The cylinder kernel which satisfies Dirichlet

B.C. on each face of the cavity is therefore

$$\overline{T}^{DD-DD-DD} = V_1^{---} - V_1^{+--} - V_1^{-+-} - V_1^{--+} + V_1^{++-} + V_1^{-++} + V_1^{+-+} - V_1^{+++} \tag{3.12}$$

b. An Alternate Way to Construct the Cylinder Kernel $\overline{T}^{DD-DD-DD}$

We can write down the explicit expression of the normalized normal modes of the scalar field $\phi(\mathbf{r})$ for 3-D cavity with Dirichlet B.C. on each face as

$$\phi_{lmn}(x,y,z) = \frac{2\sqrt{2}}{\sqrt{abc}} \sin\frac{l\pi}{a}x \sin\frac{m\pi}{b}y \sin\frac{n\pi}{c}z \tag{3.13}$$

By the definition of the cylinder kernel in (2.24), we have:

$$\begin{aligned}\overline{T}^{DD-DD-DD}(t,\mathbf{r},\mathbf{r}') &= -\sum_{l,m,n=1}^{\infty} \frac{8}{\omega_{lmn}abc}\phi_{lmn}(\mathbf{r})\phi^*_{lmn}(\mathbf{r}')e^{-t\omega_{lmn}} \\ &= -\sum_{l,m,n=1}^{\infty} \frac{8}{\omega_{lmn}abc} \sin\frac{l\pi}{a}x \sin\frac{m\pi}{b}y \sin\frac{n\pi}{c}z \sin\frac{l\pi}{a}x' \sin\frac{m\pi}{b}y' \sin\frac{n\pi}{c}z' e^{-t\omega_{lmn}}\end{aligned} \tag{3.14}$$

where $\omega_{lmn}^2 = \pi^2[(\frac{l}{a})^2 + (\frac{m}{b})^2 + (\frac{n}{c})^2]$. We can then rewrite (3.14) as

$$\begin{aligned}&\overline{T}^{DD-DD-DD}(t,\mathbf{r},\mathbf{r}') \\ &= -\sum_{l,m,n=-\infty}^{\infty} \frac{1}{\omega_{lmn}abc} \sin\frac{l\pi}{a}x \sin\frac{m\pi}{b}y \sin\frac{n\pi}{c}z \sin\frac{l\pi}{a}x' \sin\frac{m\pi}{b}y' \sin\frac{n\pi}{c}z' e^{-t\omega_{lmn}} \\ &= -\sum_{l,m,n=-\infty}^{\infty} \frac{1}{8\omega_{lmn}abc}[e^{\imath k_1(x-x')} - e^{\imath k_1(x+x')}][e^{\imath k_2(y-y')} - e^{\imath k_2(y+y')}][e^{\imath k_3(z-z')} - e^{\imath k_3(z+z')}]e^{-t\omega_{lmn}} \\ &= -\sum_{l,m,n=-\infty}^{\infty} \frac{1}{8\omega_{lmn}abc}[e^{\imath k_1(x-x')}e^{\imath k_2(y-y')}e^{\imath k_3(z-z')} \\ &\qquad - e^{\imath k_1(x+x')}e^{\imath k_2(y-y')}e^{\imath k_3(z-z')} - e^{\imath k_1(x-x')}e^{\imath k_2(y+y')}e^{\imath k_3(z-z')} - e^{\imath k_1(x-x')}e^{\imath k_2(y-y')}e^{\imath k_3(z+z')} \\ &\qquad + e^{\imath k_1(x+x')}e^{\imath k_2(y+y')}e^{\imath k_3(z-z')} + e^{\imath k_1(x+x')}e^{\imath k_2(y-y')}e^{\imath k_3(z+z')} + e^{\imath k_1(x+x')}e^{\imath k_2(y-y')}e^{\imath k_3(z+z')} \\ &\qquad - e^{\imath k_1(x+x')}e^{\imath k_2(y+y')}e^{\imath k_3(z+z')}]e^{-t\omega_{lmn}}\end{aligned} \tag{3.15}$$

Bear in mind the free cylinder kernel is defined as

$$\overline{T}(t,\mathbf{r},\mathbf{r}') = -\int \frac{1}{\omega} e^{\imath\omega(r-r')} e^{-\omega t} d\omega = -\frac{1}{2\pi^2}\frac{1}{t^2+|\mathbf{r}-\mathbf{r}'|^2} \tag{3.16}$$

Apply the Poisson summation formula, getting

$$\begin{aligned} &-\sum_{l,m,n=-\infty}^{\infty} \frac{e^{-t\omega_{lmn}}}{8\omega_{lmn}abc} e^{\imath k_1(x-x')} e^{\imath k_2(y-y')} e^{\imath k_3(z-z')} \\ &= -\frac{1}{(2a)(2b)(2c)} \sum_{l,m,n=-\infty}^{\infty} \frac{e^{-t\omega_{lmn}}}{\omega_{lmn}} e^{2\pi\imath(\frac{l\pi}{2a},\frac{m\pi}{2b},\frac{n\pi}{2c})(x-x',y-y',z-z')} \\ &= -\frac{1}{2\pi^2} \sum_{i,j,k=-\infty}^{\infty} \frac{1}{t^2+(x-x'+2ia)^2+(y-y'+2jb)^2+(z-z'+2kc)^2} = V_1^{---} \end{aligned} \tag{3.17}$$

so the cylinder kernel becomes to

$$\overline{T}^{DD-DD-DD}(t,\mathbf{r},\mathbf{r}') = V_1^{---} - V_1^{+--} - V_1^{-+-} - V_1^{--+} + V_1^{++-} + V_1^{-++} + V_1^{+-+} - V_1^{+++} \tag{3.18}$$

Now we have reproduced previous result (3.15) in an alternate way.

c. General Expression of Cylinder Kernel For Rectangular Cavity with B.C. of 1st Kind

Firstly let's see another special case: purely Neumann B.C. (NN-NN-NN). Define a Neumann Reflection Operator N_x^a as

$$N_x^a f(x) = f(2a-x) \tag{3.19}$$

which is different from D_x by a '$-$' sign. In the derivation of cylinder kernel, replace all D_x with N_x; it will be straightforward to obtain the cylinder kernel for purely Neumann rectangular cavity $\overline{T}^{NN-NN-NN}$

$$\overline{T}^{NNN}(t,\mathbf{r},\mathbf{r}') == V_1^{---} + V_1^{+--} + V_1^{-+-} + V_1^{--+} + V_1^{++-} + V_1^{-++} + V_1^{+-+} + V_1^{+++} \tag{3.20}$$

where $V_1^{\varepsilon_1\varepsilon_2\varepsilon_3}$ is defined as in (3.11).

It's possible to generalize these results to more general cases, say B.C. of 1st kind. If we represent a general cylinder kernel of 1st kind $\overline{T}^{\alpha\beta\gamma}$, where α, β, γ are restricted to either DD or NN, indicating 2 Dirichlet or Neumann B.C. on opposite faces, and define $\eta_{DD} = -1$ and $\eta_{NN} = 1$, the the cylinder kernels for rectangular cavity with B.C. of 1st kind are,

$$\overline{T}^{\alpha\beta\gamma} = V_1^{---} + \eta_\alpha V_1^{+--} + \eta_\beta V_1^{-+-} + \eta_\gamma V_1^{--+} + \eta_\alpha\eta_\beta V_1^{++-} + \eta_\beta\eta_\gamma V_1^{-++} + \eta_\alpha\eta_\gamma V_1^{+-+} + \eta_\alpha\eta_\beta\eta_\gamma V_1^{+++} \tag{3.21}$$

2. Energy Density and Total Energy of Rectangular Cavity with B.C. of 1st Kind

In our analysis, the expression of the cylinder kernel contains 8 parts; each part is related to one kind of path length and all 8 parts can be classified into 4 kinds in Table II:

Table II. Table of 4 kinds of closed paths

Type	Path Length	Number of reflections at $[x = 0, a][y = 0, b][z = 0, c]$		
Periodic	$d^{---} = \sqrt{(2la)^2 + (2mb)^2 + (2nc)^2}$	[even]	[even]	[even]
Side	$d^{+--} = \sqrt{(2la + 2x)^2 + (2mb)^2 + (2nc)^2}$	[odd]	[even]	[even]
	$d^{-+-} = \sqrt{(2la)^2 + (2mb + 2y)^2 + (2nc)^2}$	[even]	[odd]	[even]
	$d^{--+} = \sqrt{(2la)^2 + (2mb)^2 + (2nc + 2z)^2}$	[even]	[even]	[odd]
Edge	$d^{++-} = \sqrt{(2la + 2x)^2 + (2mb + 2y)^2 + (2nc)^2}$	[odd]	[odd]	[even]
	$d^{-++} = \sqrt{(2la)^2 + (2mb + 2y)^2 + (2nc + 2z)^2}$	[even]	[odd]	[odd]
	$d^{+-+} = \sqrt{(2la + 2x)^2 + (2mb)^2 + (2nc + 2z)^2}$	[odd]	[even]	[odd]
Corner	$d^{+++} = \sqrt{(2la + 2x)^2 + (2mb + 2y)^2 + (2nc + 2z)^2}$	[odd]	[odd]	[odd]

When we are interested in the Casimir energy, which is the integral of energy density over the cavity (which was studied by [38, 39, 40]), we find that all paths except corner paths contribute to the Casimir energy.

a. Contribution from Periodic Paths

The energy density contributed by periodic paths is:

$$\varepsilon_1^{---} = -\frac{1}{2}\lim_{t\to 0}\frac{\partial^2}{\partial t^2}V_1^{---} = -\frac{1}{2\pi^2}\lim_{t\to 0}\sum_{l,m,n}^{\infty}\frac{d_P^2-3t^2}{(t^2+d_P^2)^3} = -\frac{1}{2\pi^2}\lim_{t\to 0}[\frac{3}{2\pi^2 t^4}+\sum_{l,m,n}^{\infty}{}'\frac{d_P^2-3t^2}{(t^2+d_P^2)^3}] \tag{3.22}$$

where $d_P = d^{---}$ is the length of periodic paths and the primed sum $\sum'$ means the term with $(l,m,n) = (0,0,0)$ is to be omitted. The divergent term, $\frac{3}{2\pi^2 t^4}$, is just coming from $(l,m,n) = (0,0,0)$ and is a universal leading divergent term. Since d_P is position independent, when integrating the energy density over the space to get the total energy, there will be a corresponding cutoff-dependent term $\frac{3V}{2\pi^2 t^4}$ and for all other terms we can take the limit $t \to 0$ now.

The total energy coming from the periodic paths is thus

$$\begin{aligned} E_1^P = \int \varepsilon_1^{---}dV &= \frac{3V}{2\pi^2 t^4} - \frac{V}{2\pi^2}\sum_{l,m,n}^{\infty}{}'\frac{1}{[(2la)^2+(2mb)^2+(2nc)^2]^2} \\ &= -\frac{abc}{32\pi^2}Z_3(a,b,c;4) + \frac{3V}{2\pi^2 t^4} \end{aligned} \tag{3.23}$$

where $Z_n(a_1,...,a_d;s)$ is the Epstein zeta function.

b. Contribution from Side Paths

There are three kinds of side paths: d_{S_x}, d_{S_y} and d_{S_z}. Their corresponding cylinder kernels are V_1^{+--}, V_1^{-+-} and V_1^{--+}. Let's take side paths d^{S_x} as example to obtain the total energy coming from side paths.

The energy density contributed by side paths type d_{S_X} is

$$\begin{aligned}\varepsilon_1^{+--} &= -\frac{1}{2}\lim_{t\to 0}\frac{\partial^2}{\partial t^2}V_1^{+--} = -\frac{1}{2\pi^2}\lim_{t\to 0}\sum_{l,m,n}^{\infty}\frac{d_{S_x}^2-3t^2}{(t^2+d_{S_x}^2)^3}\\ &= -\frac{1}{2\pi^2}\sum_{l=-\infty}^{\infty}\frac{(2la+2x)^2-3t^2}{[t^2+(2la+2x)^2]^3}\,|_{(m,n)=(0,0)} - \frac{1}{2\pi^2}\sum_{m,n}^{\infty}{}'\sum_{l=-\infty}^{\infty}\frac{1}{d_{S_x}^4}\end{aligned} \tag{3.24}$$

Since the side path length d_{S_x} is only x-dependent, integrating the energy density over space to get the total energy is easy:

$$\begin{aligned}E_1^{S_x} = bc\int\varepsilon_1^{+--}dx &= -\frac{bc}{2\pi^2}\int_0^a\sum_{m,n}^{\infty}{}'\sum_{l=-\infty}^{\infty}\frac{1}{[(2la+2x)^2+(2mb)^2+(2nc)^2]^2}dx\\ &\quad -\frac{bc}{2\pi^2}\int_0^a\sum_{l=-\infty}^{\infty}\frac{(2la+2x)^2-3t^2}{[t^2+(2la+2x)^2]^3}dx\\ &= -\frac{bc}{64\pi}Z_2(b,c;3)+\frac{bc}{4\pi t^3}\end{aligned} \tag{3.25}$$

Again $\frac{bc}{4\pi t^3}$ is a divergent, cutoff dependent term.

Similar formulas hold for the other two side paths types, d_{S_y} and d_{S_z}:

$$\begin{aligned}E_1^{S_y} &= -\frac{ac}{64\pi}Z_2(a,c;3)+\frac{ac}{4\pi t^3}\\ E_1^{S_z} &= -\frac{ab}{64\pi}Z_2(a,b;3)+\frac{ab}{4\pi t^3}\end{aligned} \tag{3.26}$$

c. Contribution from Edge Paths

Let's first consider the edge path $d_{E_{xy}}$ and then generalize it to the other 2 kinds of edge paths, $d_{E_{yz}}$ and $d_{E_{zx}}$.

Energy density contributed by edge paths $d_{E_{xy}}$ is

$$\begin{aligned}\varepsilon_1^{++-} &= -\frac{1}{2}\lim_{t\to 0}\frac{\partial^2}{\partial t^2}V_1^{++-} = -\frac{1}{2\pi^2}\lim_{t\to 0}\sum_{l,m,n}^{\infty}\frac{d_{E_{xy}}^2-3t^2}{(t^2+d_{E_{xy}}^2)^3}\\ &= -\frac{1}{2\pi^2}\sum_{l,m=-\infty}^{\infty}\frac{d_{E_{xy}}^2-3t^2}{(t^2+d_{E_{xy}}^2)^3}\,|_{n=0} - \frac{1}{2\pi^2}\sum_{l,m=-\infty}^{\infty}\sum_{n=-\infty}^{\infty}{}'\frac{1}{d_{E_{xy}}^4}\end{aligned} \tag{3.27}$$

The edge path $d_{E_{xy}}$ is both $x-$dependent and $y-$dependent, so the integration over space

includes double integrals. Evaluate this integral to obtain the total energy from the edge path $d_{E_{xy}}$ is [15]

$$\begin{aligned} E_1^{E_{xy}} = c\int\int \varepsilon_1^{++-}dxdy &= -\frac{c}{2\pi^2}\int_0^a\int_0^b \sum_{l,m=-\infty}^{\infty}{}' \sum_{n=-\infty}^{\infty} \frac{dxdy}{[(2la+2x)^2+(2mb+2y)^2+(2nc)^2]^2} \\ &\quad -\frac{c}{2\pi^2}\int_0^a\int_0^b \sum_{l,m}^{\infty} \frac{(2la+2x)^2+(2mb+2y)^2-3t^2}{[t^2+(2la+2x)^2+(2mb+2y)^2]^3}dxdy \\ &= -\frac{\zeta(2)}{16\pi c}+\frac{c}{8\pi t^2} = -\frac{\pi}{96c}+\frac{c}{8\pi t^2} \end{aligned} \tag{3.28}$$

Similar formulas hold for the other two edge path types $d_{lmn}^{E_{yz}}$ and $d_{lmn}^{E_{zx}}$:

$$\begin{aligned} E_1^{E_{yz}} &= -\frac{\zeta(2)}{16\pi a}+\frac{a}{8\pi t^2} = -\frac{\pi}{96a}+\frac{a}{8\pi t^2} \\ E_1^{E_{zx}} &= -\frac{\zeta(2)}{16\pi b}+\frac{b}{8\pi t^2} = -\frac{\pi}{96b}+\frac{b}{8\pi t^2} \end{aligned} \tag{3.29}$$

d. Contribution from Corner Paths

The energy density contributed by corner paths d_C is

$$\varepsilon_1^{+++} = -\frac{1}{2}\lim_{t\to 0}\frac{\partial^2}{\partial t^2}V_1^{+++} = -\frac{1}{2\pi^2}\lim_{t\to 0}\sum_{l,m,n}^{\infty}\frac{d_C^2-3t^2}{[t^2+d_C^2]^3} \tag{3.30}$$

The total energy contributed by corner paths is:

$$\begin{aligned} E_1^C &= \int \varepsilon_1^{+++}dxdydz \\ &= -\frac{1}{2\pi^2}\int_0^a\int_0^b\int_0^c \sum_{l,m,n=-\infty}^{\infty} \frac{(2la+2x)^2+(2mb+2y)^2+(2nc+2z)^2-3t^2}{[t^2+(2la+2x)^2+(2mb+2y)^2+(2nc+2z)^2]^3}dxdydz \\ &= 0 \end{aligned} \tag{3.31}$$

We summarize the total energy contributed from 8 parts of 4 kinds in Table III. It's straightforward to give the general total energy expression for rectangular cavity with B.C.

of 1st kind:

$$E_1^{\alpha\beta\gamma} = E_1^P + \eta_\alpha E_1^{S_x} + \eta_\beta E_1^{S_y} + \eta_\gamma E_1^{S_z} + \eta_\alpha\eta_\beta E_1^{E_{xy}} + \eta_\beta\eta_\gamma E_1^{E_{yz}} + \eta_\alpha\eta_\gamma E_1^{E_{zx}} + \eta_\alpha\eta_\beta\eta_\gamma E_1^C \quad (3.32)$$

where $\eta_{DD} = -1$ and $\eta_{NN} = 1$ as defined before.

Table III. Table of total energy by path types, 1st kind B.C.

Type	Path Length	Total Energy
Periodic	$d_P : \sqrt{(2la)^2 + (2mb)^2 + (2nc)^2}$	$E_1^P : -\frac{abc}{32\pi^2} Z_3(a,b,c;4) + \frac{3abc}{2\pi^2 t^4}$
Side	$d_{S_x} : \sqrt{(2la+2x)^2 + (2mb)^2 + (2nc)^2}$	$E_1^{S_x} : -\frac{bc}{64\pi} Z_2(b,c;3) + \frac{bc}{4\pi t^3}$
	$d_{S_y} : \sqrt{(2la)^2 + (2mb+2y)^2 + (2nc)^2}$	$E_1^{S_y} : -\frac{ac}{64\pi} Z_2(a,c;3) + \frac{ac}{4\pi t^3}$
	$d_{S_z} : \sqrt{(2la)^2 + (2mb)^2 + (2nc+2z)^2}$	$E_1^{S_z} : -\frac{ab}{64\pi} Z_2(a,b;3) + \frac{ab}{4\pi t^3}$
Edge	$d_{E_{xy}} : \sqrt{(2la+2x)^2 + (2mb+2y)^2 + (2nc)^2}$	$E_1^{E_{xy}} : -\frac{\pi}{96c} + \frac{c}{8\pi t^2}$
	$d_{E_{yz}} : \sqrt{(2la)^2 + (2mb+2y)^2 + (2nc+2z)^2}$	$E_1^{E_{yz}} : -\frac{\pi}{96a} + \frac{a}{8\pi t^2}$
	$d_{E_{xz}} : \sqrt{(2la+2x)^2 + (2mb)^2 + (2nc+2z)^2}$	$E_1^{E_{zx}} : -\frac{\pi}{96b} + \frac{b}{8\pi t^2}$
Corner	$d_C : \sqrt{(2la+2x)^2 + (2mb+2y)^2 + (2nc+2z)^2}$	$E_1^C : 0$

3. Casimir Force for Scalar Pistons of 1st Kind

a. Casimir Force for Neumann Scalar Piston

For a rectangular cavity $a \times b \times c$ with Neumann B.C. on each face, the total energy is:

$$E_{abc}^{NNN} = E_{abc}^P + E_{abc}^{S_x} + E_{abc}^{S_y} + E_{abc}^{S_z} + E_{abc}^{E_{xy}} + E_{abc}^{E_{yz}} + E_{abc}^{E_{xz}} + E_{abc}^C \quad (3.33)$$

If we consider only $a-$dependent terms,

$$\begin{aligned} E^{NNN}_{abc}(a) =& E^{P}_{abc} + E^{S_y}_{abc} + E^{S_z}_{abc} + E^{E_{yz}}_{abc} \\ =& -\frac{abc}{32\pi^2}{\sum_{l,m,n=-\infty}^{\infty}}' \frac{1}{[(la)^2+(mb)^2+(nc)^2]^2} - \frac{ab}{64\pi}{\sum_{l,m=-\infty}^{\infty}}' \frac{1}{[(la)^2+(mb)^2]^{\frac{3}{2}}} \\ & - \frac{ac}{64\pi}{\sum_{l,n=-\infty}^{\infty}}' \frac{1}{[(la)^2+(nc)^2]^{\frac{3}{2}}} - \frac{\pi}{96}\frac{1}{a} + [\frac{3abc}{2\pi^2 t^4} + \frac{ac}{4\pi t^3} + \frac{ab}{4\pi t^3} + \frac{a}{8\pi t^2}] \end{aligned} \tag{3.34}$$

Before talking about piston, let's consider just a rectangular cavity. If we would like to calculate the force on the face $x = a$, we need to take derivative of E with respect to a. For the 4 $a-$dependent parts of E, we get the corresponding force

$$\begin{aligned} F^{P}_{cavity} =& -\frac{\partial}{\partial a}E^{P}_{cavity} = \frac{bc}{32\pi^2}{\sum_{l,m,n=-\infty}^{\infty}}' [\frac{1}{[(la)^2+(mb)^2+(nc)^2]^2} - \frac{4l^2a^2}{[(la)^2+(mb)^2+(nc)^2]^3}] \\ F^{S_y}_{cavity} =& -\frac{\partial}{\partial a}E^{S_y}_{cavity} = \frac{b}{64\pi}{\sum_{l,m=-\infty}^{\infty}}' [\frac{1}{[(la)^2+(mb)^2]^{\frac{3}{2}}} - \frac{3l^2a^2}{[(la)^2+(mb)^2]^{\frac{5}{2}}}] \\ F^{S_z}_{cavity} =& -\frac{\partial}{\partial a}E^{S_z}_{cavity} = \frac{c}{64\pi}{\sum_{l,n=-\infty}^{\infty}}' [\frac{1}{[(la)^2+(nc)^2]^{\frac{3}{2}}} - \frac{3l^2a^2}{[(la)^2+(nc)^2]^{\frac{5}{2}}}] \\ F^{E_{yz}}_{cavity} =& -\frac{\partial}{\partial a}E^{E_{yz}}_{cavity} = -\frac{\pi}{96}\frac{1}{a^2} \end{aligned} \tag{3.35}$$

Notice that here we operate on only the finite parts of E^P, E^{S_y}, E^{S_y} and $E^{E_{yz}}$, the divergent parts of them are discarded since when another rectangular cavity is introduced they will be canceled exactly. Then the force on the face $x = a$ for the cavity with Neumann B.C. on each face is

$$F^{NNN}_{cavity} = F^{P}_{cavity} + F^{S_y}_{cavity} + F^{S_z}_{cavity} + F^{E_{yz}}_{cavity} \tag{3.36}$$

Next we extend the rectangular cavity along the x direction to form a piston with the face at $x = a$ as the partition.

The total energy of the the second rectangular cavity $(L-a)\times b\times c$ is

$$E^{NNN}_{L-a,b,c} = E^{P}_{L-a,b,c} + E^{S_y}_{L-a,b,c} + E^{S_z}_{L-a,b,c} + E^{E_{yz}}_{L-a,b,c} \tag{3.37}$$

Take the limit $L\to\infty$ and bearing in mind that $Z_d(a_1,...a_d;s)|_{a_1\to\infty}\to Z_{d-1}(a_2,...a_d;s)$

$$\begin{aligned} E^{NNN}_{L-a,b,c} =& -\frac{(L-a)bc}{32\pi^2}Z_2(b,c;4) - \frac{(L-a)b}{64\pi}Z_1(b;3) - \frac{(L-a)c}{64\pi}Z_1(c;3) \\ =& \frac{abc}{32\pi^2}Z_2(b,c;4) + \frac{ab}{64\pi}Z_1(b;3) + \frac{ac}{64\pi}Z_1(c;3) \\ =& \frac{abc}{32\pi^2}{\sum_{m,n=-\infty}^{\infty}}' \frac{1}{[(mb)^2+(nc)^2]^2} + \frac{ab}{64\pi}{\sum_{m=-\infty}^{\infty}}' \frac{1}{(m|b|)^3} + \frac{ac}{64\pi}{\sum_{n=-\infty}^{\infty}}' \frac{1}{(n|c|)^3} \end{aligned} \tag{3.38}$$

Here $Z_1(b;3)$ is the Riemann Zeta function $\zeta(b;3)$ and we've discarded the $a-$independent terms. The force on partition $x=a$ contributed by the second rectangular cavity $(L-a)\times b\times c$ is

$$F^{NNN}_{L-a,b,c} = -\frac{bc}{32\pi^2}{\sum_{m,n=-\infty}^{\infty}}' \frac{1}{[((mb)^2+(nc)^2]^2} - \frac{b}{64\pi}{\sum_{m=-\infty}^{\infty}}' \frac{1}{(m|b|)^3} - \frac{c}{64\pi}{\sum_{n=-\infty}^{\infty}}' \frac{1}{(n|c|)^3} \tag{3.39}$$

This part of the force is $a-$independent; therefore, it is a constant term. Observing the relation between $E^{NNN}_{L-a,b,c}$ and $E^{NNN}_{a,b,c}$, we find

$$E^{NNN}_{L-a,b,c} = -E^{NNN}_{a,b,c}|_{l=0} \tag{3.40}$$

So we conclude that the sum of $E^{NNN}_{L-a,b,c}$ and $E^{NNN}_{a,b,c}$ will be just $E^{NNN}_{a,b,c}$ with all $l=0$ terms excluded. The total energy of the whole piston is the sum of the total energy of two rectangular cavities with B.C. of 1st kind (a-dependent parts only):

$$\begin{aligned} E^{NNN}_{1} =& E^{NNN}_{abc} + E^{NNN}_{L-a,b,c}|_{L\to\infty} = E^{NNN}_{abc}|_{l\neq 0} = E^{P}_{piston} + E^{S_y}_{piston} + E^{S_z}_{piston} + E^{E_{yz}}_{piston} \\ =& -\frac{abc}{32\pi^2}\sum_{l,m,n=-\infty;l\neq 0}^{\infty}\frac{1}{[(la)^2+(mb)^2+(nc)^2]^2} - \frac{ab}{64\pi}\sum_{l,m=-\infty;l\neq 0}^{\infty}\frac{1}{[(la)^2+(mb)^2]^{\frac{3}{2}}} \\ & -\frac{ac}{64\pi}\sum_{l,n=-\infty;l\neq 0}^{\infty}\frac{1}{[(la)^2+(nc)^2]^{\frac{3}{2}}} - \frac{\pi}{96}\frac{1}{a} \end{aligned} \tag{3.41}$$

We are ready for evaluating the piston force on the partition $x = a$. E_1^P, $E_1^{S_y}$, $E_1^{S_y}$ and $E_1^{E_{yz}}$ stand for the corresponding combined energy of the $a \times b \times c$ and $(L-a) \times b \times c$ cavities with B.C. of 1st kind.

$$\begin{aligned}
F_1^P &= -\frac{\partial}{\partial a} E_1^P = \frac{bc}{32\pi^2} \sum_{l\neq 0,m,n} \left[\frac{1}{[(la)^2+(mb)^2+(nc)^2]^2} - \frac{4l^2a^2}{[(la)^2+(mb)^2+(nc)^2]^3} \right] \\
F_1^{S_y} &= -\frac{\partial}{\partial a} E_1^{S_y} = \frac{b}{64\pi} \sum_{l\neq 0,m} \left[\frac{1}{[(la)^2+(mb)^2]^{\frac{3}{2}}} - \frac{3l^2a^2}{[(la)^2+(mb)^2]^{\frac{5}{2}}} \right] \\
F_1^{S_z} &= -\frac{\partial}{\partial a} E_1^{S_z} = \frac{c}{64\pi} \sum_{l\neq 0,n} \left[\frac{1}{[(la)^2+(nc)^2]^{\frac{3}{2}}} - \frac{3l^2a^2}{[(la)^2+(nc)^2]^{\frac{5}{2}}} \right] \\
F_1^{E_{yz}} &= -\frac{\partial}{\partial a} E_1^{E_{yz}} = -\frac{\pi}{96}\frac{1}{a^2}
\end{aligned} \tag{3.42}$$

If we let the piston bottom be the face $x = 0$ and the partition be the face $x = a$ and let $b = c$ and $\eta = \frac{a}{b}$, then $F_1^{S_y} = F_1^{S_z}$ and we can write down the Neumann piston force as

$$\begin{aligned}
F_1^{NNN} =& F_1^P + F_1^{S_y} + F_1^{S_z} + F_1^{E_{yz}} \\
=& \frac{1}{32\pi^2 b^2} \sum_{l\neq 0,m,n} \left[\frac{1}{[l^2\eta^2+m^2+n^2]^2} - \frac{4l^2\eta^2}{[l^2\eta^2+m^2+n^2]^3} \right] \\
&+ \frac{1}{32\pi b^2} \sum_{l\neq 0,n} \left[\frac{1}{[l^2\eta^2+n^2]^{\frac{3}{2}}} - \frac{3l^2\eta^2}{[l^2\eta^2+n^2]^{\frac{5}{2}}} \right] - \frac{\pi}{96b^2}\frac{1}{\eta^2}
\end{aligned} \tag{3.43}$$

Notice that

$$\begin{aligned}
\sum_{l\neq 0,m,n} =& \sum_{l\neq 0} \left[\sum_{m\neq 0,n\neq 0} + \sum_{m=0,n\neq 0} + \sum_{m\neq 0,n=0} + \sum_{m=0,n=0} \right] \\
=& 8 \sum_{l=1,m=1,n=1}^{\infty} + 8 \sum_{l=1,n=1}^{\infty} + 2 \sum_{l=1}^{\infty}
\end{aligned} \tag{3.44}$$

and

$$\sum_{l\neq 0,n} = \sum_{l\neq 0} \left[\sum_{n\neq 0} + \sum_{n=0} \right] = 4 \sum_{l=1,n=1}^{\infty} + 2 \sum_{l=1}^{\infty} \tag{3.45}$$

So we can rewrite F^{P}_{piston}, $F^{S_y}_{piston}$ and $F^{S_z}_{piston}$ as

$$\begin{aligned}
F^{P}_{1} =&\frac{1}{32\pi^2 b^2}\sum_{l\neq 0,m,n}[\frac{1}{[l^2\eta^2+m^2+n^2]^2}-\frac{4l^2\eta^2}{[l^2\eta^2+m^2+n^2]^3}]\\
=&\frac{1}{32\pi^2 b^2}(8\sum_{l=1,m=1,n=1}^{\infty}+8\sum_{l=1,n=1}^{\infty}+2\sum_{l=1}^{\infty})[\frac{1}{[l^2\eta^2+m^2+n^2]^2}-\frac{4l^2\eta^2}{[l^2\eta^2+m^2+n^2]^3}]\\
=&\frac{1}{4\pi^2 b^2}\sum_{l=1,m=1,n=1}^{\infty}[\frac{1}{[l^2\eta^2+m^2+n^2]^2}-\frac{4l^2\eta^2}{[l^2\eta^2+m^2+n^2]^3}]\\
&+\frac{1}{4\pi^2 b^2}\sum_{l=1,n=1}^{\infty}[\frac{1}{[l^2\eta^2+n^2]^2}-\frac{4l^2\eta^2}{[l^2\eta^2+n^2]^3}]-\frac{\pi^2}{480b^2\eta^4}
\end{aligned} \tag{3.46}$$

$$\begin{aligned}
F^{S_y}_{1}=F^{S_z}_{1} =&\frac{1}{64\pi b^2}\sum_{l\neq 0,n}[\frac{1}{[l^2\eta^2+n^2]^{\frac{3}{2}}}-\frac{3l^2\eta^2}{[l^2\eta^2+n^2]^{\frac{5}{2}}}]\\
=&\frac{1}{64\pi b^2}(4\sum_{l=1,n=1}^{\infty}+2\sum_{l=1}^{\infty})[\frac{1}{[l^2\eta^2+n^2]^{\frac{3}{2}}}-\frac{3l^2\eta^2}{[l^2\eta^2+n^2]^{\frac{5}{2}}}]\\
=&\frac{1}{16\pi b^2}\sum_{l=1,n=1}^{\infty}[\frac{1}{[l^2\eta^2+n^2]^{\frac{3}{2}}}-\frac{3l^2\eta^2}{[l^2\eta^2+n^2]^{\frac{5}{2}}}]-\frac{\zeta(3)}{16\pi b^2\eta^3}
\end{aligned} \tag{3.47}$$

$$F^{E_{yz}}_{1}=-\frac{\pi}{96b^2}\frac{1}{\eta^2} \tag{3.48}$$

In unit of $1/b^2$, we plot $F^{NNN}_{1}, F^{P}_{1}, F^{S_y}_{1}, F^{E_{yz}}_{1} \sim \eta$ and $F^{NNN}_{cavity}, F^{P}_{cavity}, F^{S_y}_{cavity}, F^{E_{yz}}_{cavity} \sim \eta$ in the Fig. 2. Notice that the difference between F^{NNN}_{1} and F^{NNN}_{cavity} is just a constant term $F^{NNN}_{L-a,b,c}$. We can see from Fig. 2 that for the piston geometry, $|\ F^{P}_{1}\ |>|\ F^{S_y}_{1}\ |>|\ F^{E_{yz}}_{1}\ |$, so the contributions from periodic paths F^{P}_{1} are dominant. At the limit $\eta\to\infty$, $F^{NNN}_{1}\to 0$ while $F^{NNN}_{cavity}\to[\frac{Z_2(1,1;4)}{8\pi^2}+\frac{\pi^2}{720}+\frac{\zeta(3)}{32\pi}]$. The force for the piston of infinite length is always attractive, while there is a turning point for the cavity where the force changes from attractive to repulsive.

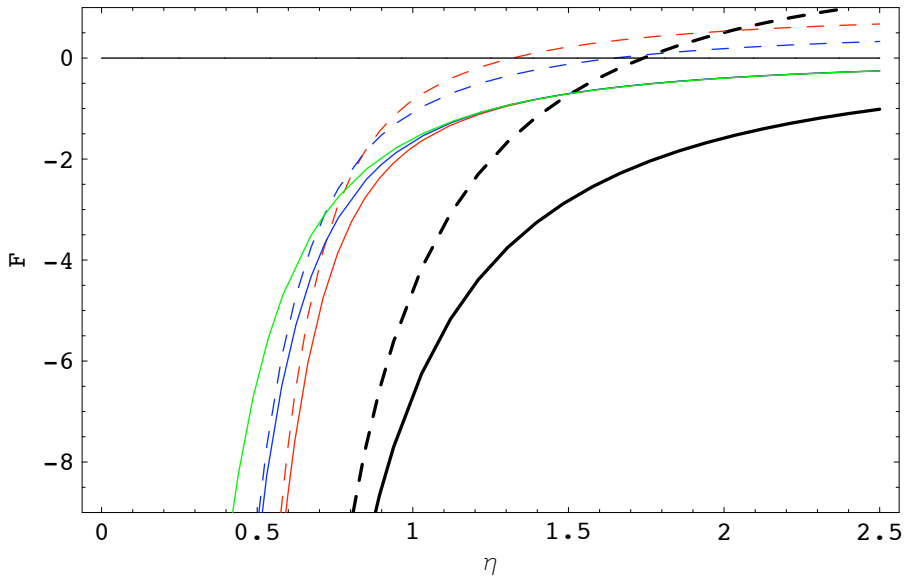

Fig. 2. The force F on a Neumann piston with square cross section ($b = c$) as functions of $\eta = a/b$, rescaled as $480F/\pi^2$. The solid black line is total force F_1^{NNN} considering the piston and the dashed black line is total force F_{cavity}^{NNN} considering only the rectangular cavity $a \times b \times c$. Solid red, solid blue and solid green stand for the contribution from periodic paths, side paths and edge paths for piston respectively, while their dashed counterparts are for the rectangular cavity $a \times b \times c$.

b. Casimir Force for General Scalar Piston with B.C. of 1st Kind

We have analyzed the piston force for the $NN-NN-NN$ type piston; it is straightforward to extend our analysis to other pistons with B.C. of 1st kind. Based on the formula of total energy in (3.32) the formula of piston force in (3.42), the piston force for general piston with B.C. of 1st kind is

$$F_1^{\alpha\beta\gamma} = F_1^P + \eta_\beta F_1^{S_y} + \eta_\gamma F_1^{S_z} + \eta_\beta\eta_\gamma F_1^{E_{yz}} \tag{3.49}$$

Note that the cutoff divergent terms of two rectangular cavities are canceled. The 1st term is a universal term standing for contribution from periodic paths; 2nd and 3rd terms are contributions from side paths, their sign are determined by the B.C. on sides, NN for '+'and DD for '-'; the last term stands for the contribution from edge path E_{yz} and its sign is the product of η_β and η_γ, determined by B.C. on sides as well. Overall, we see the B.C. on the base $x = 0$ and the partition $x = a$ does not affect the force, that is, for either NN or DD at $x = 0, a$, the force does not change. So we conclude that the piston forces are the same for piston $NN-NN-NN$ and $DD-NN-NN$. Among the other 4 kinds of pistons with B.C. of 1st kind, $NN-DD-DD$ is the same as $DD-DD-DD$ and $NN-DD-NN$ is the same as $DD-DD-NN$. So it will be adequate to study 3 pistons with B.C. of 1st kind: $NN-NN-NN$, $NN-DD-DD$ and $NN-DD-NN$. The piston forces for these 3 pistons are

$$\begin{aligned} F_1^{NNN} &= F_1^P + F_1^{S_y} + F_1^{S_z} + F_1^{E_{yz}} \\ F_1^{NDD} &= F_1^P - F_1^{S_y} - F_1^{S_z} + F_1^{E_{yz}} \\ F_1^{NDN} &= F_1^P - F_1^{S_y} + F_1^{S_z} - F_1^{E_{yz}} \end{aligned} \tag{3.50}$$

Recall that the force for two parallel plates on unit area with separation a is

$$\mathcal{F}_{plates}^N = -\frac{\pi^2}{480a^4} \tag{3.51}$$

If we would like to compare the piston force with the force of parallel plates, a natural way is to divide the piston by $\mathcal{F}^N_{plates}$. The force from periodic paths F^P_1 is (for $b = c$),

$$\begin{aligned} F^P_1 =& \frac{1}{32\pi^2 b^2} \sum_{l\neq 0,m,n} [\frac{1}{[l^2\eta^2 + m^2 + n^2]^2} - \frac{4l^2\eta^2}{[l^2\eta^2 + m^2 + n^2]^3}] \\ =& \frac{b^2\eta^4}{32\pi^2 a^4} \sum_{l\neq 0,m,n} [\frac{1}{[l^2\eta^2 + m^2 + n^2]^2} - \frac{4l^2\eta^2}{[l^2\eta^2 + m^2 + n^2]^3}] \end{aligned} \tag{3.52}$$

so the force per unit area is

$$\begin{aligned} \mathcal{F}^P_1 = \frac{F^P_1}{b^2} =& -\frac{15\eta^4}{\pi^4}[-\frac{\pi^2}{480a^4}] \sum_{l\neq 0,m,n} [\frac{1}{[l^2\eta^2 + m^2 + n^2]^2} - \frac{4l^2\eta^2}{[l^2\eta^2 + m^2 + n^2]^3}] \\ =& -\frac{15\eta^4}{\pi^4}\mathcal{F}^N_1 \sum_{l\neq 0,m,n} [\frac{1}{[l^2\eta^2 + m^2 + n^2]^2} - \frac{4l^2\eta^2}{[l^2\eta^2 + m^2 + n^2]^3}] \end{aligned} \tag{3.53}$$

Other forces per unit area are

$$\begin{aligned} \mathcal{F}^{S_y}_1 = \mathcal{F}^{S_z}_1 =& -\frac{15\eta^4}{2\pi^3}\mathcal{F}^N_1 \sum_{l\neq 0,n} [\frac{1}{[l^2\eta^2 + n^2]^{\frac{3}{2}}} - \frac{3l^2\eta^2}{[l^2\eta^2 + n^2]^{\frac{5}{2}}}] \\ \mathcal{F}^{E_{yz}}_1 =& \frac{5\eta^2}{\pi}\mathcal{F}^N_1 \end{aligned} \tag{3.54}$$

With these forces per unit area, we can convert the piston forces in (3.50) to

$$\begin{aligned} \mathcal{F}^{NNN}_1 =& \mathcal{F}^P_1 + \mathcal{F}^{S_y}_1 + \mathcal{F}^{S_z}_1 + \mathcal{F}^{E_{yz}}_1 \\ \mathcal{F}^{NDD}_1 =& \mathcal{F}^P_1 - \mathcal{F}^{S_y}_1 - \mathcal{F}^{S_z}_1 + \mathcal{F}^{E_{yz}}_1 \\ \mathcal{F}^{NDN}_1 =& \mathcal{F}^P_1 - \mathcal{F}^{E_{yz}}_1 \end{aligned} \tag{3.55}$$

We plot these 3 forces before and after division by $\mathcal{F}^N_1$ in Figs. 3 and 4. At the limit $\eta \to 0$, or $a \ll b = c$, the piston force is the same as the parallel plates force. Since the difference between piston and parallel plates is the sides, when $a \ll b = c$, the sides' effect is small enough to be ignored. However, with η increasing, the sides' effect become visible and cannot be ignored any more. When comparing with parallel plates force, we can understand the piston force as being based on the dominant term F^P_1; periodic paths'

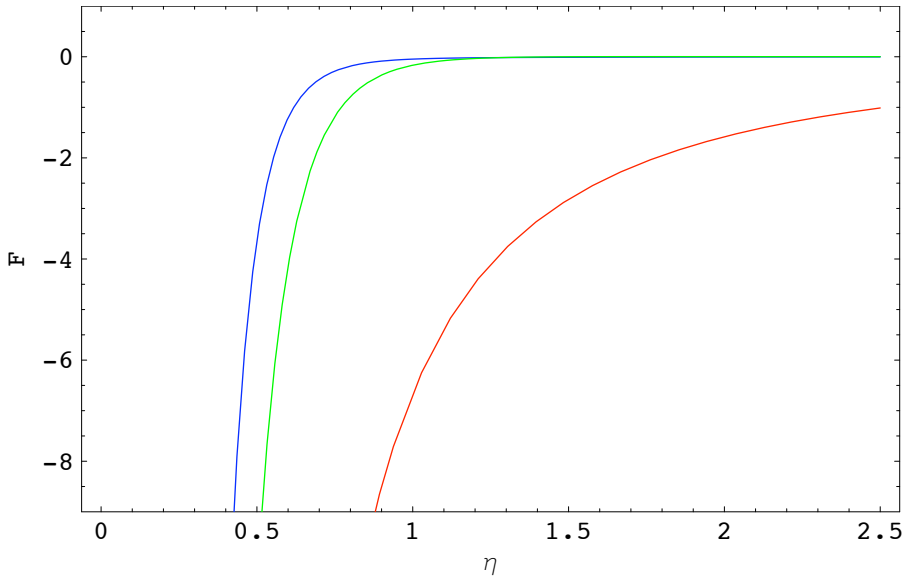

Fig. 3. The force F on a piston with square cross section ($b = c$) as functions of $\eta = a/b$. Solid red= F_1^{NNN}, solid blue= F_1^{NDD} and solid green= F_1^{NDN}.

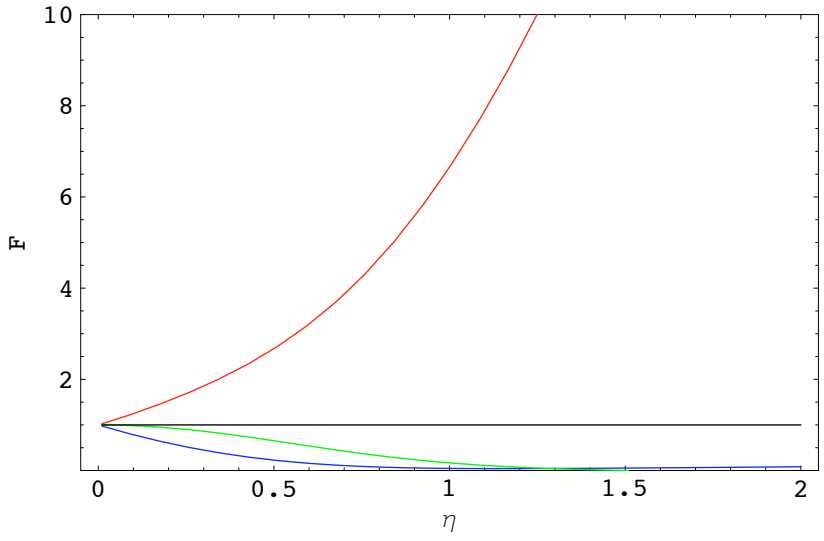

Fig. 4. The force F on a piston with square cross section ($b = c$) as functions of $\eta = a/b$, normalized to the parallel plates force $\mathcal{F}^N_{plates} = -\frac{\pi^2}{480a^4}$. Solid red= F_1^{NNN}, solid blue= F_1^{NDD} and solid green= F_1^{NDN}.

contribution provides an attractive force which reduces to the parallel-plate force at the limit $\eta \to 0$. It is augmented by side path contribution ($\eta_y F_1^{S_y}$ and $\eta_z F_1^{S_z}$) and edge path contribution ($\eta_y \eta_z F_1^{E_{yz}}$). For $NN-NN-NN$ piston, the two side path contributions and the edge path contribution all have '+' sign; they provide a contribution with same sign as the dominant term and make the attractive force's magnitude greater. Thus in the figure 4, we see F_1^{NNN} start from 1 and then increase. For $NN-DD-DD$ piston, two side paths contribute negatively (with '-' sign) and edge path still contributes positively (with '+' sign). With the knowledge that the side-path contribution is greater than the edge-path contribution, we conclude that F_1^{NDD} will decrease and be below 1. For $NN-DD-NN$ piston, the two side path contributions cancel each other and the edge path term contributes negatively (with '-' sign), so F_1^{NDD} will be slightly below 1. Based on these arguments, we conclude that F_1^{NNN} damps more slowly than the parallel-plate force $\mathcal{F}^N_{plates}$, while F_1^{NDD} and F_1^{NDN} damp more quickly than $\mathcal{F}^N_{plates}$, with F_1^{NDD} the most quickly. We can also see this from Fig. 3: F_1^{NDD} damps most quickly and F_1^{NNN} has greatest magnitude.

B. Cylinder Kernel for Rectangular Cavity with 2nd Kind of B.C.

The 2nd kind of B.C. includes one mixed B.C.. $DN-DD-DD$, $DN-DD-NN$ and $DN-NN-NN$ have the mixed B.C. on base and partition ($x = 0, a$) while $DD-DN-DD$, $NN-DN-DD$, $DD-DN-NN$ and $NN-DN-NN$ have the mixed B.C. on sides $y = 0, b$. We will take $DN-DD-DD$ as an example first, which is studied in [31] and is called hybrid B.C.

1. Cylinder Kernel for a Rectangular Cavity with Hybrid B.C.

Suppose the only Neumann B.C. is imposed at $x = a$ and Dirichlet B.C. elsewhere for the rectangular cavity. Our notation for the cylinder kernel with hybrid B.C. is $\overline{T}^{MDD}$,

where M means mixed B.C. at two faces $x = 0, a$ and D means Dirichlet B.C.. Similar to the definition of Dirichlet Reflection Operator $D_x^a f(x) = -f(2a - x)$, we could define a Neumann Reflection Operator as N_x^a as

$$N_x^a f(x) = f(2a - x) \tag{3.56}$$

Following the procedure for the derivation of cylinder kernel of purely Dirichlet B.C. but replacing the Dirichlet Reflection Operator D_x^a at $x = a$ with Neumann Reflection Operator N_x^a, we will get the cylinder kernel for hybrid B.C. as:

$$\overline{T}^{MDD} = V_2^{---} + V_2^{+--} - V_2^{-+-} - V_2^{--+} - V_2^{++-} + V_2^{-++} - V_2^{+-+} + V_2^{+++} \tag{3.57}$$

where

$$V_2^{\varepsilon_1\varepsilon_2\varepsilon_3} = -\frac{1}{2\pi^2} \sum_{l,m,n=-\infty}^{\infty} \frac{(-1)^l}{t^2 + (2la + x + \varepsilon_1 x')^2 + (2mb + y + \varepsilon_2 y')^2 + (2nc + z + \varepsilon_3 z')^2} \tag{3.58}$$

It is different from $V_1^{\varepsilon_1\varepsilon_2\varepsilon_3}$ by including an extra term $(-1)^l$ inside the summation.

For general cases of 2nd kind of B.C., define $\eta_{DD} = -1$, $\eta_{NN} = 1$ and $\eta_M = 1$; we have:

$$\overline{T}^{\alpha\beta\gamma} = V_2^{---} + \eta_\alpha V_2^{+--} + \eta_\beta V_2^{-+-} + \eta_\gamma V_2^{--+} + \eta_\alpha\eta_\beta V_2^{++-} + \eta_\beta\eta_\gamma V_2^{-++} + \eta_\alpha\eta_\gamma V_2^{+-+} + \eta_\alpha\eta_\beta\eta_\gamma V_2^{+++} \tag{3.59}$$

2. Energy Density and Total Energy for Rectangular Cavity

In the following calculation, we will ignore the universal divergent terms since the scheme of analysis is the same as before.

a. Contribution from Periodic Paths

The energy density contributed by periodic paths is:

$$\varepsilon_2^{---} = -\frac{1}{2}\lim_{t\to 0}\frac{\partial^2}{\partial t^2}V_2^{---} = -\frac{1}{2\pi^2}\lim_{t\to 0}\sum_{l,m,n}^{\infty}\frac{(-1)^l(d_P^2-3t^2)}{(t^2+d_P^2)^3} = -\frac{1}{2\pi^2}\sum_{l,m,n}^{\infty}{}'\frac{(-1)^l}{d_P^4} \tag{3.60}$$

The total energy coming from the periodic paths is:

$$E_2^P = \int \varepsilon_2^{---}dV = -\frac{abc}{32\pi^2}\sum_{l,m,n}^{\infty}{}'\frac{(-1)^l}{[(la)^2+(mb)^2+(nc)^2]^2} \tag{3.61}$$

b. Contribution from Side Paths S_z

The energy density contributed by side paths of lengths d_{S_z} is

$$\begin{aligned}\varepsilon_2^{--+} &= -\frac{1}{2}\lim_{t\to 0}\frac{\partial^2}{\partial t^2}V_2^{--+} = -\frac{1}{2\pi^2}\lim_{t\to 0}\sum_{l,m,n}^{\infty}\frac{(-1)^l(d_{S_z}^2-3t^2)}{(t^2+d_{S_z}^2)^3}\\ &= -\frac{1}{2\pi^2}\sum_{l,m}^{\infty}{}'\sum_{n=-\infty}^{\infty}\frac{(-1)^l}{d_{S_z}^4}\end{aligned} \tag{3.62}$$

Since the side path $d_{lmn}^{S_z}$ is only z-dependent, the total energy is:

$$\begin{aligned}E_2^{S_z} = ab\int \varepsilon_2^{--+}dz &= -\frac{ab}{2\pi^2}\int_0^c\sum_{l,m}^{\infty}{}'\sum_{n=-\infty}^{\infty}\frac{(-1)^l}{[(2la)^2+(2mb)^2+(2nc+2z)^2]^2}dz\\ &= -\frac{ab}{64\pi}\sum_{l,m}^{\infty}{}'\frac{(-1)^l}{[(la)^2+(mb)^2]^{\frac{3}{2}}}\end{aligned} \tag{3.63}$$

Similarly for side paths of type S_y we get,

$$E_2^{S_y} = -\frac{ac}{64\pi}\sum_{l,n}^{\infty}{}'\frac{(-1)^l}{[(la)^2+(nc)^2]^{\frac{3}{2}}} \tag{3.64}$$

c. Contribution from Side Paths S_x

The energy density contributed by the S_x side path is

$$\begin{aligned}\varepsilon_2^{+--} &= -\frac{1}{2}\lim_{t\to 0}\frac{\partial^2}{\partial t^2}V_2^{+--} = -\frac{1}{2\pi^2}\lim_{t\to 0}\sum_{l,m,n}^{\infty}\frac{(-1)^l(d_{S_x}^2-3t^2)}{(t^2+d_{S_x}^2)^3}\\ &= -\frac{1}{2\pi^2}\sum_{m,n}^{\infty}{}'\sum_{l=-\infty}^{\infty}\frac{(-1)^l}{d_{S_x}^4}\end{aligned} \tag{3.65}$$

The total energy is

$$E_2^{S_x} = ab\int\varepsilon_2^{+--}dx = -\frac{bc}{2\pi^2}\int_0^c\sum_{m,n}^{\infty}{}'\sum_{l=-\infty}^{\infty}\frac{(-1)^l}{[(2la+2x)^2+(2mb)^2+(2nc)^2]^2}dx = 0 \tag{3.66}$$

This is the significant difference: the contribution from side paths where mixed B.C. occur is zero.

d. Contribution from Edge Paths E_{yz}

The energy density contributed by edge paths is

$$\begin{aligned}\varepsilon_2^{-++} &= -\frac{1}{2}\lim_{t\to 0}\frac{\partial^2}{\partial t^2}V_2^{-++} = -\frac{1}{2\pi^2}\lim_{t\to 0}\sum_{l,m,n}^{\infty}\frac{(-1)^l(d_{E_{yz}}^2-3t^2)}{(t^2+d_{E_{yz}}^2)^3}\\ &= -\frac{1}{2\pi^2}\sum_{m,n=-\infty}^{\infty}\sum_{l=-\infty}^{\infty}{}'\frac{(-1)^l}{d_{E_{yz}}^4}\end{aligned} \tag{3.67}$$

The total energy is

$$\begin{aligned}E_2^{E_{yz}} = a\int\varepsilon_2^{-++}dydz &= -\frac{a}{2\pi^2}\int_0^b\int_0^c\sum_{m,n=-\infty}^{\infty}\sum_{l=-\infty}^{\infty}{}'\frac{(-1)^l dydz}{[(2la)^2+(2mb+2y)^2+(2nc+2z)^2]^2}\\ &= \frac{\pi}{192a}\end{aligned} \tag{3.68}$$

e. Contribution from Edge Paths E_{xz}

The energy density contributed by edge path $d_{lmn}^{E_{xz}}$ is

$$\begin{aligned}\varepsilon_2^{+-+} &= -\frac{1}{2}\lim_{t\to 0}\frac{\partial^2}{\partial t^2}V_2^{+-+} = -\frac{1}{2\pi^2}\lim_{t\to 0}\sum_{l,m,n}^{\infty}\frac{(-1)^l(d_{E_{xz}}^2-3t^2)}{(t^2+d_{E_{xz}}^2)^3}\\ &= -\frac{1}{2\pi^2}\sum_{l,n=-\infty}^{\infty}{\sum_{m=-\infty}^{\infty}}'\frac{(-1)^l}{d_{E_{xz}}^4}\end{aligned} \tag{3.69}$$

The total energy is

$$\begin{aligned}E_2^{E_{xz}} = b\int\varepsilon_2^{+-+}dxdz &= -\frac{b}{2\pi^2}\int_0^a\int_0^c\sum_{l,n=-\infty}^{\infty}{\sum_{m=-\infty}^{\infty}}'\frac{(-1)^l dxdz}{[(2la+2x)^2+(2mb)^2+(2nc+2z)^2]^2}\\ &= 0\end{aligned} \tag{3.70}$$

Same property holds for edge paths E_{xy}:

$$E_2^{E_{xz}} = 0 \tag{3.71}$$

f. Contribution from Corner Paths

The energy density contributed by corner path d_C is:

$$\varepsilon_2^{+++} = -\frac{1}{2}\lim_{t\to 0}\frac{\partial^2}{\partial t^2}V_2^{+++} = -\frac{1}{2\pi^2}\lim_{t\to 0}\sum_{l,m,n=-\infty}^{\infty}{}'\frac{(-1)^l(d_C^2-3t^2)}{[t^2+d_C^2]^3} \tag{3.72}$$

The total energy contributed by corner path is:

$$\begin{aligned}E_2^C &= \int\varepsilon_2^{+++}dxdydz\\ &= -\frac{1}{2\pi^2}\int_0^a\int_0^b\int_0^c\sum_{l,m,n=-\infty}^{\infty}{}'\frac{(-1)^l((2la+2x)^2+(2mb+2y)^2+(2nc+2z)^2-3t^2)}{[t^2+(2la+2x)^2+(2mb+2y)^2+(2nc+2z)^2]^3}dxdydz\\ &= 0\end{aligned} \tag{3.73}$$

Thus we have obtained the total energy contributed from all paths, listed in Table IV:

Table IV. Table of total energy by path types for 2nd kind B.C., mixed B.C. on base and partition

Path Type	Total Energy
Periodic Path	$E_2^P = -\frac{abc}{32\pi^2}\sum{}' \frac{(-1)^l}{[(la)^2+(mb)^2+(nc)^2]^2}$
Side Paths	$E_2^{S_x} = 0$
	$E_2^{S_y} = -\frac{ac}{64\pi}\sum{}' \frac{(-1)^l}{[(la)^2+(nc)^2]^{\frac{3}{2}}}$
	$E_2^{S_z} = -\frac{ab}{64\pi}\sum{}' \frac{(-1)^l}{[(la)^2+(mb)^2]^{\frac{3}{2}}}$
Edge Paths	$E_2^{E_{xy}} = 0$
	$E_2^{E_{yz}} = \frac{\pi}{192a}$
	$E_2^{E_{xz}} = 0$
Corner Path	$E_2^C = 0$

The total energy for a general rectangular cavity with 2nd kind B.C. is

$$E_2^{\alpha\beta\gamma} = E_2^P + \eta_\alpha E_2^{S_x} + \eta_\beta E_2^{S_y} + \eta_\gamma E_2^{S_z} + \eta_\alpha\eta_\beta E_2^{E_{xy}} + \eta_\beta\eta_\gamma E_2^{E_{yz}} + \eta_\alpha\eta_\gamma E_2^{E_{xz}} + \eta_\alpha\eta_\beta\eta_\gamma E_2^C \quad (3.74)$$

where $\eta_{DD} = -1$, $\eta_{NN} = 1$ and $\eta_M = 1$ as defined before.

For the purpose of studying the piston with hybrid B.C. (Neumann B.C. at $x = a$ and Dirichlet B.C. elsewhere)

$$E_2^{MDD} = E_2^P + E_2^{S_x} - E_2^{S_y} - E_2^{S_z} - E_2^{E_{xy}} + E_2^{E_{yz}} - E_2^{E_{xz}} \quad (3.75)$$

3. Casimir Force for Hybrid Scalar Piston

The total energy of a rectangular cavity $a \times b \times c$ with Neumann B.C. at $x = a$ and Dirichlet B.C. elsewhere is written in (3.75). Since our concern is the $a-$dependent terms, we shorten this to

$$E_{abc}^{MDD} = E_{abc}^{P} - E_{abc}^{S_y} - E_{abc}^{S_z} + E_{abc}^{E_{yz}} \tag{3.76}$$

Next we extend the rectangular cavity along the x direction to form a piston with the $x = a$ face as the partition; the total energy of the the second rectangular cavity $(L-a) \times b \times c$ is

$$E_{L-a,b,c}^{MDD} = E_{L-a,b,c}^{P} - E_{L-a,b,c}^{S_y} - E_{L-a,b,c}^{S_z} + E_{L-a,b,c}^{E_{yz}} \tag{3.77}$$

The total energy of the whole piston is the sum of the total energy of two rectangular cavities with B.C. of 2nd kind:

$$\begin{aligned} E_2^{MDD} =& E_{abc}^{MDD} + E_{L-a,b,c}^{MDD}|_{L\to\infty} \\ =& -\frac{abc}{32\pi^2} \sum_{l\neq 0,m,n} \frac{(-1)^l}{[(la)^2+(mb)^2+(nc)^2]^2} + \frac{ab}{64\pi} \sum_{l\neq 0,m} \frac{(-1)^l}{[(la)^2+(mb)^2]^{\frac{3}{2}}} \\ &+ \frac{ac}{64\pi} \sum_{l\neq 0,n} \frac{(-1)^l}{[(la)^2+(nc)^2]^{\frac{3}{2}}} + \frac{\pi}{192}\frac{1}{a} \end{aligned} \tag{3.78}$$

Taking the derivative of E with respect to a, we can get the force,

$$F_2^{MDD} = F_2^{P} - F_2^{S_y} - F_2^{S_z} + F_2^{E_{yz}} \tag{3.79}$$

where

$$
\begin{aligned}
F_2^P &= -\frac{\partial}{\partial a}E_2^P = \frac{bc}{32\pi^2}\sum_{l\neq 0,m,n}[\frac{(-1)^l}{[(la)^2+(mb)^2+(nc)^2]^2} - \frac{(-1)^l 4l^2a^2}{[(la)^2+(mb)^2+(nc)^2]^3}] \\
F^{S_y} &= -\frac{\partial}{\partial a}E_2^{S_y} = \frac{b}{64\pi}\sum_{l\neq 0,m}[\frac{(-1)^l}{[(la)^2+(mb)^2]^{\frac{3}{2}}} - \frac{(-1)^l 3l^2a^2}{[(la)^2+(mb)^2]^{\frac{5}{2}}}] \\
F^{S_z} &= -\frac{\partial}{\partial a}E_2^{S_z} = \frac{c}{64\pi}\sum_{l\neq 0,n}[\frac{(-1)^l}{[(la)^2+(nc)^2]^{\frac{3}{2}}} - \frac{(-1)^l 3l^2a^2}{[(la)^2+(nc)^2]^{\frac{5}{2}}}] \\
F_2^{E_{yz}} &= -\frac{\partial}{\partial a}E_2^{E_{yz}} = \frac{\pi}{192}\frac{1}{a^2}
\end{aligned}
\tag{3.80}
$$

Letting $b = c$ and $\eta = \frac{a}{c}$, we can rewrite the piston force as

$$
\begin{aligned}
F_2^P &= \frac{1}{32\pi^2 b^2}\sum_{l\neq 0,m,n}[\frac{(-1)^l}{[l^2\eta^2+m^2+n^2]^2} - \frac{(-1)^l 4l^2\eta^2}{[l^2\eta^2+m^2+n^2]^3}] \\
F_2^{S_y} &= F_2^{S_z} = \frac{1}{64\pi b^2}\sum_{l\neq 0,n}[\frac{(-1)^l}{[l^2\eta^2+n^2]^{\frac{3}{2}}} - \frac{(-1)^l 3l^2\eta^2}{[l^2\eta^2+n^2]^{\frac{5}{2}}}] \\
F_2^{E_{yz}} &= \frac{\pi}{192b^2}\frac{1}{\eta^2}
\end{aligned}
\tag{3.81}
$$

We can easily extend our argument to more general cases such as $DN-DD-NN$ and $DN-NN-NN$. From (3.74) the Casimir force F_2^{MDN} for $DN-DD-NN$ piston ($\eta_\alpha = 1, \eta_\beta = -1, \eta_{\gamma=1}$) and F_2^{MNN} for $DN-NN-NN$ piston ($\eta_\alpha = 1, \eta_\beta = 1, \eta_\gamma = 1$) are

$$
\begin{aligned}
F_2^{MNN} =& F_2^P + F_2^{S_y} + F_2^{S_z} + F_2^{E_{yz}} \\
F_2^{MDN} =& F_2^P - F_2^{S_y} + F_2^{S_z} - F_2^{E_{yz}} = F_2^P - F_2^{E_{yz}}
\end{aligned}
\tag{3.82}
$$

In Fig.5, we plot F_2^{MNN}, F_2^{MDN} and F_2^{MDD}. At the limit $\eta \to 0$, the piston force is the same as the parallel-plate force with Dirichlet B.C. on one plate and Neumann B.C. on the other plate. The periodic paths' contribution F_2^P is still the dominant term, so the force is always repulsive. The sides' effect are brought in with η increasing. For side paths and edge paths, when they have same sign as the periodic paths, we call it contributing positively, otherwise negatively. For F_2^{MNN}, side paths and edge paths all contribute positively, so it

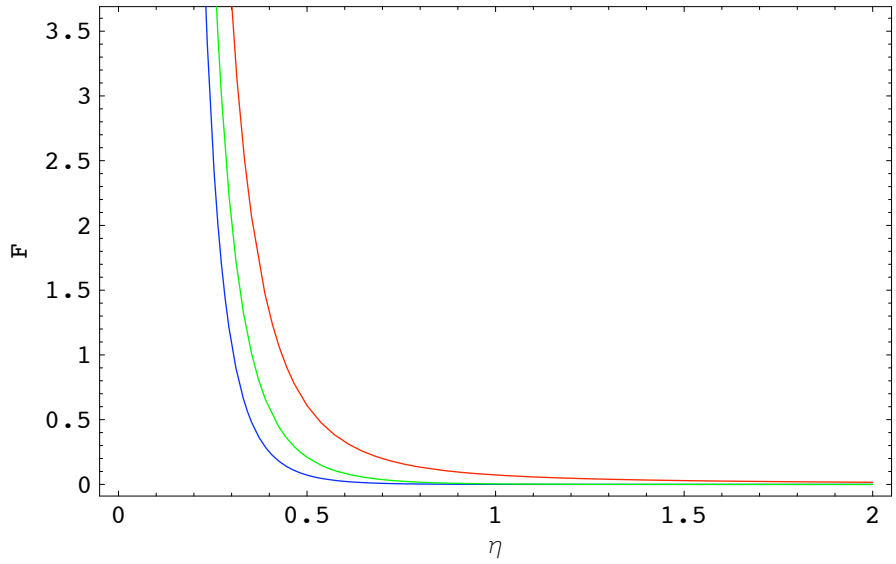

Fig. 5. The force F on a piston with square cross section ($b = c$) as functions of $\eta = a/b$. red=$F_2^{DN-NN-NN}$, blue=$F_2^{DN-DD-DD}$ and green=$F_2^{DN-DD-NN}$.

has the greatest magnitude. For F_2^{MDD}, side paths and contribute negatively and edge path contribute positively, so it has the least magnitude and damps most quickly. F_2^{MDN} is in the middle since side paths' contribution is greater than edges'.

4. Casimir Force for Scalar Piston with the Mixed B.C. on Sides

There is another kind of B.C. for the piston with the partition at $x = a$, which has both Dirichlet/Neumann B.C. at $x = 0, a$, but mixed B.C. at $y = 0, b$ or $z = 0, c$, such as $NN - DN - NN$ and $NN - DN - DD$. We fix the mixed B.C. at $y = 0, b$, that is, Dirichlet B.C. at $y = 0$ and Neumann at $y = b$. The total energy for each kind of path will differ from the previous cases; we have to make some adaptations for the position change of mixed B.C. as in Table V.

Since the partition is still at $x = a$, for the Casimir force, we need only the a-dependent terms; there are only 2 such now, E_2^P and $E_2^{S_z}$. The corresponding piston forces from these

Table V. Table of total energy by path types for 2nd kind B.C., mixed B.C. on sides

Path Type	Total Energy
Periodic Path	$E_2^P = -\frac{abc}{32\pi^2}\sum{}' \frac{(-1)^m}{[(la)^2+(mb)^2+(nc)^2]^2}$
Side Paths	$E_2^{S_x} = -\frac{bc}{64\pi}\sum{}' \frac{(-1)^m}{[(mb)^2+(nc)^2]^{\frac{3}{2}}}$
	$E_2^{S_y} = 0$
	$E_2^{S_z} = -\frac{ab}{64\pi}\sum{}' \frac{(-1)^m}{[(la)^2+(mb)^2]^{\frac{3}{2}}}$
Edge Paths	$E_2^{E_{xy}} = 0$
	$E_2^{E_{yz}} = 0$
	$E_2^{E_{xz}} = \frac{\pi}{192b}$
Corner Path	$E_2^C = 0$

two energies are

$$
\begin{aligned}
F_2^P &= \frac{1}{32\pi^2 b^2}\sum_{l\neq 0,m,n}\left[\frac{(-1)^m}{[l^2\eta^2+m^2+n^2]^2} - \frac{(-1)^m 4l^2\eta^2}{[l^2\eta^2+m^2+n^2]^3}\right] \\
F_2^{S_z} &= \frac{1}{64\pi b^2}\sum_{l\neq 0,n}\left[\frac{(-1)^m}{[l^2\eta^2+n^2]^{\frac{3}{2}}} - \frac{(-1)^m 3l^2\eta^2}{[l^2\eta^2+n^2]^{\frac{5}{2}}}\right]
\end{aligned}
\tag{3.83}
$$

So the Casimir force becomes

$$
\begin{aligned}
F_2^{DMN} &= F_2^{NMN} = F_2^P + F_2^{S_z} \\
F_2^{DMD} &= F_2^{NMD} = F_2^P - F_2^{S_z}
\end{aligned}
\tag{3.84}
$$

These two forces are plotted in Fig. 6. At the limit $\eta \to 0$, the piston force is the same as the force between two Neumann parallel plates. The force is always attractive. There is no edge effect. F_2^{NMD} damps more quickly than F_2^{NMN}.

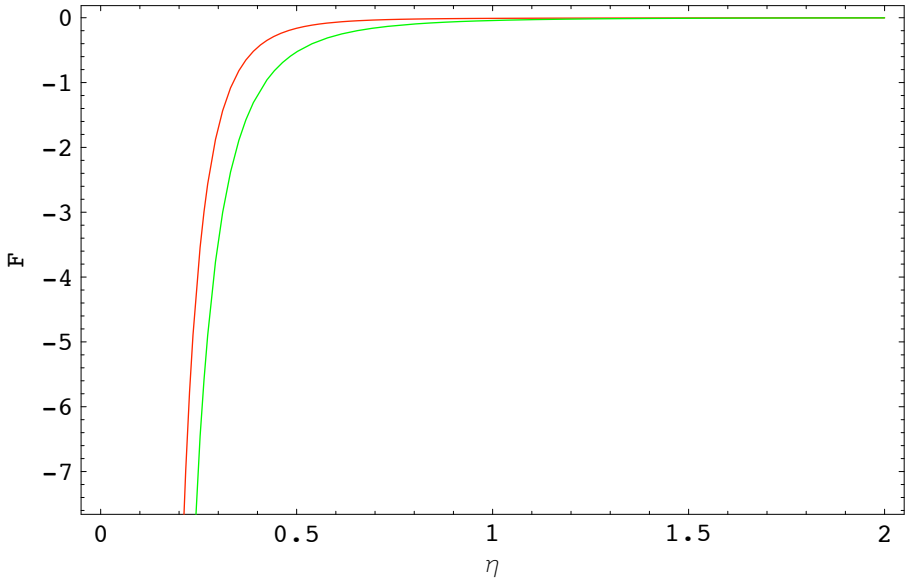

Fig. 6. The force F on a piston with square cross section ($b = c$) as functions of $\eta = a/b$. Red=F_2^{NMD} and Green=F_2^{NMN}.

C. Casimir Force for Scalar Piston with B.C. of 3rd Kind

The 3rd kind of B.C. means, there are two pair of faces with mixed B.C. and the other pair have both Dirichlet B.C. or both Neumann B.C. on the opposite faces. This kind of B.C. includes: $DN-DN-DD$, $DN-DN-NN$, $DD-DN-DN$, $NN-DN-DN$.

1. Cylinder Kernel for Scalar Piston with 3rd Kind of B.C.

$$\overline{T}^{\alpha\beta\gamma} = V_3^{---} + \eta_\alpha V_3^{+--} + \eta_\beta V_3^{-+-} + \eta_\gamma V_3^{--+} + \eta_\alpha\eta_\beta V_3^{++-} + \eta_\beta\eta_\gamma V_3^{-++} + \eta_\alpha\eta_\gamma V_3^{+-+} + \eta_\alpha\eta_\beta\eta_\gamma V_3^{+++} \tag{3.85}$$

where

$$V_3^{\varepsilon_1\varepsilon_2\varepsilon_3} = -\frac{1}{2\pi^2}\sum_{l,m,n=-\infty}^{\infty}\frac{(-1)^l(-1)^m}{t^2+(2la+x+\varepsilon_1 x)^2+(2mb+y+\varepsilon_2 y)^2+(2nc+z+\varepsilon_3 z)^2} \tag{3.86}$$

2. Casimir Force for Scalar Piston with 3rd Kind of B.C.

a. When Mixed B.C. Are on Base and Partition $x = 0, a$

When the two mixed B.C. are imposed at $x = 0, a$ and $y = 0, b$, such as $DN - DN - DD$, $DN - DN - NN$, the total energy contributed by different kinds of paths is listed in Table VI:

Table VI. Table of total energy by path types for 3rd B.C., mixed B.C. on base and partition

Path Type	Total Energy
Periodic Path	$E_3^P = -\frac{abc}{32\pi^2}\sum{}' \frac{(-1)^l(-1)^m}{[(la)^2+(mb)^2+(nc)^2]^2}$
Side Paths	$E_3^{S_x} = 0$
	$E_3^{S_y} = 0$
	$E_3^{S_z} = -\frac{ab}{64\pi}\sum{}' \frac{(-1)^l(-1)^m}{[(la)^2+(mb)^2]^{\frac{3}{2}}}$
Edge Paths	$E_3^{E^{xy}} = 0$
	$E_3^{E^{yz}} = 0$
	$E_3^{E^{xz}} = 0$
Corner Path	$E_3^C = 0$

There are only two nonzero terms E_3^P and $E_3^{S_z}$; they are both $a-$dependent. The corresponding piston forces from these two energies are

$$\begin{aligned} F_3^P &= \frac{1}{32\pi^2 b^2}\sum_{l\neq 0,m,n}\left[\frac{(-1)^l(-1)^m}{[l^2\eta^2+m^2+n^2]^2} - \frac{(-1)^l(-1)^m 4l^2\eta^2}{[l^2\eta^2+m^2+n^2]^3}\right] \\ F_3^{S_z} &= \frac{1}{64\pi b^2}\sum_{l\neq 0,n}\left[\frac{(-1)^l(-1)^m}{[l^2\eta^2+n^2]^{\frac{3}{2}}} - \frac{(-1)^l(-1)^m 3l^2\eta^2}{[l^2\eta^2+n^2]^{\frac{5}{2}}}\right] \end{aligned} \tag{3.87}$$

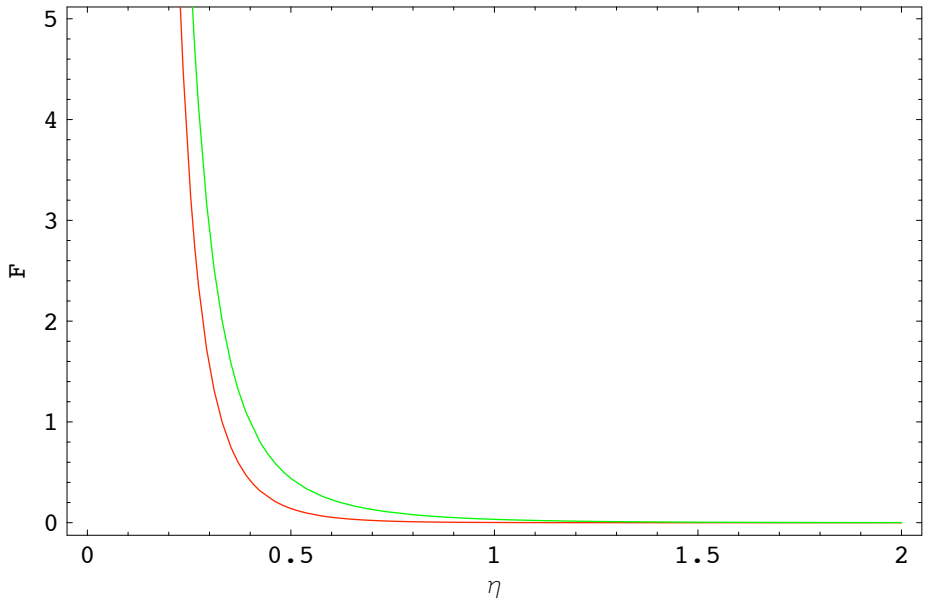

Fig. 7. The force F on a piston with square cross section ($b = c$) as functions of $\eta = a/b$. Red=F_3^{MMD} and Green=F_3^{MMN}.

So the Casimir force becomes

$$\begin{aligned} F_3^{MMN} &= F_3^P + F_3^{S_z} \\ F_3^{MMD} &= F_3^P - F_3^{S_z} \end{aligned} \tag{3.88}$$

These two force are plotted in Fig. 7. They are both repulsive and reduce to the force between two parallel plates with Dirichlet B.C. on one plate and Neumann B.C. on another as $\eta \to 0$.

b. When Mixed B.C. Are Not on Base and Partition $x = 0, a$

When the two mixed B.C. are imposed at $y = 0, b$ and $z = 0, c$, the cases $DD - DN - DN$ and $NN - DN - DN$, we have both Dirichlet or both Neumann B.C. on base and partition. The total energy contributed by different kinds of paths is listed in Table VII:

Table VII. Table of total energy by path types for 3rd B.C., mixed B.C. on sides

Path Type	Total Energy
Periodic Path	$E_3^P = -\frac{abc}{32\pi^2}\sum{}' \frac{(-1)^m(-1)^n}{[(la)^2+(mb)^2+(nc)^2]^2}$
Side Paths	$E_3^{S_x} = -\frac{bc}{64\pi}\sum{}' \frac{(-1)^m(-1)^n}{[(mb)^2+(nc)^2]^{\frac{3}{2}}}$
	$E_3^{S_y} = 0$
	$E_3^{S_z} = 0$
Edge Paths	$E_3^{E_{xy}} = 0$
	$E_3^{E_{yz}} = 0$
	$E_3^{E_{xz}} = 0$
Corner Path	$E_3^C = 0$

The only $a-$dependent term is E_3^P, so the piston force is

$$F_3^{NMM} = F_3^{DMM} = F_3^P = \frac{1}{32\pi^2 b^2}\sum_{l\neq 0,m,n}\left[\frac{(-1)^m(-1)^n}{[l^2\eta^2+m^2+n^2]^2} - \frac{(-1)^m(-1)^n 4l^2\eta^2}{[l^2\eta^2+m^2+n^2]^3}\right] \tag{3.89}$$

This force are plotted in Fig. 8. It is attractive and reduces to the Neumann parallel-plate force as $\eta \to 0$.

D. Casimir Force for Scalar Piston with 4th Kind of B.C.

The 4th kind of B.C. means, the three pair of faces are all equipped with mixed B.C. on the opposite faces: $DN - DN - DN$.

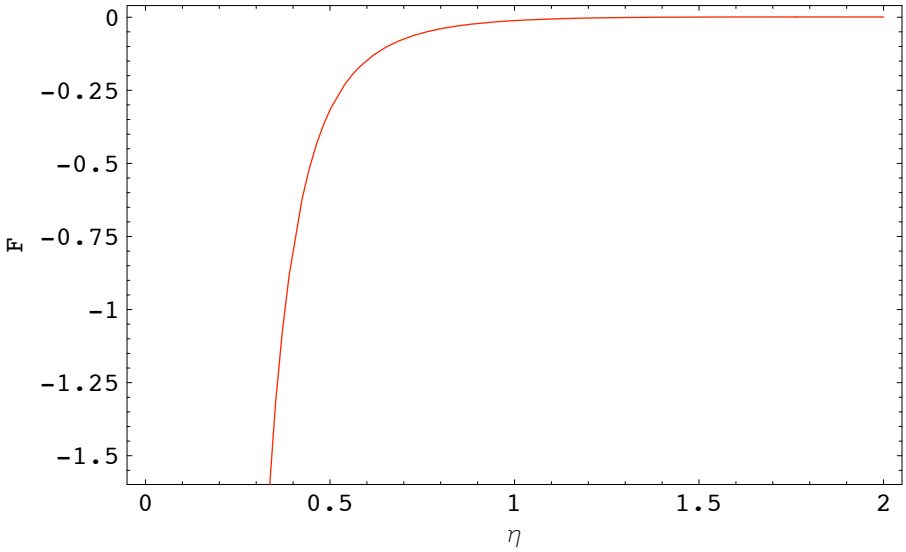

Fig. 8. The force F_3^{NMM} on a piston with square cross section ($b = c$) as functions of $\eta = a/b$.

1. Cylinder Kernel for Scalar Piston with 4th Kind of B.C.

$$\overline{T}^{\alpha\beta\gamma} = V_4^{---} + \eta_\alpha V_4^{+--} + \eta_\beta V_4^{-+-} + \eta_\gamma V_4^{--+} + \eta_\alpha\eta_\beta V_4^{++-} + \eta_\beta\eta_\gamma V_4^{-++} + \eta_\alpha\eta_\gamma V_4^{+-+} + \eta_\alpha\eta_\beta\eta_\gamma V_4^{+++} \tag{3.90}$$

where

$$V_4^{\varepsilon_1\varepsilon_2\varepsilon_3} = -\frac{1}{2\pi^2}\sum_{l,m,n=-\infty}^{\infty}\frac{(-1)^l(-1)^m(-1)^n}{t^2+(2la+x+\varepsilon_1 x)^2+(2mb+y+\varepsilon_2 y)^2+(2nc+z+\varepsilon_3 z)^2} \tag{3.91}$$

2. Casimir Force for Scalar Piston with 4th Kind of B.C.

The only nonzero $a-$dependent term is $E_4^P = -\frac{abc}{32\pi^2}\sum'\frac{(-1)^l(-1)^m(-1)^n}{[(la)^2+(mb)^2+(nc)^2]^2}$. So the piston force is

$$F_4^{MMM} = F_4^P = \frac{1}{32\pi^2 b^2}\sum_{l\neq 0,m,n}\left[\frac{(-1)^l(-1)^m(-1)^n}{[l^2\eta^2+m^2+n^2]^2} - \frac{(-1)^l(-1)^m(-1)^n 4l^2\eta^2}{[l^2\eta^2+m^2+n^2]^3}\right] \tag{3.92}$$

This force is plotted in Fig. 9.

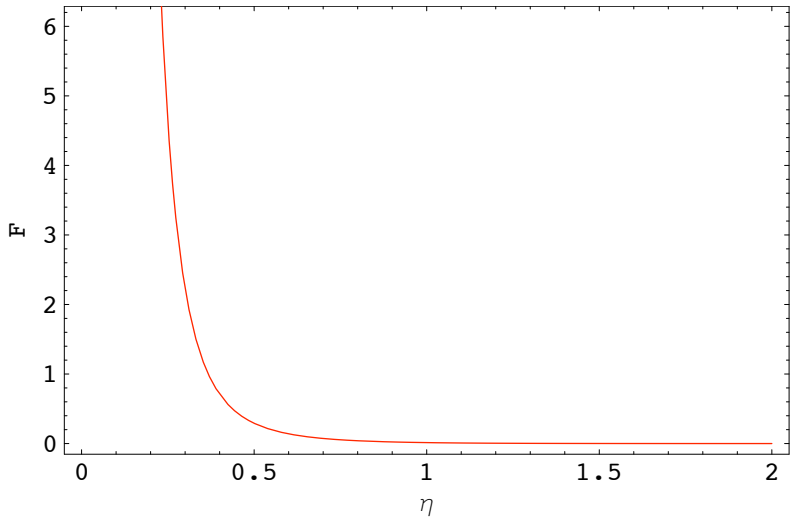

Fig. 9. The force F_4^{MMM} on a piston with square cross section ($b = c$) as function of $\eta = a/b$.

E. Conclusion

For a rectangular piston geometry, which includes 2 rectangular cavities $a \times b \times c$ and $(L-a) \times b \times c$, if we fix the partition on the $x = a$ face, there are 4 kinds of possible B.C. for the cavity $a \times b \times c$; the B.C. for the cavity $(L-a) \times b \times c$ will be the same. The general properties for each kind of B.C. are: (1) There are only 4 $a-$dependent terms, which are contributed by periodic paths, side paths S_y and S_z and edge paths E_{yz}. For some kinds of B.C., side paths' contribution and edge paths' contribution might be absent; however, periodic paths' contribution always stays and dominates. (2) The relative weight from different kinds of paths is different; the contribution from periodic path always dominates, then that of the side paths, then that of edge paths the least if it exists. (3) When the mixed B.C. are at $x = 0, a$, the piston force on the partition is always repulsive with the parallel-plate force as the $a \to 0$ limit. But when DD or NN B.C. are at $x = 0, a$, the piston force is always attractive. Let's rewrite the general formula for piston force as

$$F^{\alpha\beta\gamma} = F^P + \eta_\beta F^{S_y} + \eta_\gamma F^{S_z} + \eta_\beta \eta_\gamma F^{E_{yz}} \tag{3.93}$$

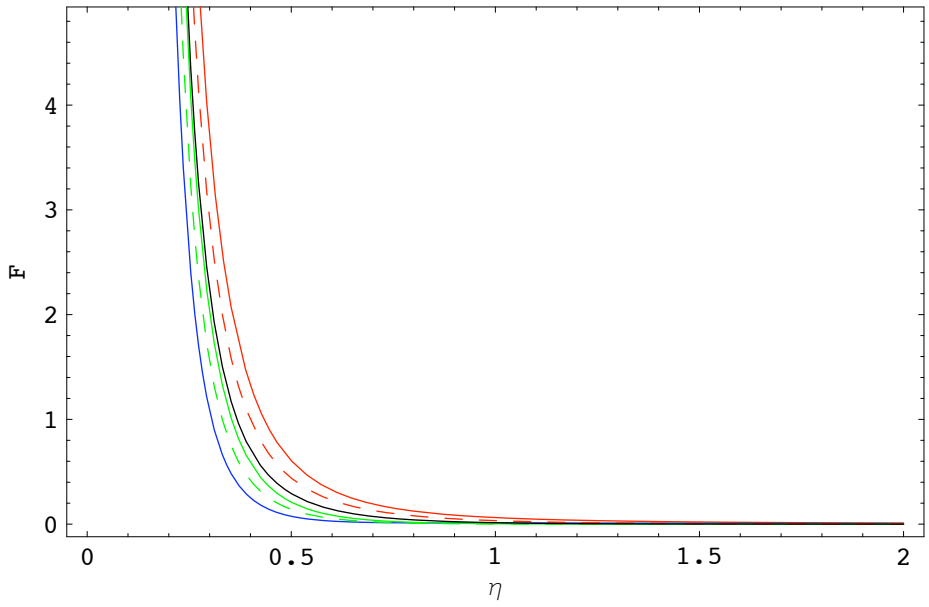

Fig. 10. The force F on a piston with square cross section ($b = c$) as functions of $\eta = a/b$. Solid red= F_2^{MNN}, dashed red= F_3^{MMN}, solid black= F_4^{MMM}, solid green= F_2^{MDN}, dashed green= F_3^{MMD} and solid blue= F_2^{MDD}.

Again α, β, γ take a value from DD, NN and M and $\eta_{DD} = -1$, $\eta_{NN} = 1$ and $\eta_M = 1$. Notice that η_α does not appear in this formula; η_β and η_γ determine the sign of side paths and the product of η_β and η_γ determines the sign of edge paths. (4) When no mixed B.C. is included on sides ($y = 0, b; z = 0, c$), we have a contribution from each kind of path. When 1 mixed B.C. is included on the sides, the energy from edge paths will be zero and hence $F^{E_{yz}}$ is absent; furthermore, when the mixed B.C. are at $y = 0, b$, then E_{S_y} is zero and F_{S_y} will be absent and similarly $F_{S_z} = 0$ when the mixed B.C. are at $z = 0, c$. When the B.C. on sides are both mixed B.C., we see that the contributions from side paths and edge paths are all absent and only periodic paths contribute.

We plot the piston force for all cases with mixed B.C. at $x = 0, a$ in Fig. 10. Neumann B.C. on sides make a positive contribution to the force since $\eta_{NN} = 1$, while Dirichlet B.C. on sides make a negative contribution due to $\eta_{DD} = -1$. For mixed B.C. on sides, although $\eta_M = 1$ the corresponding energy is absent so there is no side-path contribution; that is why

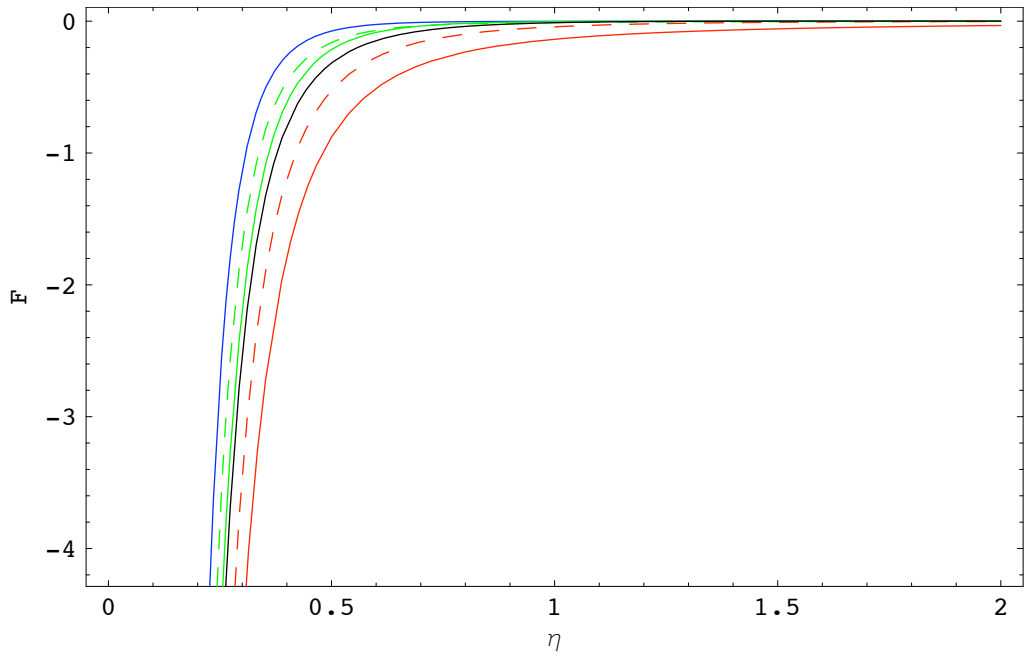

Fig. 11. The force F on a piston with square cross section ($b = c$) as functions of $\eta = a/b$. Solid red= F_1^{NNN}, dashed red= F_2^{NMN}, solid black= F_3^{NMM}, solid green= F_1^{NDN}, dashed green= F_2^{NMD} and solid blue= F_1^{NDD}.

the mixed B.C. effect is intermediate in strength between Neumann and Dirichlet B.C.. The same argument applies for the piston with Neumann B.C. at both $x = 0$ and $x = a$, the forces are plotted in Fig. 11. Since η_α does not affect the piston force, if we switch NN on $x = 0, a$ to DD, the piston force will stay unchanged for corresponding B.C.. At the limit $\eta \to 0$, we can omit the effect from sides and the piston will reduce to corresponding parallel plates. As η increases, the piston force damps rapidly but the effect from sides becomes greater.

CHAPTER IV

3D PISTON FOR ELECTROMAGNETIC FIELD—HERTZ POTENTIAL APPROACH

We have studied the 3D piston thoroughly for a scalar field, with general B.C. considered. If we can relate the Electromagnetic (EM) piston problem to corresponding scalar piston problems, it will be significantly convenient. A candidate to do so is Hertz potentials, which represent the EM field by 2 scalar fields. The essential equation of EM field is the Maxwell's equation:

$$\nabla \cdot \mathbf{E} = 0; \qquad \nabla \times \mathbf{B} = 0 \tag{4.1}$$

We can obtain $\mathbf{E}$ and $\mathbf{B}$ from the 4-vector $(\Phi, \mathbf{A})$ under Lorentz gauge $\nabla \cdot \mathbf{A} + \partial_t \Phi = 0$

$$\begin{aligned} \mathbf{E} &= -\nabla\Phi - \partial_t \mathbf{A} \\ \mathbf{B} &= \nabla \times \mathbf{A} \end{aligned} \tag{4.2}$$

However, that is not the only way to express the EM field. Let us define two vectors as below [41, 42, 43]:

$$(\Phi, \mathbf{A}) = (-\nabla \cdot \mathbf{\Pi}_e, \partial_t \mathbf{\Pi}_e + \nabla \times \mathbf{\Pi}_m) \tag{4.3}$$

We can rewrite the Maxwell's equation and get $\mathbf{E}$ and $\mathbf{B}$ expressed in terms of $\mathbf{\Pi}_e$ and $\mathbf{\Pi}_m$; they are the so called Hertz potentials. For a highly symmetric geometry such as a rectangular cavity, it turns out very convenient to express the EM field by two scalar fields, also called Hertz potentials. We can single out one particular direction, say $\vec{e}_3$, and choose the Hertz potentials as $\mathbf{\Pi}_e = \varphi \vec{e}_3$ and $\mathbf{\Pi}_m = \psi \vec{e}_3$; then [42]

$$(\Phi, \mathbf{A}) = (-\partial_3 \phi, \partial_2 \psi, -\partial_1 \psi, \partial_0 \varphi) \tag{4.4}$$

It's straightforward that if ϕ and ψ satisfy the wave equation themselves, $\Box\phi = 0$ and $\Box\psi = 0$, then the Maxwell's equation is satisfied. We can always obtain $\mathbf{E}$ and $\mathbf{B}$ expressed

by these 2 Hertz potentials:

$$\begin{aligned}\mathbf{E} &= -\nabla\Phi - \partial_t\mathbf{A} = (\partial_1\partial_3\phi - \partial_0\partial_2\psi, \partial_2\partial_3\phi + \partial_0\partial_1\psi, \partial_3^2\phi - \partial_0^2\phi)\\ \mathbf{B} &= \nabla\times\mathbf{A} = (\partial_0\partial_2\phi - \partial_1\partial_3\psi, -\partial_0\partial_1\phi + \partial_2\partial_3\psi, \partial_3^2\psi - \partial_0^2\psi)\end{aligned} \tag{4.5}$$

For a surface, there are 2 typical boundary conditions for the EM field: Conducting Boundary Condition (CBC) indicates $E_t = 0, B_n = 0$ on the boundary and Permeable Boundary Condition (PBC) requires $E_n = 0, B_t = 0$ on the boundary. We investigate the piston with all faces CBC as our first example and then generalize to other kind of B.C..

A. Purely Conducting Piston

1. Implication of B.C.

A purely conducting piston is an extension of a rectangular cavity with CBC on each face. So we start our argument from a rectangular cavity. The CBC on each face requires that **E** and **B** have to satisfy the following equations

$$\begin{aligned} B_x|_{x=0,a} &= 0 \quad E_y = E_z|_{x=0,a} = 0\\ B_y|_{y=0,b} &= 0 \quad E_x = E_z|_{y=0,b} = 0\\ B_z|_{z=0,c} &= 0 \quad E_x = E_y|_{z=0,c} = 0\end{aligned} \tag{4.6}$$

Substituting (4.6) to (4.5), we obtain the corresponding constraints on the 2 scalar fields ϕ and ψ:

$$\begin{aligned} \phi_x|_{x=0,a} &= 0 \quad \partial_x\psi_x|_{x=0,a} = 0\\ \phi_y|_{y=0,b} &= 0 \quad \partial_y\psi_y|_{y=0,b} = 0\\ \partial_z\phi_z|_{z=0,c} &= 0 \quad \psi_z|_{z=0,c} = 0\end{aligned} \tag{4.7}$$

Therefore the appropriate normal modes of the Hertz potentials for the conducting cavity are

$$\begin{aligned}\phi_{lmn}(x,y,z) &= D_{lmn}\frac{\sin\frac{l\pi}{a}x\sin\frac{m\pi}{b}y\cos\frac{n\pi}{c}ze^{-i\omega_{lmn}t}}{|k^{\perp}_{lmn}|\sqrt{2\omega_{lmn}}}\\ \psi_{lmn}(x,y,z) &= D_{lmn}\frac{\cos\frac{l\pi}{a}x\cos\frac{m\pi}{b}y\sin\frac{n\pi}{c}ze^{-i\omega_{lmn}t}}{|k^{\perp}_{lmn}|\sqrt{2\omega_{lmn}}}\end{aligned} \tag{4.8}$$

where $\omega^2_{lmn} = k_1^2 + k_2^2 + k_3^2$, $k^2_{\perp} = k_1^2 + k_2^2$ and $k_1 = \frac{l\pi}{a}, k_2 = \frac{m\pi}{b}, k_3 = \frac{n\pi}{c}$. It follows from the canonical normalization conditions for **E** and **B** that:

$$|D_{lmn}|^2 = \frac{\epsilon_{0l}\epsilon_{0m}\epsilon_{0n}}{abc} \tag{4.9}$$

where $\epsilon_{0i} = 1$ for $i = 0$ and $\epsilon_{0i} = 2$ otherwise. Now we can go forward to give the expressions for the vacuum expectation value (VEV) of each components of **E** and **B**.

$$E^2_3(t-t',\mathbf{r},\mathbf{r}') = \sum_{l,m,n=1}^{\infty}\frac{|D_{lmn}|^2(k_1^2+k_2^2)}{2\omega_{lmn}}\sin k_1x\sin k_2y\cos k_3z\sin k_1x'\sin k_2y'\cos k_3z'e^{i\omega(t-t')} \tag{4.10}$$

$$\begin{aligned}E^2_{\perp}(t-t',\mathbf{r},\mathbf{r}') = &\sum_{l,m,n=1}^{\infty}\frac{|D_{lmn}|^2(k_2^2+k_3^2)}{2\omega_{lmn}}\cos k_1x\sin k_2y\sin k_3z\cos k_1x'\sin k_2y'\sin k_3z'e^{i\omega(t-t')}\\ &+\sum_{l,m,n}^{\infty}\frac{|D_{lmn}|^2(k_1^2+k_3^2)}{2\omega_{lmn}}\sin k_1x\cos k_2y\sin k_3z\sin k_1x'\cos k_2y'\sin k_3z'e^{i\omega(t-t')}\end{aligned} \tag{4.11}$$

$$B^2_3(t-t',\mathbf{r},\mathbf{r}') = \sum_{l,m,n=1}^{\infty}\frac{|D_{lmn}|^2(k_1^2+k_2^2)}{2\omega_{lmn}}\cos k_1x\cos k_2y\sin k_3z\cos k_1x'\cos k_2y'\sin k_3z'e^{i\omega(t-t')} \tag{4.12}$$

$$B_{\perp}^{2}(t-t',\mathbf{r},\mathbf{r}') = \sum_{l,m,n=1}^{\infty} \frac{|D_{lmn}|^2(k_2^2+k_3^2)}{2\omega_{lmn}} \sin k_1 x \cos k_2 y \cos k_3 z \sin k_1 x' \cos k_2 y' \cos k_3 z' e^{i\omega(t-t')} + \sum_{l,m,n}^{\infty} \frac{|D_{lmn}|^2(k_1^2+k_3^2)}{2\omega_{lmn}} \cos k_1 x \sin k_2 y \cos k_3 z \cos k_1 x' \sin k_2 y' \cos k_3 z' e^{i\omega(t-t')} \tag{4.13}$$

If we define $i\omega_{lmn}(t-t')$ as $-\omega_{lmn}\tau$ and convert (k_1^2, k_2^2, k_3^2) to $(-\partial_1^2, -\partial_2^2, -\partial_3^2)$, recalling the cylinder kernel definition in (3.15), we can relate the expressions above to cylinder kernels of the scalar field with various B.C.:

$$E_3^2(t,\mathbf{r},\mathbf{r}') = \frac{1}{2}(\partial_1^2+\partial_2^2)\overline{T}^{DDN}(t,\mathbf{r},\mathbf{r}') \tag{4.14}$$

$$E_{\perp}^2(t,\mathbf{r},\mathbf{r}') = \frac{1}{2}(\partial_2^2+\partial_3^2)\overline{T}^{NDD}(t,\mathbf{r},\mathbf{r}') + \frac{1}{2}(\partial_1^2+\partial_3^2)\overline{T}^{DND}(t,\mathbf{r},\mathbf{r}') \tag{4.15}$$

$$B_3^2(t,\mathbf{r},\mathbf{r}') = \frac{1}{2}(\partial_1^2+\partial_2^2)\overline{T}^{NND}(t,\mathbf{r},\mathbf{r}') \tag{4.16}$$

$$B_{\perp}^2(t,\mathbf{r},\mathbf{r}') = \frac{1}{2}(\partial_2^2+\partial_3^2)\overline{T}^{DNN}(t,\mathbf{r},\mathbf{r}') + \frac{1}{2}(\partial_1^2+\partial_3^2)\overline{T}^{NDN}(t,\mathbf{r},\mathbf{r}') \tag{4.17}$$

2. Energy Density and Total Energy

The energy density of EM field can be read from the stress tensor of the 00 component.

$$\begin{aligned}\varepsilon^{CCC}(\tau,\mathbf{r},\mathbf{r}) &= T_{00}(\tau,\mathbf{r},\mathbf{r}) = \frac{1}{2}(\mathbf{E}^2+\mathbf{B}^2)\\ &= \frac{1}{4}[(\partial_1^2+\partial_2^2)(\overline{T}^{DDN}+\overline{T}^{NND}) + (\partial_2^2+\partial_3^2)(\overline{T}^{NDD}+\overline{T}^{DNN}) + (\partial_1^2+\partial_3^2)(\overline{T}^{DND}+\overline{T}^{NDN})]\end{aligned} \tag{4.18}$$

Notice that the cylinder kernel $\overline{T}$ satisfies Laplace Equation:

$$(\partial_1^2+\partial_2^2+\partial_3^2)\overline{T} = \partial_0^2\overline{T} = -\partial_\tau^2\overline{T} \tag{4.19}$$

so the energy density can be simplified to

$$\varepsilon^{CCC}(\tau,\mathbf{r},\mathbf{r}) = -\partial_\tau^2 V_1^{---} - \partial_1^2 V_1^{-++} - \partial_2^2 V_1^{+-+} - \partial_3^2 V_1^{++-} \tag{4.20}$$

ecause that

$$\begin{aligned}
\partial_1^2 V_1^{-++} &= \partial_\tau^2 V_1^{-++} - \frac{4}{\pi^2}\sum_{lmn}^{\infty}\frac{(2la)^2 - t^2}{(d_{lmn}^{E_{yz}})^6} \\
\partial_2^2 V_1^{+-+} &= \partial_\tau^2 V_1^{+-+} - \frac{4}{\pi^2}\sum_{lmn}^{\infty}\frac{(2mb)^2 - t^2}{(d_{lmn}^{E_{xz}})^6} \\
\partial_3^2 V_1^{++-} &= \partial_\tau^2 V_1^{++-} - \frac{4}{\pi^2}\sum_{lmn}^{\infty}\frac{(2nc)^2 - t^2}{(d_{lmn}^{E_{xy}})^6}
\end{aligned} \tag{4.21}$$

he energy density for a rectangular cavity with CBC on each face is

$$\begin{aligned}
\varepsilon^{CCC}(\tau, \mathbf{r}, \mathbf{r}) = &- \partial_\tau^2[V_1^{---} + V_1^{-++} + V_1^{+-+} + V_1^{++-}] \\
&+ \frac{4}{\pi^2}\sum_{lmn}^{\infty}[\frac{(2la)^2 - t^2}{(d_{lmn}^{E_{yz}})^6} + \frac{(2mb)^2 - t^2}{(d_{lmn}^{E_{xz}})^6} + \frac{(2nc)^2 - t^2}{(d_{lmn}^{E_{xy}})^6}]
\end{aligned} \tag{4.22}$$

Integrate over the cavity to get the total energy:

$$\begin{aligned}
E_{abc}^{CCC} =& 2[E_1^P + E_1^{E_{yz}} + E_1^{E_{xz}} + E_1^{E_{xy}}] + \frac{\pi}{24a} + \frac{\pi}{24b} + \frac{\pi}{24c} \\
=& E_1^{DDD} + E_1^{NNN} + \frac{\pi}{24a} + \frac{\pi}{24b} + \frac{\pi}{24c} \\
=& -\frac{abc}{16\pi^2} Z_3(a, b, c; 4) + \frac{\pi}{48a} + \frac{\pi}{48b} + \frac{\pi}{48c}
\end{aligned} \tag{4.23}$$

3. Casimir Force for Purely Conducting Piston

We extend the rectangular cavity along the x direction to form a piston with the partition at $x = a$. The energy of the second rectangular cavity $(L - a) \times b \times c$ is

$$\begin{aligned}
E_{(L-a)bc}^{CCC}|_{L\to\infty} =& -\frac{(L-a)bc}{16\pi^2}{\sum_{l,m,n=-\infty}^{\infty}}' \frac{1}{[(l(L-a))^2 + (mb)^2 + (nc)^2]^2} + \frac{\pi}{48(L-a)} \\
=& \frac{abc}{16\pi^2}{\sum_{m,n=-\infty}^{\infty}}' \frac{1}{[(mb)^2 + (nc)^2]^2}
\end{aligned} \tag{4.24}$$

Here we discard the $a-$independent terms. The total energy of the piston is the sum of energies from two rectangular cavities: $a \times b \times c$ and $(L-a) \times b \times c$.

$$\begin{aligned} E^{CCC} =& E^{CCC}_{abc} + E^{CCC}_{L-a,b,c}|_{L\to\infty} \\ =& -\frac{abc}{16\pi^2} {\sum_{l,m,n=-\infty}^{\infty}}' \frac{1}{[(la)^2+(mb)^2+(nc)^2]^2} + \frac{\pi}{48a} + \frac{abc}{16\pi^2} {\sum_{m,n=-\infty}^{\infty}}' \frac{1}{[((mb)^2+(nc)^2]^2} \\ =& -\frac{abc}{16\pi^2} \sum_{l,m,n=-\infty;l\neq 0}^{\infty} \frac{1}{[(la)^2+(mb)^2+(nc)^2]^2} + \frac{\pi}{48a} \end{aligned} \tag{4.25}$$

We are ready to evaluate the piston force on the partition $x = a$.

$$F^{CCC} = -\frac{\partial}{\partial a} E^{CCC} = \frac{bc}{16\pi^2} \sum_{l\neq 0} [\frac{1}{[(la)^2+(mb)^2+(nc)^2]^2} - \frac{4l^2a^2}{[(la)^2+(mb)^2+(nc)^2]^3}] + \frac{\pi}{48}\frac{1}{a^2} \tag{4.26}$$

Let $b = c$ and $\eta = \frac{a}{b}$; the piston force for a purely conducting piston can be rewritten as

$$F^{CCC} = \frac{1}{16\pi^2 b^2} \sum_{l\neq 0,m,n} [\frac{1}{[l^2\eta^2+m^2+n^2]^2} - \frac{4l^2\eta^2}{[l^2\eta^2+m^2+n^2]^3}] + \frac{\pi}{48b^2}\frac{1}{\eta^2} \tag{4.27}$$

It is plotted in Fig. 12 as function of η. From (4.23), we see the relation between the force for purely conducting piston and the force for purely Dirichlet/Neumann piston:

$$F^{CCC} = F^{DDD} + F^{NNN} + \frac{\pi}{24\eta^2} = F^{DDN} + F^{DND} \tag{4.28}$$

The piston force is always attractive and the piston force $F^{CCC}|_{\eta\to\infty} = 0$ at the limit $\eta \to \infty$.

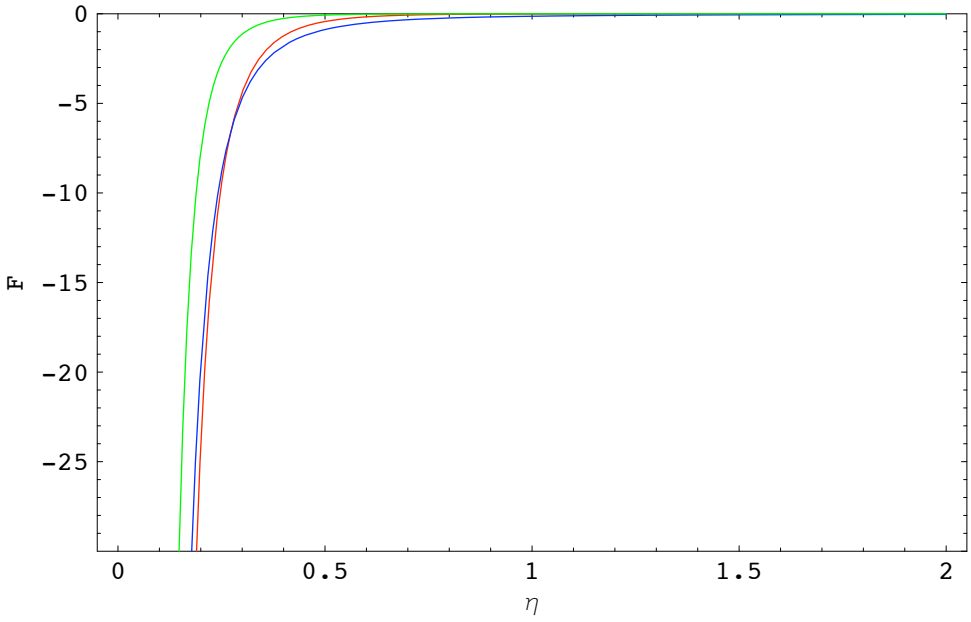

Fig. 12. The force F on a piston with square cross section ($b = c$) as functions of $\eta = a/b$. Solid red= F^{CCC}, solid blue= F^{NNN} and solid green= F^{DDD}.

4. Purely Permeable Piston

A purely permeable piston is extended by a rectangular cavity with PBC on each face. The CBC on each face requires that **E** and **B** to satisfy

$$\begin{aligned} B_y = B_z|_{x=0,a} &= 0 \quad E_x|_{x=0,a} = 0 \\ B_x = B_z|_{y=0,b} &= 0 \quad E_y|_{y=0,b} = 0 \\ B_x = B_y|_{z=0,c} &= 0 \quad E_z|_{z=0,c} = 0 \end{aligned} \tag{4.29}$$

Correspondingly, the 2 scalar fields ϕ and ψ satisfy

$$\begin{aligned} \partial_x \phi_x|_{x=0,a} &= 0 \quad \psi_x|_{x=0,a} = 0 \\ \partial_y \phi_y|_{y=0,b} &= 0 \quad \psi_y|_{y=0,b} = 0 \\ \partial_z \phi_z|_{z=0,c} &= 0 \quad \partial_z \psi_z|_{z=0,c} = 0 \end{aligned} \tag{4.30}$$

Therefore the appropriate normal modes for a purely permeable cavity are

$$\begin{aligned}\phi_{lmn}(x,y,z) &= D_{lmn}\frac{\cos\frac{l\pi}{a}x\cos\frac{m\pi}{b}y\sin\frac{n\pi}{c}ze^{-i\omega_{lmn}t}}{|k^{\perp}_{lmn}|\sqrt{2\omega_{lmn}}}\\ \psi_{lmn}(x,y,z) &= D_{lmn}\frac{\sin\frac{l\pi}{a}x\sin\frac{m\pi}{b}y\cos\frac{n\pi}{c}ze^{-i\omega_{lmn}t}}{|k^{\perp}_{lmn}|\sqrt{2\omega_{lmn}}}\end{aligned} \tag{4.31}$$

Comparing with the purely conducting cavity, the 2 scalar fields just exchange their values, $\phi \rightleftharpoons \psi$, which results in the exchange between $\mathbf{E}$ and $\mathbf{B}$; however, the energy density $\varepsilon = \frac{1}{2}(\mathbf{E}^2 + \mathbf{B}^2)$ stays unchanged. In other words, $\varepsilon^{CCC} = \varepsilon^{PPP}$. Therefore for the purely permeable piston, the piston force F^{PPP} will be exactly the same as F^{CCC}. The similar conclusion applies to other situations as well, such as $F^{PCC} = F^{CPP}$. We call this phenomenon *"B.C. Duality"*:

For a rectangular cavity with CBC and PBC on all 6 faces, if we replace CBC by PBC and replace PBC by CBC, then the two scalar field exchange to each other, $(\phi, \psi) \to (\psi, \phi)$, which makes $\mathbf{E}$ and $\mathbf{B}$ exchange their values but maintains the energy density $\varepsilon = \frac{1}{2}(\mathbf{E}^2+\mathbf{B}^2)$ unchanged.

5. Piston with PBC at $x = 0, a$ and CBC at $y = 0, b; z = 0, c$ (PCC)

The normal modes for this kind of piston are

$$\begin{aligned}\phi_{lmn}(x,y,z) &= D_{lmn}\frac{\cos\frac{l\pi}{a}x\sin\frac{m\pi}{b}y\cos\frac{n\pi}{c}ze^{-i\omega_{lmn}t}}{|k^{\perp}_{lmn}|\sqrt{2\omega_{lmn}}}\\ \psi_{lmn}(x,y,z) &= D_{lmn}\frac{\sin\frac{l\pi}{a}x\cos\frac{m\pi}{b}y\sin\frac{n\pi}{c}ze^{-i\omega_{lmn}t}}{|k^{\perp}_{lmn}|\sqrt{2\omega_{lmn}}}\end{aligned} \tag{4.32}$$

The energy density is

$$\begin{aligned}\varepsilon^{PCC} &= \frac{1}{4}[(\partial_1^2+\partial_2^2)(\overline{T}^{NDN}+\overline{T}^{DND})+(\partial_2^2+\partial_3^2)(\overline{T}^{DDD}+\overline{T}^{NNN})+(\partial_1^2+\partial_3^2)(\overline{T}^{NND}+\overline{T}^{DDN})\\ &= -\partial_\tau^2 V_1^{---}-\partial_1^2 V_1^{-++}+\partial_2^2 V_1^{+-+}+\partial_3^2 V_1^{++-}\\ &= -\partial_\tau^2[V_1^{---}+V_1^{-++}-V_1^{+-+}-V_1^{+++}]+\frac{4}{\pi^2}\sum_{lmn}^{\infty}[\frac{(2la)^2-t^2}{(d_{lmn}^{E_{yz}})^6}-\frac{(2mb)^2-t^2}{(d_{lmn}^{E_{xz}})^6}-\frac{(2nc)^2-t^2}{(d_{lmn}^{E_{xy}})^6}]\end{aligned} \tag{4.33}$$

The total energy for the cavity $a\times b\times c$ is

$$\begin{aligned}E_{abc}^{PCC} &= 2[E_1^P+E_1^{E_{yz}}-E_1^{E_{xz}}-E_1^{E_{xy}}]+\frac{\pi}{24a}-\frac{\pi}{24b}-\frac{\pi}{24c}\\ &= -\frac{abc}{16\pi^2}Z_3(a,b,c;4)+\frac{\pi}{48a}-\frac{\pi}{48b}-\frac{\pi}{48c}\end{aligned} \tag{4.34}$$

The $a-$dependent parts in E_{abc}^{PCC} are the same as in E_{abc}^{CCC}:

$$E_{abc}^{PCC}(a)=E_{abc}^{CCC}(a)=-\frac{abc}{16\pi^2}Z_3(a,b,c;4)+\frac{\pi}{48a} \tag{4.35}$$

Therefore the piston force F^{PCC} is the same as F^{CCC} as well. To summarize, we have found 4 equivalent cases:

$$F^{CCC}=F^{PPP}=F^{CPP}=F^{PCC} \tag{4.36}$$

6. Piston with CBC at $x=0,a;z=0,c$ and PBC at $y=0,b$ (CPC)

The total energy for the cavity $a\times b\times c$ can be obtained by rotating the PCC cavity along z-axis

$$\begin{aligned}E_{abc}^{CPC} &= 2[E_1^P-E_1^{E_{yz}}+E_1^{E_{xz}}-E_1^{E_{xy}}]-\frac{\pi}{24a}+\frac{\pi}{24b}-\frac{\pi}{24c}\\ &= -\frac{abc}{16\pi^2}Z_3(a,b,c;4)-\frac{\pi}{48a}+\frac{\pi}{48b}-\frac{\pi}{48c}\end{aligned} \tag{4.37}$$

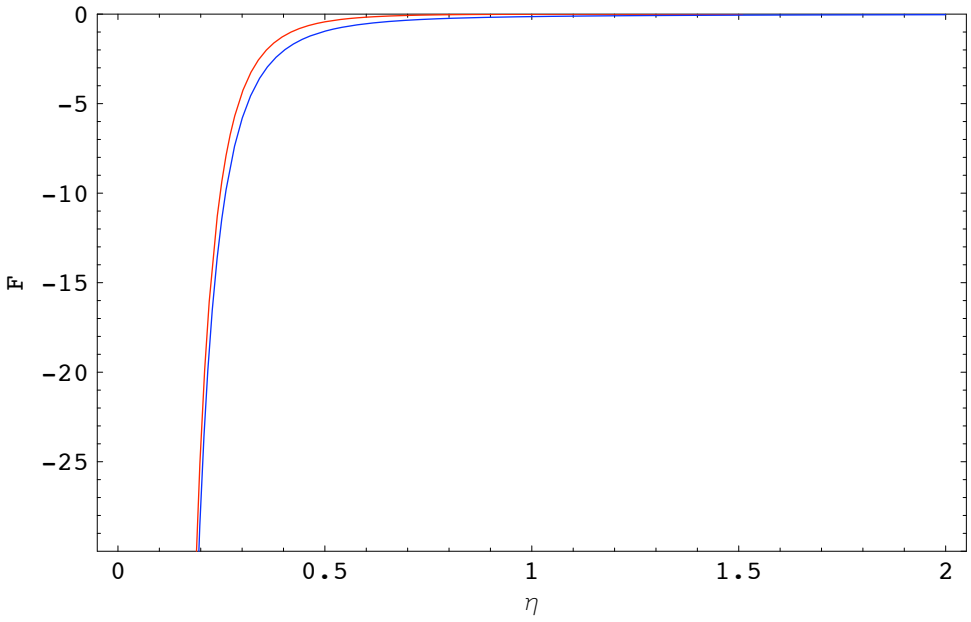

Fig. 13. The force F on a piston with square cross section ($b = c$) as functions of $\eta = a/b$. Solid red= F^{PCC} and solid blue= F^{CPC}.

The $a-$dependent parts in E^{CPC}_{abc} are

$$\begin{aligned} E^{CPC}_{abc} &= -\frac{abc}{16\pi^2} Z_3(a,b,c;4) - \frac{\pi}{48a} \\ &= [-\frac{abc}{16\pi^2} Z_3(a,b,c;4) + \frac{\pi}{48a}] - \frac{\pi}{24a} \\ &= E^{PCC}_{abc} - \frac{\pi}{24a} \end{aligned} \tag{4.38}$$

Therefore the relation between F^{CPC} and F^{PCC} is

$$F^{CPC} = F^{PCC} - \frac{\pi}{24\eta^2} = F^{DDD} + F^{NNN} \tag{4.39}$$

The piston force F^{CPC} is plotted in Fig. 13 along with F^{PCC}; they are both attractive.

B. Permeable Piston with a PBC Partition

1. Implication of B.C.

We investigate the cavity with PBC at $x = a$ and CBC elsewhere. The appropriate normal modes for the cavity are:

$$\begin{aligned}\phi_{lmn}(x,y,z) &= D_{lmn}\frac{\sin\frac{(l+\frac{1}{2})\pi}{a}x\sin\frac{m\pi}{b}y\cos\frac{n\pi}{c}ze^{-i\omega_{lmn}t}}{|k^{\perp}_{lmn}|\sqrt{2\omega_{lmn}}}\\ \psi_{lmn}(x,y,z) &= D_{lmn}\frac{\cos\frac{(l+\frac{1}{2})\pi}{a}x\cos\frac{m\pi}{b}y\sin\frac{n\pi}{c}ze^{-i\omega_{lmn}t}}{|k^{\perp}_{lmn}|\sqrt{2\omega_{lmn}}}\end{aligned} \tag{4.40}$$

where $\omega^2_{lmn} = k_1^2 + k_2^2 + k_3^2$, $k^2_{\perp} = k_1^2 + k_2^2$ and $k_1 = \frac{(l+\frac{1}{2})\pi}{a}, k_2 = \frac{m\pi}{b}, k_3 = \frac{n\pi}{c}$. Now we can go forward to give the expressions for each component of **E** and **B**.

$$E^2_3(t-t',\mathbf{r},\mathbf{r}') = \sum_{l,m,n}^{\infty}\frac{|D_{lmn}|^2(k_1^2+k_2^2)}{2\omega_{lmn}}\cos k_1x\sin k_2y\cos k_3z\cos k_1x'\sin k_2y'\cos k_3z'e^{i\omega_{lmn}(t-t')} \tag{4.41}$$

$$\begin{aligned}E^2_{\perp}(t-t',\mathbf{r},\mathbf{r}') = &\sum_{l,m,n}^{\infty}\frac{|D_{lmn}|^2(k_2^2+k_3^2)}{2\omega_{lmn}}\sin k_1x\sin k_2y\sin k_3z\sin k_1x'\sin k_2y'\sin k_3z'e^{i\omega_{lmn}(t-t')}\\ &+\sum_{l,m,n}^{\infty}\frac{|D_{lmn}|^2(k_1^2+k_3^2)}{2\omega_{lmn}}\cos k_1x\cos k_2y\sin k_3z\cos k_1x'\cos k_2y'\sin k_3z'e^{i\omega_{lmn}(t-t')}\end{aligned} \tag{4.42}$$

$$B^2_3(t-t',\mathbf{r},\mathbf{r}') = \sum_{l,m,n}^{\infty}\frac{|D_{lmn}|^2(k_1^2+k_2^2)}{2\omega_{lmn}}\sin k_1x\cos k_2y\sin k_3z\sin k_1x'\cos k_2y'\sin k_3z'e^{i\omega_{lmn}(t-t')} \tag{4.43}$$

$$\begin{aligned}B^2_{\perp}(t-t',\mathbf{r},\mathbf{r}') = &\sum_{l,m,n}^{\infty}\frac{|D_{lmn}|^2(k_2^2+k_3^2)}{2\omega_{lmn}}\cos k_1x\cos k_2y\cos k_3z\cos k_1x'\cos k_2y'\cos k_3z'e^{i\omega(t-t')}\\ &+\sum_{l,m,n}^{\infty}\frac{|D_{lmn}|^2(k_1^2+k_3^2)}{2\omega_{lmn}}\sin k_1x\sin k_2y\cos k_3z\sin k_1x'\sin k_2y'\cos k_3z'e^{i\omega(t-t')}\end{aligned} \tag{4.44}$$

Recall from Chapter III that $k_1 = \frac{(l+\frac{1}{2})\pi}{a}$ is related to the mixed B.C. on the scalar field. Therefore with the cylinder kernels defined in chapter III, we can rewrite E_i^2 and B_i^2 as

$$E_3^2(t,\mathbf{r},\mathbf{r}') = \frac{1}{4}(\partial_1^2+\partial_2^2)\overline{T}^{MDN}(t,\mathbf{r},\mathbf{r}') \tag{4.45}$$

$$E_\perp^2(t,\mathbf{r},\mathbf{r}') = \frac{1}{4}(\partial_2^2+\partial_3^2)\overline{T}^{MDD}(t,\mathbf{r},\mathbf{r}') + \frac{1}{4}(\partial_1^2+\partial_3^2)\overline{T}^{MND}(t,\mathbf{r},\mathbf{r}') \tag{4.46}$$

$$B_3^2(t,\mathbf{r},\mathbf{r}') = \frac{1}{4}(\partial_1^2+\partial_2^2)\overline{T}^{MND}(t,\mathbf{r},\mathbf{r}') \tag{4.47}$$

$$B_\perp^2(t,\mathbf{r},\mathbf{r}') = \frac{1}{4}(\partial_2^2+\partial_3^2)\overline{T}^{MNN}(t,\mathbf{r},\mathbf{r}') + \frac{1}{4}(\partial_1^2+\partial_3^2)\overline{T}^{MDN}(t,\mathbf{r},\mathbf{r}') \tag{4.48}$$

2. Energy Density and Total Energy

The energy density is

$$\varepsilon^{MCC} = \frac{1}{4}[(\partial_1^2+\partial_2^2)(\overline{T}^{MDN}+\overline{T}^{MND}) + (\partial_2^2+\partial_3^2)(\overline{T}^{MDD}+\overline{T}^{MNN}) + (\partial_1^2+\partial_3^2)(\overline{T}^{MND}+\overline{T}^{MDN})] \tag{4.49}$$

Notice that $\overline{T}$ satisfies the Laplace equation,

$$(\partial_1^2+\partial_2^2+\partial_3^2)\overline{T} = \partial_0^2\overline{T} = -\partial_\tau^2\overline{T} \tag{4.50}$$

so the energy density can be simplified to:

$$\begin{aligned}\varepsilon^{MCC} &= -\partial_\tau^2 V_2^{---} - \partial_\tau^2 V_2^{+--} - \partial_1^2 V_2^{-++} - \partial_1^2 V_2^{+++} \\ &= -\partial_\tau^2[V_2^{---}+V_2^{+--}+V_2^{-++}+V_2^{+++}] + \frac{4}{\pi^2}\sum_{lmn}^{\infty}(-1)^l[\frac{(2la)^2}{(d_{lmn}^{E_{yz}})^6} + \frac{(2la+2x)^2}{(d_{lmn}^{C})^6}\end{aligned} \tag{4.51}$$

Integrate over the cavity to get the total energy:

$$\begin{aligned}E^{MCC} &= 2[E_2^P + E_2^{S_x} + E_2^{E_{yz}} + E_2^C] - \frac{\pi}{48a} \\ &= 2E_2^P - 2E_2^{E_{yz}} = E_2^{MDN} + E_2^{MND}\end{aligned} \tag{4.52}$$

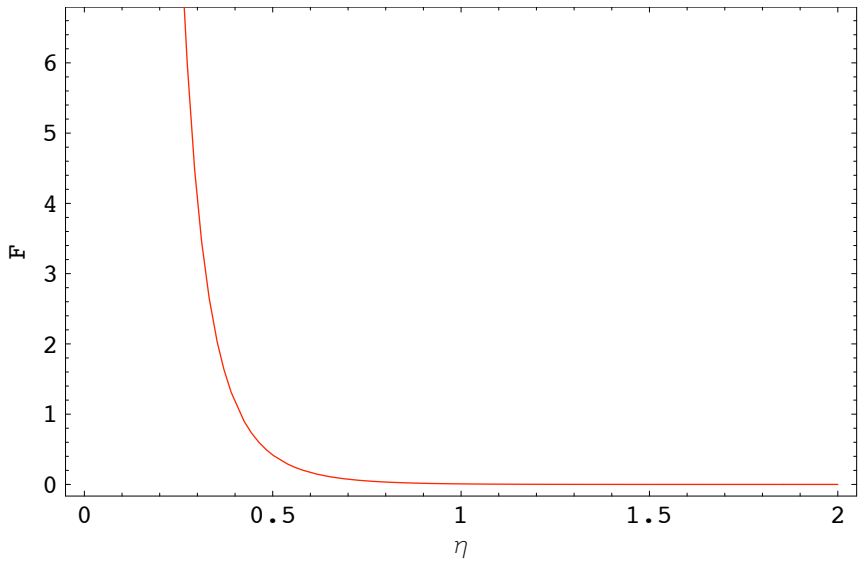

Fig. 14. The force F on a piston with square cross section ($b = c$) as functions of $\eta = a/b$. Solid red= $F^{MCC} = F^{MPP}$.

Note that $E_2^{S_x} = 0$, $E_2^C = 0$ and $E_2^{E_{yz}} = \frac{\pi}{192a}$.

3. Piston Force

By the B.C. duality, for the piston with CBC at the partition $x = 0$ and PBC elsewhere, the piston force F^{MCC} will be the same as F^{MPP}. It is plotted in Fig. 14.

$$F^{MCC} = F^{MPP} = F_2^{MDN} + F_2^{MND} \tag{4.53}$$

4. CP-PP-CC

When the B.C. on sides are not all CBC, but rather PBC at $y = 0, b$ and CBC at $z = 0, c$, the normal modes are

$$\begin{aligned}
\phi_{lmn}(x,y,z) &= D_{lmn} \frac{\sin \frac{(l+\frac{1}{2})\pi}{a} x \cos \frac{m\pi}{b} y \cos \frac{n\pi}{c} z e^{-i\omega_{lmn} t}}{|k^{\perp}_{lmn}| \sqrt{2\omega_{lmn}}} \\
\psi_{lmn}(x,y,z) &= D_{lmn} \frac{\cos \frac{(l+\frac{1}{2})\pi}{a} x \sin \frac{m\pi}{b} y \sin \frac{n\pi}{c} z e^{-i\omega_{lmn} t}}{|k^{\perp}_{lmn}| \sqrt{2\omega_{lmn}}}
\end{aligned} \tag{4.54}$$

Total energy for a cavity is

$$\begin{aligned}\varepsilon^{MPC} =&\frac{1}{4}[(\partial_1^2+\partial_2^2)(\overline{T}^{MDD}+\overline{T}^{MNN})+(\partial_2^2+\partial_3^2)(\overline{T}^{MND}+\overline{T}^{MDN})+(\partial_1^2+\partial_3^2)(\overline{T}^{MND}+\overline{T}^{MDN})\\ =&-\partial_\tau^2 V_2^{---}-\partial_\tau^2 V_2^{+--}-\partial_3^2 V_2^{-++}-\partial_3^2 V_2^{+++}\\ =&-\partial_\tau^2[V_2^{---}+V_2^{+--}+V_2^{-++}+V_2^{+++}]+\frac{4}{\pi^2}\sum_{lmn}^{\infty}(-1)^l[\frac{(2nc+2z)^2}{(d_{lmn}^{E_{yz}})^6}+\frac{(2nc+2z)^2}{(d_{lmn}^{C})^6}]\\ =&2[E_2^P+E_2^{S_x}+E_2^{E_{yz}}+E_2^C]-\frac{\pi}{96a}\\ =&2(E_2^P+0+\frac{\pi}{192a}+0)-\frac{\pi}{96a}=2E_2^P\end{aligned} \tag{4.55}$$

Note that $E_2^{S_x}=0$ and $E_2^C=0$, so the total energy

$$E^{MPC}=2E_2^P=2E_2^{MND}-\frac{\pi}{96a} \tag{4.56}$$

$$F^{MPC}=2F_2^{MND}-\frac{\pi}{96a^2}=\frac{F^{MDD}+F^{NN}}{2}+F^{MDN} \tag{4.57}$$

It is plotted in Fig. 15 along with F^{MCC}; they are both repulsive.

C. Piston with Mixed B.C.

There are various B.C. for a piston with mixed B.C. on some sides: CC-CP-CC (PP-CP-PP), CC-CP-PP (PP-CP-CC); CC-CP-CP, PP-CP-CP, CP-CP-CC, CP-CP-PP; CP-CP-CP.

1. CC-CP-CC

The normal modes are

$$\begin{aligned}\phi_{lmn}(x,y,z)&=D_{lmn}\frac{\sin\frac{l\pi}{a}x\sin\frac{(m+\frac{1}{2})\pi}{b}y\cos\frac{n\pi}{c}ze^{-i\omega_{lmn}t}}{|k_{lmn}^{\perp}|\sqrt{2\omega_{lmn}}}\\ \psi_{lmn}(x,y,z)&=D_{lmn}\frac{\cos\frac{l\pi}{a}x\cos\frac{(m+\frac{1}{2})\pi}{b}y\sin\frac{n\pi}{c}ze^{-i\omega_{lmn}t}}{|k_{lmn}^{\perp}|\sqrt{2\omega_{lmn}}}\end{aligned} \tag{4.58}$$

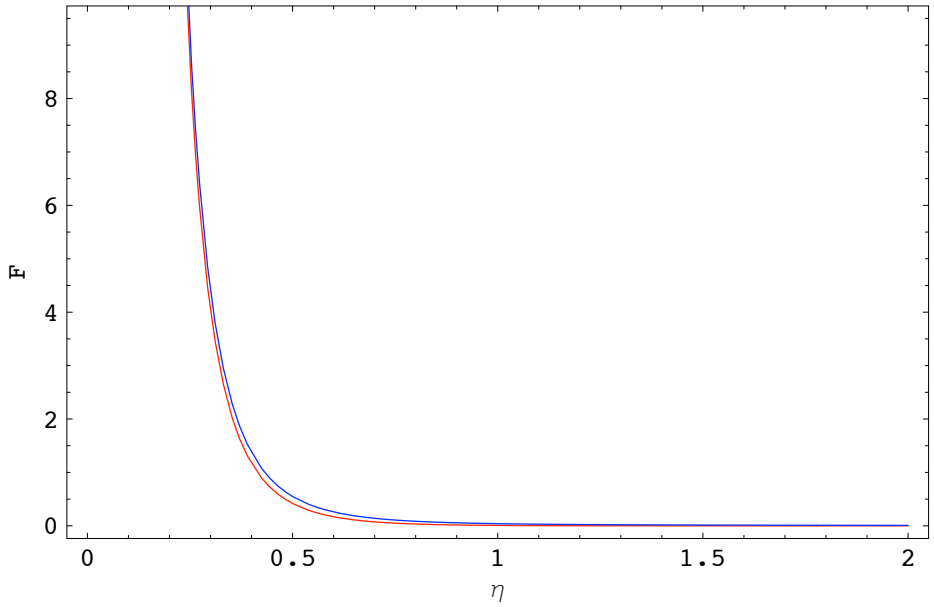

Fig. 15. The force F on a piston with square cross section ($b = c$) as functions of $\eta = a/b$. Solid red= $F^{MCC} = F^{MPP}$, solid blue= F^{MPC}.

Total energy for a cavity is

$$\varepsilon^{CMC}(\tau, \mathbf{r}, \mathbf{r}) = \frac{1}{4}[(\partial_1^2 + \partial_2^2)(\overline{T}^{DMD} + \overline{T}^{NMN}) + (\partial_2^2 + \partial_3^2)(\overline{T}^{DMD} + \overline{T}^{NMN}) + (\partial_1^2 + \partial_3^2)(\overline{T}^{DMN} + \overline{T}^{NMD})] \tag{4.59}$$

The $a-$dependent terms are V_2^{---}, V_2^{+-+}, V_2^{++-} and V_2^{-++}.

$$\begin{aligned} &\varepsilon^{CMC} \\ &= \frac{1}{4}[(\partial_1^2 + \partial_2^2)(\overline{T}^{DMD} + \overline{T}^{NMN}) + (\partial_2^2 + \partial_3^2)(\overline{T}^{DMD} + \overline{T}^{NMN}) + (\partial_1^2 + \partial_3^2)(\overline{T}^{NMD} + \overline{T}^{DMN})] \\ &= -\partial_\tau^2 V_2^{---} - \partial_\tau^2 V_2^{-+-} \\ &E^{CMC} = 2[E_2^P + E_2^{S_y}] = 2E_2^P = E^{NMN} + E^{DMD} \end{aligned} \tag{4.60}$$

Note that $E_2^{S_y} = 0$. Then the piston force can be related to scalar piston forces as

$$F^{CMC} = F^{NMN} + F^{DMD} \tag{4.61}$$

2. CC-CP-PP

The normal modes are

$$\begin{aligned}\phi_{lmn}(x,y,z) &= D_{lmn}\frac{\sin\frac{l\pi}{a}x\sin\frac{(m+\frac{1}{2})\pi}{b}y\sin\frac{n\pi}{c}ze^{-i\omega_{lmn}t}}{|k^{\perp}_{lmn}|\sqrt{2\omega_{lmn}}}\\ \psi_{lmn}(x,y,z) &= D_{lmn}\frac{\cos\frac{l\pi}{a}x\cos\frac{(m+\frac{1}{2})\pi}{b}y\cos\frac{n\pi}{c}ze^{-i\omega_{lmn}t}}{|k^{\perp}_{lmn}|\sqrt{2\omega_{lmn}}}\end{aligned} \tag{4.62}$$

Total energy for a cavity is

$$\begin{aligned}&\varepsilon^{CMP}(\tau,\mathbf{r},\mathbf{r})\\ &= \frac{1}{4}[(\partial_1^2+\partial_2^2)(\overline{T}^{DMD}+\overline{T}^{NMN})+(\partial_2^2+\partial_3^2)(\overline{T}^{DMD}+\overline{T}^{NMN})+(\partial_1^2+\partial_3^2)(\overline{T}^{NMD}+\overline{T}^{DMN})]\end{aligned} \tag{4.63}$$

The $a-$dependent terms are V_2^{---}, V_2^{+-+}, V_2^{++-} and V_2^{-++}.

$$\begin{aligned}&\varepsilon^{CMP}\\ &= \frac{1}{4}[(\partial_1^2+\partial_2^2)(\overline{T}^{DMD}+\overline{T}^{NMN})+(\partial_2^2+\partial_3^2)(\overline{T}^{DMD}+\overline{T}^{NMN})+(\partial_1^2+\partial_3^2)(\overline{T}^{NMD}+\overline{T}^{DMN})]\\ &= -\partial_\tau^2 V_2^{---}-\partial_\tau^2 V_2^{-+-}\\ &E^{CMP} = 2[E_2^P+E_2^{S_y}] = 2E_2^P\end{aligned} \tag{4.64}$$

This is the same as ε^{CMC}, so the piston force is again $F^{CMP} = F^{CMC} = F^{NMN} + F^{DMD}$.

3. CC-CP-CP

The normal modes are

$$\begin{aligned}\phi_{lmn}(x,y,z) &= \sum_{l,m,n}^{\infty} D_{lmn} \frac{\sin\frac{l\pi}{a}x \sin\frac{(m+\frac{1}{2})\pi}{b}y \sin\frac{(n+\frac{1}{2})\pi}{c}z e^{-i\omega_{lmn}t}}{|k^{\perp}_{lmn}|\sqrt{2\omega_{lmn}}} \\ \psi_{lmn}(x,y,z) &= \sum_{l,m,n}^{\infty} D_{lmn} \frac{\cos\frac{l\pi}{a}x \cos\frac{(m+\frac{1}{2})\pi}{b}y \cos\frac{(n+\frac{1}{2})\pi}{c}z e^{-i\omega_{lmn}t}}{|k^{\perp}_{lmn}|\sqrt{2\omega_{lmn}}}\end{aligned} \tag{4.65}$$

Total energy for a cavity is

$$\begin{aligned}&\varepsilon^{CMM}(\tau,\mathbf{r},\mathbf{r}) = \\ &\frac{1}{4}[(\partial_1^2+\partial_2^2)(\overline{T}^{DMM}+\overline{T}^{NMM})+(\partial_2^2+\partial_3^2)(\overline{T}^{DMM}+\overline{T}^{NMM})+(\partial_1^2+\partial_3^2)(\overline{T}^{NMM}+\overline{T}^{DMM})] \\ =&\frac{1}{2}(\partial_1^2+\partial_2^2+\partial_3^2)(\overline{T}^{DMM}+\overline{T}^{NMM}) = \frac{1}{2}\partial_\tau^2(\overline{T}^{DMM}+\overline{T}^{NMM})\end{aligned} \tag{4.66}$$

The $a-$dependent terms are V_3^{---}, V_3^{+-+}, V_3^{++-} and V_3^{-++}.

$$\begin{aligned}\varepsilon^{CMM}(\tau,\mathbf{r},\mathbf{r}) =& -\partial_\tau^2[V_3^{---}+V_3^{+-+}+V_3^{++-}+V_3^{-++}] \\ E^{CMM} =& 2[E_2^P+E_3^{S_y}+E_3^{S_z}+E_3^{E_{yz}}]\end{aligned} \tag{4.67}$$

however, $E_3^{S_y} = E_3^{S_z} = E_3^{E_{yz}} = 0$, so

$$E^{CMM}(\tau,\mathbf{r},\mathbf{r}) = 2E_3^P = 2F_3^P \tag{4.68}$$

Therefore, $F^{CMM} = 2F^{NMM}$.

We plot F^{CMC} and F^{CMM} in Fig. 16; they are both attractive.

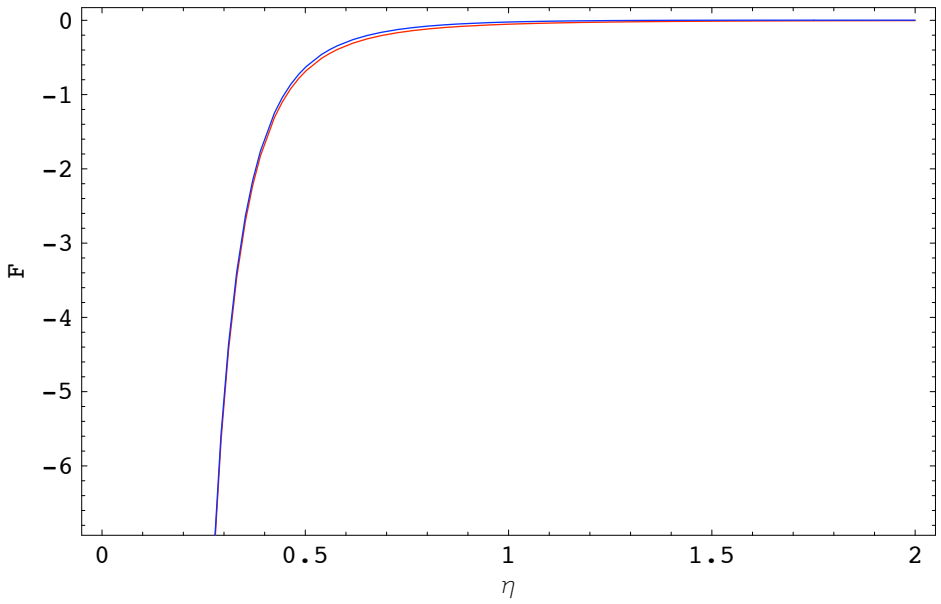

Fig. 16. The force F on a piston with square cross section ($b = c$) as functions of $\eta = a/b$. Solid red= $F^{CMC} = F^{CMP}$, solid blue= F^{CMM}.

4. CP-CP-CC

The normal modes are

$$\begin{aligned}\phi_{lmn}(x,y,z) &= D_{lmn}\frac{\sin\frac{(l+\frac{1}{2})\pi}{a}x\sin\frac{(m+\frac{1}{2})\pi}{b}y\sin\frac{n\pi}{c}ze^{-i\omega_{lmn}t}}{|k^{\perp}_{lmn}|\sqrt{2\omega_{lmn}}}\\ \psi_{lmn}(x,y,z) &= D_{lmn}\frac{\cos\frac{(l+\frac{1}{2})\pi}{a}x\cos\frac{(m+\frac{1}{2})\pi}{b}y\cos\frac{n\pi}{c}ze^{-i\omega_{lmn}t}}{|k^{\perp}_{lmn}|\sqrt{2\omega_{lmn}}}\end{aligned} \tag{4.69}$$

Total energy for a cavity is

$$\begin{aligned}&\varepsilon^{MMC}(\tau,\mathbf{r},\mathbf{r})\\ &= \frac{1}{4}[(\partial_1^2+\partial_2^2)(\overline{T}^{MMN}+\overline{T}^{MMD})+(\partial_2^2+\partial_3^2)(\overline{T}^{MMN}+\overline{T}^{MMD})+(\partial_1^2+\partial_3^2)(\overline{T}^{MMN}+\overline{T}^{MMD})]\\ &= \frac{1}{2}(\partial_1^2+\partial_2^2+\partial_3^2)(\overline{T}^{MMN}+\overline{T}^{MMD}) = -\frac{1}{2}\partial_\tau^2(\overline{T}^{MMN}+\overline{T}^{MMD})\end{aligned} \tag{4.70}$$

The $a-$dependent terms are V_3^{---}, V_3^{+-+}, V_3^{++-} and V_3^{-++}.

$$\begin{aligned}\varepsilon^{MMC}(\tau,\mathbf{r},\mathbf{r}) =& -\partial_\tau^2[V_3^{---}+V_3^{+-+}-V_3^{++-}-V_3^{-++}]\\ E^{MMC} =& 2[E_3^P+E_3^{S_y}-E_3^{S_z}-E_3^{E_{yz}}]\end{aligned} \tag{4.71}$$

however, $E_3^{S_y}=E_3^{S_z}=E_3^{E_{yz}}=0$, so

$$E^{MMC}(\tau,\mathbf{r},\mathbf{r}) = 2E_3^P = E^{MMN}+E^{MMD} \tag{4.72}$$

The piston force is $F^{MMC}=F^{MMN}+F^{MMD}$.

5. CP-CP-CP

The normal modes are

$$\begin{aligned}\phi_{lmn}(x,y,z) &= D_{lmn}\frac{\sin\frac{(l+\frac{1}{2})\pi}{a}x\sin\frac{(m+\frac{1}{2})\pi}{b}y\sin\frac{(n+\frac{1}{2})\pi}{c}ze^{-i\omega_{lmn}t}}{|k_{lmn}^{\perp}|\sqrt{2\omega_{lmn}}}\\ \psi_{lmn}(x,y,z) &= D_{lmn}\frac{\cos\frac{(l+\frac{1}{2})\pi}{a}x\cos\frac{(m+\frac{1}{2})\pi}{b}y\cos\frac{(n+\frac{1}{2})\pi}{c}ze^{-i\omega_{lmn}t}}{|k_{lmn}^{\perp}|\sqrt{2\omega_{lmn}}}\end{aligned} \tag{4.73}$$

Total energy for a cavity is

$$\begin{aligned}&\varepsilon^{MMM}(\tau,\mathbf{r},\mathbf{r})\\ &=\frac{1}{4}[(\partial_1^2+\partial_2^2)(\overline{T}^{MMM}+\overline{T}^{MMM})+(\partial_2^2+\partial_3^2)(\overline{T}^{MMM}+\overline{T}^{MMM})+(\partial_1^2+\partial_3^2)(\overline{T}^{MMM}+\overline{T}^{MMM})]\\ &=\frac{1}{2}(\partial_1^2+\partial_2^2+\partial_3^2)(\overline{T}^{MMM}+\overline{T}^{MMM})=-\partial_\tau^2\overline{T}^{MMM}\end{aligned} \tag{4.74}$$

The $a-$dependent terms are V_4^{---}, V_4^{+-+}, V_4^{++-} and V_4^{-++}.

$$\begin{aligned}\varepsilon^{MMM}(\tau,\mathbf{r},\mathbf{r}) =& -\partial_\tau^2[V_4^{---}+V_4^{+-+}+V_4^{++-}+V_4^{-++}]\\ E^{MMM} =& 2[E_4^P+E_4^{S_y}+E_4^{S_z}+E_4^{E_{yz}}]\end{aligned} \tag{4.75}$$

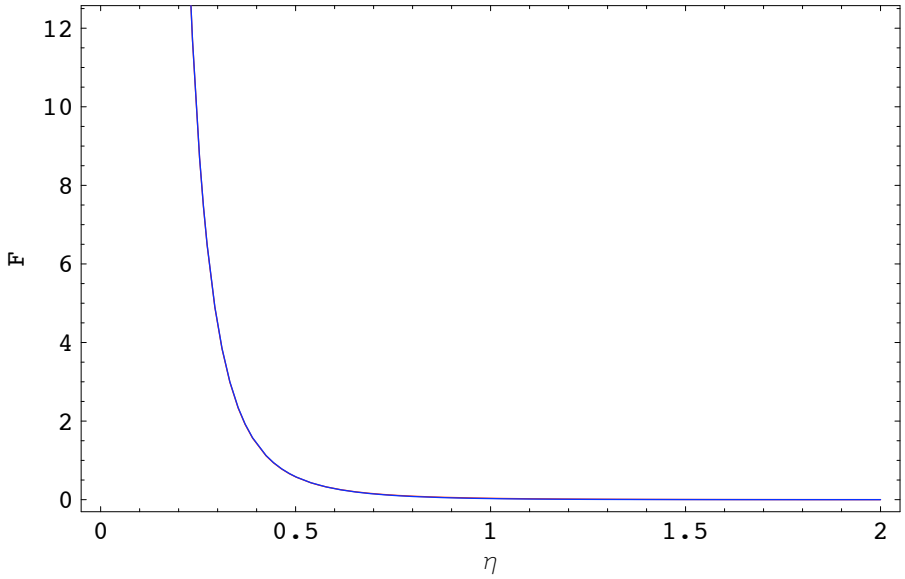

Fig. 17. The force F on a piston with square cross section ($b = c$) as functions of $\eta = a/b$. Solid red= F^{MMC}, solid blue= F^{MMM}.

however, $E_4^{S_y} = E_4^{S_z} = E_4^{E_{yz}} = 0$, so

$$E^{MMM}(\tau, \mathbf{r}, \mathbf{r}) = 2E_4^P = 2E^{MMM} \tag{4.76}$$

The piston force is $F^{MMM} = 2F^{MMM}$. F^{MMC} and F^{MMM} are plotted in Fig. 17; they are both repulsive.

D. Conclusion

For a piston with partition fixed at $x = a$, different B.C. yield different piston forces. B.C. duality provides the symmetry between 2 Hertz potentials ϕ and ψ when considering total energy, that makes two pistons with exactly opposite B.C. have identical piston force. Again the piston force turns out to be determined by a-dependent terms, which are contributed by periodic paths (V^{---}), side paths (V^{+-+} and V^{++-}) and edge paths (V^{-++}). Since we have related EM piston energy to the scalar cylinder kernel, it is straightforward to re-

Table VIII. Table of the relations between EM pistons and scalar pistons

B.C. Type	Equivalent Cases	Total Energy
CC-CC-CC	PP-PP-PP; PP-CC-CC; CC-PP-PP	$F^{CCC} = F_1^{DDN} + F_1^{DND}$
CC-PP-CC	PP-CC-PP	$F^{CPC} = F_1^{DDD} + F_1^{NNN}$
CC-CP-CC	CC-CP-PP; PP-PC-PP	$F^{CMC} = F_2^{NMN} + F_2^{DMD}$
CC-CP-CP	PP-CP-CP	$F^{CMM} = 2F_3^{NMM}$
CP-CC-CC	PC-PP-PP	$F^{MCC} = F_2^{MDN} + F_2^{MND}$
CP-PP-CC	PC-CC-PP	$F^{MPC} = F_2^{MDD} + F_2^{MNN}$
CP-CP-CC	CP-CP-PP	$F^{MMC} = F_3^{MMN} + F_3^{MMD}$
CP-CP-CP	PC-PC-PC	$F^{MMM} = 2F_4^{MMM}$

late EM piston force to the corresponding scalar piston force as well. We summarize the equivalent B.C. and the relations between EM pistons and scalar pistons in the table VIII. Recall that the subscripts $1, 2, 3, 4$ represent 1st, 2nd, 3rd and 4th kind B.C. for scalar piston. When the B.C. at $x = 0, a$ are both CBC/PBC, the piston force is always atractive; while when mixed B.C. are at $x = 0, a$, the piston force is always repulsive. Periodic paths' contribution always stays and dominates, while side paths' and edge paths' contribution is a perturbation to periodic paths' and might be absent for some cases, we call this part as side effect. At the limit $a \to 0$, these side effects are relatively small and can be ignored, so that in essence we have two parallel plates; as a increases, the side effect increases correspondingly; it could be either positive (same sign as periodic paths' contribution) or negative (opposite sign to periodic paths' contribution). In other words, the side effect becomes more and more visible when a increases and as a result, the total energy damps more

quickly or less according to its sign.

In summary, the EM piston has been studied by means of 2 Hertz potentials, thus **E** and **B** have been decomposed into 2 scalar fields. The EM fields **E** and **B** are constrained by either conducting or permeable B.C. and therefore induce corresponding B.C. for the 2 Hertz potentials ϕ and ψ, so that total energy and piston force of the EM piston can be represented by corresponding quantities of the scalar piston. It is convenient to use the known scalar piston results to deduce EM piston results, and that provides a way to analyze the EM piston from the point of view of classical paths; for a specific EM piston, we can tell which kinds of paths contribute more, less, or just are absent.

CHAPTER V

MULTIPLE REFLECTION EXPANSION ANALYSIS

All analysis in previous chapters dealt with flat surfaces, in which cases we can always apply the method of images to construct the corresponding Green functions such as cylinder kernel. When it comes to curved surfaces, method of images does not apply; we have to find an alternate way to construct the cylinder kernel. The multiple reflection expansion (MRE for short) is the closest counterpart for curved surfaces of the method of images for flat surfaces. Definitely the mathematics for curved surfaces is much more complicated.

A free Green's function $G^f(r, r')$ represents the propagation from point x to point x' directly. However, when boundary conditions are introduced, the Green's function will be confined to satisfy them (Dirichlet B.C. or Neumann B.C.). The confined Green's function can be developed by summing up the direct propagation: $x \to x'$, propagation with 1 reflection on the boundary S: $x \to S \to x'$, propagation with 2 reflections on the boundary S: $x \to S \to S \to x'$, and all propagations with higher number of reflections [44, 45].

For the whole space, the reduced Green's function in (2.9) is

$$G^f(\mathbf{r}, \mathbf{r}', \omega) = \frac{e^{\imath\omega|\mathbf{r}-\mathbf{r}'|}}{4\pi \mid \mathbf{r} - \mathbf{r}' \mid} \tag{5.1}$$

This is the Green's function without any boundary, which encounters a direct propagation from $\mathbf{r}$ to $\mathbf{r}'$. If we are looking for the Green's function which satisfies Dirichlet B.C. or Neumann B.C. on an arbitrary smooth surface S, MRE provides (at least formally) the Green's function which satisfies the corresponding B.C. as a summation on number of

reflections over the surface.

$$\begin{aligned} G^D(r,r') =& G^f(r,r') - < direct\ propagation > \\ & - 2\int_S d\mathbf{S}_\alpha \frac{\partial G^f(r,\alpha)}{\partial \mathbf{n}_\alpha} G^f(\alpha,r') - - - - - - - - - - - < 1st\ reflection > \\ & + 2^2 \int_S \int_S d\mathbf{S}_\alpha d\mathbf{S}_\beta \frac{\partial G^f(r,\alpha)}{\partial \mathbf{n}_\alpha} \frac{\partial G^f(\alpha,\beta)}{\partial \mathbf{n}_\beta} G^f(\beta,r') - - < 2nd\ reflection > \\ & - 2^3 \int_S \int_S \int_S d\mathbf{S}_\alpha d\mathbf{S}_\beta d\mathbf{S}_\gamma \frac{\partial G^f(r,\alpha)}{\partial \mathbf{n}_\alpha} \frac{\partial G^f(\alpha,\beta)}{\partial \mathbf{n}_\beta} \frac{\partial G^f(\beta,\gamma)}{\partial \mathbf{n}_\gamma} G^f(\gamma,r') + ... \end{aligned} \tag{5.2}$$

where r' is the starting point, the path reflects on S at points α, β, γ,..., and it finally goes to r. For Neumann B.C. the '$-$' sign for odd number reflection terms should be converted to '+' [11, 44, 45, 46, 47].

A. Reproduction of Method of Images for Flat Surfaces

The relation between the reduced Green's function for the whole space and the cylinder kernel for the whole space is

$$\overline{T}^f(r,r',t) = \frac{2}{\pi} L_\omega[ImG^f(r,r',\omega)] = \frac{2}{\pi} L_\omega[\frac{\sin\omega|rr'|}{4\pi|rr'|}] = -\frac{1}{2\pi^2}\frac{1}{t^2+|rr'|^2} \tag{5.3}$$

where L_ω is the Laplace transform operator with respect to ω. This relation gives a way to construct the cylinder kernel by Laplace transform of the corresponding reduced Green's function. Suppose we are looking for the cylinder kernel satisfying Dirichlet B.C. on a surface S and for now we have known the reduced Green's function (5.2) satisfying Dirichlet B.C.. If we take Laplace transform on both sides of (5.2), we will get the proper cylinder kernel satisfying Dirichlet B.C. $\overline{T}^D(r,r')$. The first term of the reduced Green's function, $G^f(r,r')$, corresponds to the direct propagation; after Laplace transform, it will be converted

into the free cylinder kernel $\overline{T}^f(r,r')$. The second term corresponds to the 1st reflection.

$$\begin{aligned} -2\int_S d\mathbf{S}_\alpha \frac{\partial G^f(r,\alpha)}{\partial \mathbf{n}_\alpha} G^f(\alpha,r') &= -2\int_S dS_\alpha \cos\theta_1 \frac{\partial}{\partial r_1}\left(\frac{e^{\imath\omega r_1}}{4\pi r_1}\right)\left(\frac{e^{\imath\omega r_2}}{4\pi r_2}\right) \\ &= -\frac{1}{8\pi^2}\int_S dS_\alpha \cos\theta_1 \left(\frac{\imath\omega}{r_1 r_2} e^{\imath\omega(r_1+r_2)} - \frac{1}{r_1^2 r_2} e^{\imath\omega(r_1+r_2)}\right) \end{aligned} \tag{5.4}$$

where $r_1 = |r\alpha|$, $r_2 = |\alpha r'|$ and θ_1 is the angle between the vector from r to α and the normal to the surface at point α. We take the Laplace transform for 1st reflection term (with $l = r_1 + r_2$):

$$\begin{aligned} \frac{2}{\pi} L\left[-2\int_S d\mathbf{S}_\alpha \frac{\partial G^f(r,\alpha)}{\partial \mathbf{n}_\alpha} G^f(\alpha,r')\right] &= \frac{2}{\pi} L\left[-\frac{1}{8\pi^2}\int_S dS_\alpha \cos\theta_1 \left(\frac{\imath\omega}{r_1 r_2} e^{\imath\omega(r_1+r_2)} - \frac{1}{r_1^2 r_2} e^{\imath\omega(r_1+r_2)}\right)\right] \\ &= \frac{1}{4\pi^3}\int_S dS_\alpha \cos\theta_1 \left[\frac{1}{r_1 r_2}\frac{l^2-t^2}{(l^2+t^2)^2} + \frac{1}{r_1^2 r_2}\frac{l}{t^2+l^2}\right] \end{aligned} \tag{5.5}$$

For the 2nd and higher orders of reflection more work is needed. Repeated paths and degenerate paths are involved and divergence analysis has to be made carefully [47]. By taking Laplace transform of the MRE of the reduced Green's function, we could apply numerical approximation for higher order reflections [12, 48, 49, 50].

For the purpose of comparing with method of images, let's analyze in detail the 1st reflection term (5.5). If we take the flat surface as example, we should reproduce the results of the method of images. Consider the case where the surface S stands for two parallel plates ($S_1 + S_2$) satisfying Dirichlet boundary conditions at both $x = 0$ (S_1) and $x = a$ (S_2). The cylinder kernel constructed by the method of images is

$$\overline{T}^D(r,r') = \overline{T}^f(r,r') + D_0\overline{T}^f(r,r') + D_a\overline{T}^f(r,r') + ... \tag{5.6}$$

Thus the 1st reflection term of cylinder kernel reflected by S_1 from point $r : (x,0,0)$

to $r' : (x', 0, 0)$ is

$$D_0\overline{T}^f(r, r')|_{r=r'} = \frac{1}{2\pi^2}\frac{1}{t^2 + (x + x')^2}|_{r=r'} = \frac{1}{2\pi^2}\frac{1}{t^2 + (2x)^2} \tag{5.7}$$

The other 1st reflection term $D_a\overline{T}^f(r, r')$ stands for the 1st reflection term reflected by S_2.

From MRE, the 1st reflection term of cylinder kernel reflected by S_1 is

$$\overline{T}_1^{MRE} = \frac{1}{4\pi^3}\int_{S_1} dS_\alpha = \cos\theta_1[\frac{1}{r_1 r_2}\frac{l^2 - t^2}{(l^2 + t^2)^2} + \frac{1}{r_1^2 r_2}\frac{l}{t^2 + l^2}] \tag{5.8}$$

When we put the two points identical; $r = r'$, we will have $r_1 = r_2 = \frac{l}{2}$, $cos\theta_1 = \frac{x}{l/2}$ and $dS = \pi dy^2 = \frac{\pi}{4}dl^2$. Substituting into (5.8) we got

$$\begin{aligned}
\overline{T}_1^{MRE} &= \frac{1}{4\pi^3}\int_{S_1}\frac{\pi}{4}dl^2\,(\frac{x}{l/2})[\frac{4}{l^2}\frac{l^2 - t^2}{(l^2 + t^2)^2} + \frac{8}{l^3}\frac{l}{t^2 + l^2}] \\
&= \frac{x}{4\pi^2}\int_{l_{min}}^{\infty} dl\,[\frac{12}{t^2}(\frac{1}{l^2} - \frac{1}{l^2 + t^2}) - \frac{8t^2}{l^2(l^2 + t^2)^2}] \\
&= \frac{x}{4\pi^2}[\frac{12}{t^2}(-\frac{1}{l} - \frac{1}{t}\arctan\frac{l}{t}) + (\frac{12}{lt^2} - \frac{4}{l}\frac{l}{t^2 + l^2} + \frac{12}{t^3}\arctan\frac{l}{t})]|_{l_{min}}^{\infty} \\
&= -\frac{x}{\pi^2}\frac{1}{l(t^2 + l^2)}|_{l_{min}}^{\infty} = \frac{x}{\pi^2}\frac{1}{l_{min}(t^2 + l_{min}^2)} \\
&= \frac{1}{2\pi^2}\frac{1}{t^2 + (l_{min})^2} = \frac{1}{2\pi^2}\frac{1}{t^2 + (2x)^2}
\end{aligned} \tag{5.9}$$

where $l_{min} = 2x$. The energy density contributed by the 1st reflection term is

$$\varepsilon|_{1st}^{MRE} = -\frac{1}{2}\lim_{t\longrightarrow 0}\frac{\partial^2}{\partial t^2}\overline{T}_1^{MRE} = \frac{1}{2\pi^2}\frac{1}{l_{min}^4} \tag{5.10}$$

So we conclude that, for flat surfaces, the 1st reflection term from MRE is exactly the same as $D_0\overline{T}$ from the method of images; higher order reflections are expected to be the same as well. We could understand the method of images as one special application of MRE when the surface is flat. For curved surfaces, the method of images fails; however, MRE can generalize its application to any surface.

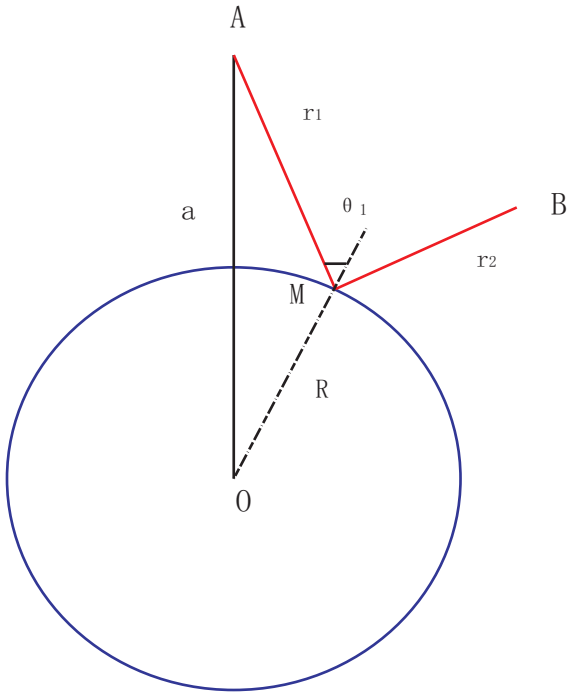

Fig. 18. A classical path starting from A (a from the center of sphere) is reflected off a sphere (with radius R) to B, the path length $l = r_1 + r_2$, the angle between AM and the normal at M is θ_1.

B. Reproduction of the Optical Approach's Result for a Sphere

We take 2-dimensional sphere in 3-dimensional space as a typical geometry to analyze how MRE works with curved surfaces. We will start with the MRE of the reduced Green's function as in (5.2). Now the boundary S stands for a sphere with radius R. By taking the Laplace transform of (5.2), the reduced Green's function satisfying Dirichlet B.C. on the sphere is converted to the cylinder kernel satisfying the same B.C.. Let's make a thorough study of the 1st reflection term of the cylinder kernel,

$$\overline{T}_1^{MRE} = \frac{1}{4\pi^3}\int_S dS_\alpha \cos\theta_1 [\frac{1}{r_1 r_2}\frac{l^2 - t^2}{(l^2+t^2)^2} + \frac{1}{r_1^2 r_2}\frac{l}{t^2+l^2}] \tag{5.11}$$

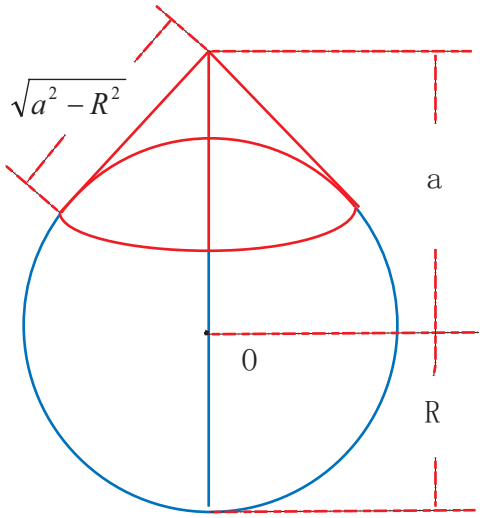

Fig. 19. The surface integral over the whole sphere is divided into 2 parts: visible region $l \in (l_{min}, l'_{max})$ and shadow region $l \in (l'_{max}, l_{max})$, where $l_{min} = 2(a-R)$, $l'_{max} = \sqrt{a^2-R^2}$ and $l_{max} = 2(a+R)$.

where r_1, r_2, θ_1 are shown in Fig. 18. When putting $r = r'$,

$$\begin{aligned} r_1 &= r_2 = \frac{l}{2} \\ \cos\theta_1 &= -\frac{R^2 + r_1^2 - a^2}{2Rr_1} = -\frac{R^2 + l^2/4 - a^2}{Rl} \\ dS &= \frac{2\pi R}{a} r_1 dr_1 = \frac{\pi R}{2a} l\, dl \end{aligned} \tag{5.12}$$

(5.11) can be written as

$$\begin{aligned} \overline{T}_1^{MRE} &= -\frac{1}{2\pi^2 a} \int_{l_{min}}^{l_{max}} dl\,(R^2 + l^2/4 - a^2)[\frac{1}{l^2}\frac{l^2 - t^2}{(l^2+t^2)^2} + \frac{2}{l^2}\frac{1}{t^2+l^2}] \\ &= -\frac{1}{2\pi^2 a}(\int_{l_{min}}^{l'_{max}} dl + \int_{l'_{max}}^{l_{max}} dl)(R^2 + l^2/4 - a^2)[\frac{1}{l^2}\frac{l^2 - t^2}{(l^2+t^2)^2} + \frac{2}{l^2}\frac{1}{t^2+l^2}] \end{aligned} \tag{5.13}$$

where $l_{max} = 2(a+R)$, $l'_{max} = 2\sqrt{a^2-R^2}$, $l_{min} = 2(a-R)$ and $a = R + l_{min}/2$ are shown in

Fig. 19. The integral from visible region ($l \in (l_{min}, l'_{max})$) gives

$$\begin{aligned}\overline{T}_{1v}^{MRE} &= -\frac{1}{2\pi^2 a}\int_{l_{min}}^{l'_{max}} dl\,(R^2 + l^2/4 - a^2)[\frac{1}{l^2}\frac{l^2 - t^2}{(l^2 + t^2)^2} + \frac{2}{l^2}\frac{1}{t^2 + l^2}] \\ &= \frac{R^2 - a^2}{2\pi^2 a}\frac{1}{l(t^2 + l^2)}|_{l_{min}}^{l'_{max}} + \frac{1}{8\pi^2 a}\frac{l}{t^2 + l^2}|_{l_{min}}^{l'_{max}} - \frac{1}{4\pi^2 at}\arctan\frac{l}{t}|_{l_{min}}^{l'_{max}} \\ &= \frac{R}{a}\frac{1}{2\pi^2}\frac{1}{t^2 + l_{min}^2} + \frac{1}{4\pi^2 at}\arctan\frac{l_{min}}{t} - \frac{1}{4\pi^2 at}\arctan\frac{l'_{max}}{t}\end{aligned} \tag{5.14}$$

The integral from shadow region ($l \in (l'_{max}, l_{max})$) gives

$$\begin{aligned}\overline{T}_{1s}^{MRE} &= -\frac{1}{2\pi^2 a}\int_{l'_{max}}^{l_{max}} dl\,(R^2 + l^2/4 - a^2)[\frac{1}{l^2}\frac{l^2 - t^2}{(l^2 + t^2)^2} + \frac{2}{l^2}\frac{1}{t^2 + l^2}] \\ &= \frac{R}{a}\frac{1}{2\pi^2}\frac{1}{t^2 + l_{max}^2} + \frac{1}{4\pi^2 at}\arctan\frac{l'_{max}}{t} - \frac{1}{4\pi^2 at}\arctan\frac{l_{max}}{t}\end{aligned} \tag{5.15}$$

Now we add the contributions from visible region and shadow region together, the 1st reflection term of the cylinder kernel is

$$\begin{aligned}\overline{T}_1^{MRE} &= \overline{T}_{1v}^{MRE} + \overline{T}_{1s}^{MRE} \\ &= \frac{R}{a}\frac{1}{2\pi^2}\frac{1}{t^2 + l_{max}^2} + \frac{R}{a}\frac{1}{2\pi^2}\frac{1}{t^2 + l_{max}^2} + \frac{1}{4\pi^2 at}\arctan\frac{l_{min}}{t} - \frac{1}{4\pi^2 at}\arctan\frac{l_{max}}{t}\end{aligned} \tag{5.16}$$

The third term can be expanded in the order of t as

$$\frac{1}{4\pi^2 at}\arctan\frac{l_{min}}{t} = \frac{1}{4\pi^2 a}(-\frac{1}{l_{min}} + \frac{t^2}{3l_{min}^3} - \frac{t^4}{5l_{min}^5}) + O[t^6] \tag{5.17}$$

Similarly for the fourth term,

$$\frac{1}{4\pi^2 at}\arctan\frac{l_{max}}{t} = \frac{1}{4\pi^2 a}(-\frac{1}{l_{max}} + \frac{t^2}{3l_{max}^3} - \frac{t^4}{5l_{max}^5}) + O[t^6] \tag{5.18}$$

Next we consider the energy density contributed by the 1st reflection term,

$$\begin{aligned}\varepsilon|_1^{MRE} &= -\frac{1}{2}\lim_{t\longrightarrow 0}\frac{\partial^2}{\partial t^2}\overline{T}_1^{MRE} \\ &= \frac{R}{a}\frac{1}{2\pi^2}(\frac{1}{l_{min}^4} + \frac{1}{l_{max}^4} - \frac{l_{min}}{6R}\frac{1}{l_{min}^4} + \frac{l_{max}}{6R}\frac{1}{l_{max}^4})\end{aligned} \tag{5.19}$$

Since $l_{min} \ll l_{max}$ and $l_{min} \ll 6R$, we conclude that the first term $\frac{R}{a}\frac{1}{2\pi^2}\frac{1}{l_{min}^4}$ dominates the energy density in the 1st reflection. This dominant term differs from the energy density contributed by the 1st reflection on a plate in (5.10) by an extra coefficient $\frac{R}{a}$, We call this coefficient "geometrical factor" ($g_1 = \frac{R}{a}$) as it reflects information on the curved surface. Correspondingly, the 1st term dominates the 1st reflection term of the cylinder kernel in (5.16).

The similarity between the formulas for curved and flat surfaces is that they both correspond to the minimal length l_{min} with one reflection on the surface; since minimal length corresponds to the optical ray length between two points when one reflection is involved, this gives a hint for us to understand the role that the boundary plays in MRE, that is, the surface integral over boundary is trying to find the minimal length of a closed path and a coefficient is coming out from the surface integral to reflect the geometrical effect.

Let's recall the optical approach's formula for energy density ,

$$\varepsilon^{optical} = -\frac{1}{2\pi^2}\sum_r (-1)^r \frac{\sqrt{\triangle_r}}{l_r^3} \tag{5.20}$$

where $\triangle_r$ is called "enlargement factor" [12, 48, 49, 50]. For the 1st reflection the enlargement factor is

$$\triangle_1 = \frac{1}{(l_{min} + \frac{l_{min}^2}{2R})^2} = \frac{1}{l_{min}^2}\frac{1}{(1 + \frac{l_{min}}{2R})^2} \tag{5.21}$$

The energy density contributed by the 1st reflection is,

$$\varepsilon_1^{optical} = \frac{1}{2\pi^2}\frac{\sqrt{\triangle_1}}{l_{min}^3} = \frac{1}{1 + \frac{l_{min}}{2R}}\frac{1}{2\pi^2}\frac{1}{l_{min}^4} = \frac{R}{a}\frac{1}{2\pi^2}\frac{1}{l_{min}^4} \tag{5.22}$$

The enlargement factor $\triangle_1$ defined in the optical approach and the geometrical factor g_1 defined in MRE are exactly the same and energy density in the optical approach corresponds to the dominant term in MRE approach. Note that MRE involves the whole surface, the

whole sphere in this case, and it provides an exact solution, while optical approximation, as it implies, provides an approximate solution. The relation between them lies, the optical approximation estimates the dominant contriution in MRE.

For higher order reflection, the optical approach needs numerical methods to obtain the enlargement factors and minimal length for periodic paths [12]; in the MRE method, when we deal with the minimal length and the geometrical factor (counterpart of enlargement factor), we did not provide easier math; that is, MRE also needs numerical methods for higher order reflections. However, in the lowest order we got consistent expression for energy density as the optical approach from another point of view. By introducing the MRE of the cylinder kernel, we naturally find connections between energy density and lengths of closed paths, and explain that the geometrical factor is coming from the surface integral and is strongly geometry-dependent.

CHAPTER VI

CONCLUSION

With the relation between cylinder kernel and energy density in (2.27), once we know the cylinder kernel, we can evaluate the Casimir energy and the Casimir force. There are two ways basically to construct the cylinder kernel: (1). Base the cylinder kernel on the summation (integration) of eigenfunctions as in (3.14); (2). Base the cylinder kernel on the method of images and sum over number of reflections as in (3.10). The cylinder kernel contains a cutoff parameter t (which should not be understood as physical time) by including an exponential term $e^{-\omega t}$. We can thus see clearly the cutoff dependence, the divergent terms resulted by cutoff dependence are easily isolated from the finite terms ($\propto t^0$, no cutoff dependence).

A typical application to scalar rectangular cavity brings 8 parts for the cylinder kernel, with the 8 parts classified to 4 kinds by type of classical paths: periodic paths, side paths, edge paths and corner paths. Therefore the total energy is composed of 8 terms contributed by different kind of paths. When considering the contribution from each kind of paths to the total energy, the periodic paths weigh highest and edge paths least; corner paths does not contribute to the total energy. There are various possible B.C. for a rectangular cavity by imposing different B.C. on each face. It turns out B.C. makes significant change to the cylinder kernel thus the total energy. Dirichlet B.C. or Neumann B.C. on each face will determine the sign of the contribution of side paths with Neumann B.C. + and Dirichlet B.C. −. Sign of contribution of edge paths are determined by B.C. of 2 faces which join at that edge, same B.C. on those 2 faces gives + and different B.C. −. The sign of periodic paths instead keeps unchanged no matter what B.C. are on the 6 faces.

A scalar piston is extended by a rectangular cavity and then composed of the original cavity and the extended cavity. The total energy of the piston is the summation of the

total energies of that two cavities. Comparing to a single rectangular cavity, the piston force converges to 0 at the limit of infinite separation while the cavity force converges to a nonzero constant, which is not reasonable. Another big change from cavity to piston lies in, for a cavity, periodic paths, side paths and edge paths always contribute to the total energy while for a piston only periodic paths always do so; side paths and edge paths may be absent depending on B.C.. The periodic paths determine the sign of the piston force and side paths and edge paths' contribution (if it exists) can be viewed as perturbation to the periodic paths'. When the B.C. on the partition (the movable face inside the piston) and the face parallel to the partition are the same, the piston force will be always attractive; when the B.C. are different, the piston force will be always repulsive. At the limit of small separation, the piston will be reduced to the parallel plates and perturbation from side paths and edge paths go to zero.

For the EM piston, we use 2 Hertz potentials ϕ and ψ to represent the EM field then the constraint on $\mathbf{E}$ and $\mathbf{B}$ resulted from the B.C. (CBC or PBC) on boundary are converted to corresponding constraint on the 2 scalar fields (Hertz potentials). The piston force of EM piston is closely related to the piston forces of 2 corresponding scalar piston. The piston force is attractive when the B.C. on the partition and the face parallel to the partition are the same and repulsive when they are different. The piston force converges to zero as the separation goes to infinity.

Cylinder kernel analysis from the point of view of classical paths obtains consistent conclusion as optical approximation did for purely Dirichlet/Neumann piston and purely conducting piston. For the rectangular cavity and piston (flat surface) they are both exact. For curved surface, such as sphere, the optical approximation is not exact any more and it does make some approximation. In comparison with the MRE (which is exact since it constructs an exact Green's function), the optical approach approximates the energy density by taking into account the enlargement factor and it turns out this approximation covers

the dominant term in the MRE approach by using surface integral. The MRE approach provides more accurate results with some correction terms, however, when the points in concern is close enough to the surface, the correction terms to the dominant term are relatively small, therefore optical approximation provides results with reasonable accuracy.

REFERENCES

[1] H. B. G. Casimir *Proc. Kon. Nederl. Akad. Wet.* **51**: 793 (1948).

[2] B. S. DeWitt *Phys. Rep.* **6**: 295 (1975).

[3] M.J. Sparnaay, *Physica* **24**: 751 (1958).

[4] S. K. Lamoreaux *Phys. Rev. Lett.* **78**: 5 (1997).

[5] H. B. G. Casimir, D. Polder *Phys. Rev.* **73**: 360 (1948).

[6] M. Bordag, *The Casimir effect 50 years later: proceedings of the Fourth Workshop on Quantum Field Theory Under the Influence of External C*, (Baker&Taylor Books, NC, 1999)

[7] G. Plunien, B. Muller, W. Greiner *Phys. Rep.* **134**: 89 (1986).

[8] T. Emig, A. Hanke, R. Golestanian, and M. Kardar *Phys. Rev. L* **87**: 260402 (2001).

[9] M. Bordag, U. Mohideen, V. M. Mostepanenko *Phys. Rep.* **353**: 1 (2001).

[10] S. Leseduarte, A. Romeo *Ann. Phys. (N.Y.)* **250**:448 (1996)

[11] R. Balian, B. Duplantier *Ann. Phys. (N.Y.)* **112**:165 (1978)

[12] A. Scardicchio, R. L. Jaffe *Nucl. Phys. B* **704**:552 (2005)

[13] K. A. Milton, L. L. Deraad and J. Schwinger *Ann. Phys. (N.Y.)* **115**:338 (1978)

[14] M. Bordag, E. Elizalde and J. Kirsten *J. Math. Phys.* **37**:895 (1996)

[15] S. A. Fulling, *J. Phys. A* **36**:6857 (2003)

[16] S. A. Fulling, *Physics Letter B* **624**:281 (2005)

[17] S. Hacyan, R. Jauregui, F. Soto, C. Villarreal *J. Phys. A* **23**:2401 (1990)

[18] R. M. Cavalcanti *Phys. Rev. D* **69**:065015 (2004)

[19] A. Roy, C. Y. Lin, U. Mohideen *Phys. Rev. L* **81**:004549 (1998)

[20] G. Bressi, G. Carugno, R. Onofrio, G. Ruoso *Phys. Rev. L* **88**:041804 (2002)

[21] K. A. Milton, *The Casimir Effect: Physical Manifestations of Zero-Point Energy* (World Scientific, NJ, 2001)

[22] S. A. Fulling, L. Kaplan, K. Kirsten, Z. H. Liu, K. A. Milton *J. Phys. A* **42**: 155402 (2009)

[23] Z. H. Liu, S. A. Fulling *New J. Phys.* **8**:234 (2006)

[24] A. Abramowitz and I. A. Stegun, Handbook of Mathematical Functions Dept. of Commerce, Washington DC 1964.

[25] W. Lukosz *Z. Physik* **258**:99 (1973)

[26] M. P. Hertzberg, R. L. Jaffe, A. Scardicchio *Phys. Rev. L* **95**:250402 (2005)

[27] G. Barton *Phys. Rev. D* **73**:065018 (2006)

[28] M. P. Hertzberg, R. L. Jaffe, M. Kardar, A. Scardicchio, *Phys. Rev. D* **76**:045016 (2007)

[29] A. Edery *Phys. Rev. D* **75**:105012 (2007)

[30] A. Edery, I. MacDonald *JHEP* **09**:005 (2007)

[31] X. Zhai, X. Li *Phys. Rev. D* **76**:047704 (2007)

[32] L. P. Teo *J. Phys. A* **42**:105403 (2009)

[33] S. C. Lim, L. P. Teo *New J. Phys.* **11**:013055 (2009)

[34] S. C. Lim, L. P. Teo *Eur. Phys. J. C* **60**:323 (2009)

[35] V. N. Marachevsky, *Phys. Rev. D* **75**:085019 (2007)

[36] V. N. Marachevsky, *J. Phys. A* **41**:164007 (2008)

[37] J. Bondurant, S. A. Fulling, *J. Phys. A* **38**:1505 (2005)

[38] R. B. Rodrigues, N. F. Svaiter, *Phys. Rev. D* **56**:4 (1997)

[39] A. A. Actor, *Ann. of Phys.* **230**:303 (1994)

[40] J. Ambjørn, S. Wolfram, *Ann. of Phys.* **147**:1 (1983)

[41] S. Hacyan, R. Jauregui, F. Soto, C. Villarreal *J. Phys. A* **23**:2401 (1990)

[42] S. Hacyan, R. Jauregui, C. Villarreal *Phys. Rev. A* **47**:4204 (1993)

[43] M. Crocee, D. A. Dalvit, F. C. Lombardo, F. D. Mazzitelli,*J. Opt. B* **7**:s32 (2005)

[44] T. H. Hansson, R. L. Jaffe *Ann. Phys. (N.Y.)* **151**:204 (1983)

[45] R. Balian, C. Bloch, *Ann. of Phys.* **60**:401 (1970)

[46] R. Balian, C. Bloch, *Ann. of Phys.* **64**:271 (1971)

[47] R. Balian, C. Bloch, *Ann. of Phys.* **69**:76 (1972)

[48] R. L. Jaffe, A. Scardicchio *Phys. Rev. L* **92**:070402 (2004)

[49] O. Schroeder, A. Scardicchio, R. L. Jaffe *Phys. Rev. A* **72**:012105 (2005)

[50] A. Scardicchio, R. L. Jaffe *Nucl. Phys. B* **743**:249 (2006)

VITA

Name: Zhonghai Liu

Address: Texas A&M University Physics Department

College Station, TX, 77843-4242

Telephone: 979-422-8169

Email: zliu@physics.tamu.edu

EDUCATION

University of Science and Technology of China, Hefei, Anhui, P. R. China B.S. in Physics, Theoretical Physics, May 2003

Texas A&M University, Department of Physics , College Station, M.S. in Physics, Theoretical Physics, August 2006

PUBLICATIONS

1. Z. H. Liu, S. A. Fulling, Casimir energy with a Robin boundary: The multiple reflection cylinder kernel expansion, *New J. Phys.* **8**:234 (2006)

2. R. Estrada, S. A. Fulling, Z. H. Liu, L. Kaplan, K. Kirsten, K. A. Milton, Vacuum stress-energy density and its gravitational implications, *J. Phys. A* **41**:164055 (2008)

3. S. A. Fulling, L. Kaplan, K. Kirsten, Z. H. Liu and K. A. Milton, Vacuum stress and closed paths in rectangles, pistons and pistols, *J. Phys. A* **42**: 155402 (2009)